

Spatiotemporal Causal Inference with Arbitrary Spillover and Carryover Effects: Airstrikes and Insurgent Violence in the Iraq War*

Mitsuru Mukaigawara[†] Kosuke Imai[‡] Jason Lyall[§] Georgia Papadogeorgou[¶]

November 7, 2025

Abstract

Social scientists now routinely draw on high-frequency, high-granularity “microlevel” data to estimate the causal effects of subnational interventions. To date, most researchers aggregate these data into panels, often tied to large-scale administrative units. This approach has two limitations. First, data (over)aggregation obscures valuable spatial and temporal information, heightening the risk of mistaken inferences. Second, existing panel approaches either ignore spatial spillover and temporal carryover effects completely or impose overly restrictive assumptions. We introduce a general methodological framework and an accompanying open-source R package, `geocausal`, that enable spatiotemporal causal inference with arbitrary spillover and carryover effects. Using this framework, we demonstrate how to define and estimate causal quantities of interest, explore heterogeneous treatment effects, conduct causal mediation analysis, and perform data visualization. We apply our methodology to the Iraq War (2003–11), where we reexamine long-standing questions about the effects of airstrikes on insurgent violence.

Keywords: Spatial spillover; carryover effects; causal inference; heterogeneous treatment effects; causal mediation; microlevel data; counterinsurgency; Iraq

*All of the proposed methods can be implemented via an R package, `geocausal` (Mukaigawara et al., 2024), which is freely available for download at the [Comprehensive R Archive Network](#). We thank the National Science Foundation for partial support (No. 2124124, 2124463, and 2124323). In addition, Imai acknowledges the Sloan Foundation (# 2020–13946) for financial support and Lyall gratefully acknowledges financial support from the Air Force Office of Scientific Research (Grant # FA9550-14-1-0072). The findings and conclusions reached here do not reflect the official views or policy of the United States Government or Air Force.

[†]Ph.D. Candidate, Department of Government, Harvard University, 1737 Cambridge Street, Cambridge MA, 02138. Email: mitsuru_mukaigawara@g.harvard.edu, URL: <https://www.mitsurumukaigawara.com>

[‡]Professor, Department of Government and Department of Statistics, Harvard University. 1737 Cambridge Street, Institute for Quantitative Social Science, Cambridge MA, 02138. Email: imai@harvard.edu, URL: <https://imai.fas.harvard.edu>

[§]James Wright Chair in Transnational Studies and Associate Professor, Department of Government, Dartmouth College, Hanover, NH 03755. Email: jason.lyall@dartmouth.edu, URL: <https://www.jasonlyall.com>

[¶]Assistant Professor, Department of Statistics, University of Florida, Gainesville FL 32603. Email: gpapadogeorgou@ufl.edu, URL: <https://gpapadogeorgou.netlify.com>

1 Introduction

Social scientists now routinely draw on high-frequency, high-granularity “microlevel” data to estimate the causal effects of subnational interventions across a wide range of disciplines. While collection methods vary, these microlevel data represent information measured at individual units of analysis (e.g., households, villages) that contain precise spatial (e.g., latitude/longitude coordinates) and temporal data (e.g., date, time) that enable fine-grained causal inference.

Prominent applications of microlevel data include the study of patterns of civil war violence (Kalyvas, 2006; Raleigh and Karlsen, 2010; Schon and Koren, 2022) and repression (Rozenas and Zhukov, 2019), the effects of development assistance and humanitarian aid (Sexton, 2016; Kotsadam et al., 2018), the local effects of natural disasters (Young and Hsiang, 2024), air pollution and health outcomes (Huang et al., 2024), and the dynamics of protests and riots (Chenoweth, Pinckney and Lewis, 2018; Keremoglu, Hellmeier and Weidmann, 2022). The rise of social media and mobility data has supercharged this trend: tens of millions of geotagged social media posts (Xu, Lu and Wei, 2025), and even billions of call-logs from individual cell phones (Aiken et al., 2022), have been collected with spatial and temporal information as discrete as one meter resolution and one second intervals.

Yet methods for causal inference have not kept pace with this microlevel turn. Indeed, nearly all of these studies share a common methodological problem: to use standard methods of causal inference, they aggregate their microlevel data into coarse panel data formats that discard geospatial and temporal information. In practice, scholars bundle these microlevel data at larger spatial levels (e.g., administrative units like districts or provinces) and time periods (e.g., months, or even years) to facilitate causal inference. Doing so, however, has several drawbacks, including an inability to assess spatial spillover and temporal carryover effects of a given intervention.¹

To illustrate these problems, consider the following example. Imagine conducting an evaluation of a short-term village-level aid program’s ability to reduce insurgent attacks in a conflict-setting like Afghanistan or Iraq. At present, the most common inferential approach is to assign treatment and outcome data to much larger administrative units like districts or provinces over lengthy time intervals of up to a year to create panel data for statistical analysis (e.g., Berman, Shapiro and Felter, 2011; Sexton, 2016; Sexton and Zurcher, 2024; Crost, Felter and Johnston, 2014; Dasgupta, Gawande and Kapur, 2017; Weintraub, 2016; Findley et al., 2023). This approach, however, risks introducing potential bias, partly by increasing sensitivity to decisions about data aggregation (Zhukov et al., 2024). Causal mechanisms also become harder to test as the distance increases between the actual sites of the intervention and outcomes and the chosen administrative units.

¹We define *spillover* as a situation where the effects of an intervention can influence outcomes in neighboring or related units. *Carryover effect* occurs when an intervention’s effects persist across subsequent time periods even when the original treatment has concluded. Spillover and carryover effects represent interference across units that violates the stable unit treatment value assumption (SUTVA) underpinning many standard models of causal inference.

Moreover, this approach hardwires spatial and temporal boundaries, leaving us unable to explore spillover and carryover effects. It is possible, for example, that the effects of aid reach across district lines or diffuse to neighboring villages but not across entire districts; both scenarios would be obscured by coarse district-level aggregation. Similarly, short-term effects might be missed entirely if time units are too lengthy. And, because existing methods struggle to observe spillover and carryover effects, our theories tend to be impoverished when hypothesizing about the extent of an intervention’s causal effects.

To address these challenges, we introduce a new statistical framework for geospatial causal inference to assist researchers working with microlevel data. Our approach offers three methodological contributions to the small but growing literature addressing the problem of geospatial causal inference. First, we tackle the question of unstructured inference — contexts where treatments may affect outcomes across multiple, arbitrary, places and times — by adopting a spatial point process modeling approach. That is, we do not assume a finite and fixed set of potential intervention locations or impose structural assumptions about unit separation and aggregation, two common solutions in the existing literature ([Wang et al., 2020](#); [Tchetgen Tchetgen, Fulcher and Shpitser, 2021](#)).

Instead, we extend the general methodology proposed by [Papadogeorgou et al. \(2022\)](#) that preserves granular spatial and temporal attributes of microlevel data, allowing treatments and outcomes to be represented as data patterns at the intervention site. Our approach avoids the pitfalls of (over)aggregation and, in particular, does not restrict the nature and extent of spillover and carryover effects. In turn, our methodology allows researchers to specify different counterfactual distributions of a given intervention to assess how it affects outcomes for multiple researcher-defined spatial and temporal windows.

Second, we show how to estimate heterogeneous treatment effects. Despite well-known concerns that spatial context can shape local effects, existing methods for estimating heterogeneous treatment effects are unable to address spatiotemporal variables without making drastic assumptions, including viewing interventions as fixed within finite spatial units ([Zhang and Ning, 2023](#)). By contrast, our framework can incorporate spatial moderators that might condition the causal effects of different distributions of an intervention.

Third, while a large literature now exists on causal mechanisms (see [Imai et al., 2011](#); [Acharya, Blackwell and Sen, 2016](#); [VanderWeele, 2015](#), and references therein), existing methods either ignore the spatial dimensions of mediators ([Hizli et al., 2023](#)) or, alternatively, rely on simple time-series of low-dimensional spatial summaries ([Runge et al., 2015](#)). Our approach improves causal mediation analysis by retaining the spatiotemporal nature of microlevel data, allowing for more fine-grained testing of potential causal mechanisms.

Finally, we provide an open R package, `geocausal`, that implements all of these methods, including identifying and estimating counterfactual treatment distributions, exploring heterogeneous effects and causal mediation, and performing data visualization and analysis.

We apply our method to several interrelated debates in the now-vast literature on counterinsurgency. More specifically, we examine the causal effects of American airstrikes on insurgent violence during the Iraq War (2003–11). We draw on two declassified datasets from the US military that detail daily US airstrikes and insurgent violence with a high degree of spatial fidelity (typically, to ten meter precision). We examine whether US airstrikes affected insurgent attacks and explore whether these effects are heterogeneous given the traits of nearby US military units, including their level of mechanization and troop density, as well as proximity to US bases. We also test whether civilian harm, as measured by satellite imagery of targeted locations, mediates the effects of airstrikes on the intensity, location, and timing of subsequent insurgent attacks. These questions are often treated separately in standalone studies. We take a different path; our framework offers a unified approach for estimating the causal effects of airstrikes, military forces, and civilian harm, while also capturing spillover and carryover effects of counterfactual microlevel interventions.

We find that intensifying US airstrikes increases insurgent violence. Moreover, these increases are highest in areas with highly mechanized forces and US bases. Our approach also sheds light into the post-strike timing of insurgent retaliation: the observed increase in attacks becomes statistically significant after 7–10 days of intensified airstrikes. Contrary to prior studies, we find little evidence that these causal effects are mediated by civilian harm. Airstrikes that bombed civilian homes and buildings are no more likely to spark increased insurgent attacks than those that hit military targets like groups of rebels. These findings suggest that insurgent attacks are motivated by a desire to demonstrate resolve by inflicting costly punishment on occupying forces rather than revenge and grievances born from civilian harm.

Our paper is organized in five sections. In Section 2, we introduce our motivating application and debates about the causal effects of airstrikes in counterinsurgency wars. In Section 3, we discuss the details of our proposed methodology. We then describe our causal assumptions and estimators in Section 4. Our findings are presented in Section 5. We conclude in Section 6.

2 Airstrikes and Insurgent Violence in Iraq

We focus on US airstrikes and their effects on subsequent violence by Iraqi rebels as our motivating application. We first detail existing debates about the effects, and effectiveness, of airstrikes in counterinsurgency wars below before describing our microlevel data.

2.1 Debates About Airpower and Counterinsurgency

A series of theoretical and policy debates has arisen around the efficacy and effects of airpower in counterinsurgency wars.² Scholars have increasingly adopted a quantitative microlevel approach to identifying the causal effects of airstrikes in both historical wars like Vietnam (Kocher, Pepinsky and Kalyvas, 2011; Dell and Querubin, 2018) and more contemporary air campaigns in Pakistan (Johnston and Sar-

²On the history of airpower in counterinsurgency, see Corum and Johnson (2003) and Newton (2019).

bahi, 2016; Rigterink, 2021), Syria (Schwab, Krause and Massoud, 2023), Afghanistan (Allen, Bell and Machain, 2021; Lyall, 2019), and Iraq (Krick, Petkun and Revkin, 2025; Papadogeorgou et al., 2022; Khan and Gopal, 2017).

To date, however, these microlevel studies have relied upon research designs that aggregate along coarse spatial and temporal windows. In one influential study, for example, the effects of American airstrikes in Vietnam are assumed to be fixed to a 2km radius around bombed hamlets and their effects on territorial control measured with a one-time change between July and December 1969 (Kocher, Pepinsky and Kalyvas, 2011). Using these same data, Dell and Querubin (2018) uses a 5km radius and quarterly changes in territorial control scores. Similarly, a study of US drone strikes in Pakistan aggregates these pinpoint bombings to a much larger agency-week panel that uses fixed 25km intervals to search for possible spillover (Johnston and Sarbahi, 2016). Simply put, these studies rely on panel designs that can obscure dynamics at the intervention sites, are likely to struggle to capture spillover effects, and are often too coarse to identify fast-moving action-reaction cycles.

To highlight our approach to spatiotemporal causal inference, we engage three interrelated questions in the debate over airpower in counterinsurgency wars. First, we examine often-heated debates about whether airstrikes are an effective tool for reducing insurgent violence. Second, we explore the possibility that airstrikes produce heterogeneous effects on insurgent violence depending on the mechanization levels of soldiers deployed at or near bombed locations. Finally, we test the claim that airstrikes causing civilian harm are especially prone to generating increased insurgent violence. These questions have typically been studied in isolation. We instead offer a unified framework for estimating effects that shed light on how airstrikes create incentives for insurgents to restore their reputation for resolve by attacking counterinsurgent forces, thereby increasing short-term violence.

We begin with the question of whether airstrikes increase, decrease, or have no effect on subsequent insurgent violence. Prior research has found that airstrikes can degrade insurgent capabilities and deter recruitment of would-be replacements, resulting in reduced military capacity and thus fewer attacks (Johnston and Sarbahi, 2016; Gordon, 2022). Other studies have suggested that insurgents adapt quickly to airpower; decreases in violence, if any, will be modest and short-lived as rebels return to original baseline of attacks (Foster, 1928). Still others have proposed that airstrikes enflame insurgent attacks, for two reasons. First, airstrikes might harm civilians indiscriminately, leading them to take up arms to seek revenge, particularly in rebel-controlled areas (Balcells, 2017; Kalyvas, 2006, 167-69). Second, harmed civilians might share information with insurgents about counterinsurgent locations and behavior, increasing rebel capacity for taking action (Condra et al., 2011; Shaver and Shapiro, 2021). Each view implicitly suggests that revenge and information-sharing should be localized to the bombed area. Revenge-seekers, for example, are most likely to strike close to home, where they hold a natural advantage in understanding the local terrain and context. Tips from civilians to rebels are likewise

context-specific; useful intelligence will most likely be about the movement of counterinsurgent forces near, if not in, the bombed location. The timing of insurgent responses is also left unclear in these theories: we might expect immediate reactions as aggrieved individuals seize on the first opportunity to strike back or, alternatively, slow-burning grievances that are nurtured for months, perhaps years, before being acted on.

We propose an alternative explanation for why airstrikes might increase insurgent attacks. Airstrikes can indeed impose costs on insurgent organizations, including killing commanders and ordinary rebels alike, frustrating open movement, and persuading locals to withhold support from a now-weakened insurgency. Rather than deter, however, airstrikes can create incentives for insurgents to strike back quickly to demonstrate that they retain the ability to hurt counterinsurgent forces (Lyall, 2019). A quick response helps maintain a reputation for resolve in the eyes of both the counterinsurgent forces and locals who might be considering defecting to the government side.

This resolve-based argument generates several empirical predictions about insurgent behavior. For example, insurgent retaliation should occur quickly after airstrikes. Insurgents should also target counterinsurgent forces, especially mechanized ones, since hitting “hard” targets is the surest path toward demonstrating resolve. Reputation-seeking insurgents may venture farther afield to find targets to strike; we should expect spatial spillover to extend from the original airstrike location to neighboring locations, including roadways marked by a high density of counterinsurgent forces (especially their bases). Given these incentives, we expect insurgent violence to be unconnected to civilian harm, whether measured by fatalities or property damage. Resolve, rather than revenge, should animate the nature of the insurgent reply to airstrikes.

For our second empirical test, we investigate whether airstrikes have heterogeneous treatment effects. To do so, we explore whether the presence of mechanized forces (defined as units with a high ratio of motorized vehicles to soldiers) increases or decreases post-airstrike insurgent violence. Both positions find support in the existing literature. Some argue, for example, that mechanized forces perform poorly in counterinsurgency: their reliance on presence patrols cuts them off from the civilian population, and thus information about the insurgents, rendering their violence more indiscriminate (Lyall and Wilson, 2009). If correct, we should observe increased rebel attacks as the number and level of mechanization increases among occupying forces in areas that have been bombed.

Others, however, contend that mechanized forces deter insurgent violence, help secure territorial control, and lead fence-sitting civilians to feel more secure and thus more willing to share tips that enable counterinsurgent forces to destroy rebel capacity (Van Wie and Walden, 2022a; Kalyvas, 2006). If this position is correct, we should observe decreased post-strike insurgent violence in areas where mechanized forces are stationed. Our proposed resolve-based explanation anticipates that insurgents should seek out mechanized forces to signal resolve and, as a result, these areas should witness increased

post-strike attacks.

Our final empirical test examines whether civilian harm mediates the effects of airstrikes on subsequent insurgent attacks. To date, a near consensus exists that civilian harm generates grievances, leads to increased support for rebels (including providing tips), and delegitimizes the counterinsurgent (Krick, Petkun and Revkin, 2025; Shaver and Shapiro, 2021; Condra and Shapiro, 2012). We should therefore expect to observe increased insurgent attacks after airstrikes that harm civilians or damage property. Existing theories are less clear on when and where we should observe these effects, though it is reasonable to assume that the sharpest increase in attacks should occur where direct harm is inflicted. Our resolve-based explanation suggests a different behavioral expectation: we anticipate that insurgent attacks will remain unaffected by the scale of civilian harm. While insurgents may recruit by appealing to harmed individuals, their targeting will be shaped primarily by a desire to restore their reputations for military capacity in a given area.

2.2 Motivating application

We draw on the Iraq War (2003–11) to illustrate our proposed methodology. The Iraq War has played an outsized role in the development of US counterinsurgency doctrine (Petersen, 2024; *U.S. Army Field Manual No.3-24*, 2007) as well as debates about the utility of airpower (Biddle, 2006; Papadogeorgou et al., 2022), mechanized forces (Lyall and Wilson, 2009; Van Wie and Walden, 2022a), and aid in these settings (Berman, Shapiro and Felter, 2011; Zürcher, 2017; Binetti, 2025). With at least 151,000 Iraqi civilian deaths in 2003–06 alone (Alkhuzai et al., 2008), the war has also become a touchstone for debates around the effects of civilian casualties on subsequent insurgent violence (Condra et al., 2011; Shaver and Shapiro, 2021) as well as calculating, and mitigating, civilian harm (Khan and Gopal, 2017; Silverman, 2020). We note, too, that the Iraq War remains one of the best documented wars given its high profile and declassification of relevant datasets, even if important data limitations remain.

We combine two declassified datasets to test the relationship between airstrikes, civilian harm, and insurgent attacks. We first draw on the US Air Force’s own dataset of airstrikes and shows of force (simulated bombing runs) in Iraq. These records include the date, aircraft type, and precise geographic coordinates (in Military Grid Reference System, or MGRS) for each air event along with information on the number and type of weapon released. We then cross-referenced these data with two additional data sources to record civilian harm. First, using a purpose-built program and at least two human coders, we identified the intended target of the airstrike using historical satellite imagery.³ We then superimposed an estimated blast radius on the selected imagery to represent the ordinance dropped during a given airstrike. We categorized targets within the blast radius into eight broad groups: residential compounds, other buildings, farms, roads, settlements, unpopulated areas, unclassifiable areas due to poor imagery,

³We detail our coding procedures in SI Section A.

and others. We treat airstrikes on residential compounds and settlements as “civilian,” while roads and unpopulated areas, where strikes typically targeted mobile insurgent bands, are treated as “military” in nature. These data provide a much more nuanced account of civilian harm than (often unreliable) counts of civilians killed. Second, as a robustness check, we cross-referenced these airstrikes with records of civilian casualties from Iraq Body Count (see <https://www.iraqbodycount.org/>) and newspaper searches to provide estimates of civilians killed and injured for each airstrike.⁴

We use a declassified version of the Department of Defense’s Combined Information Data Network Exchange (CIDNE) dataset to record insurgent attacks against American and allied forces. CIDNE records the date, location (in MGRS), and type of insurgent attack, including Small Arms Fire (SAF) and Improvised Explosive Devices (IEDs), the two most frequent type of attack. We focus our attention on the most intense period of fighting (February 2007–July 2008), which includes so-called “Surge” and subsequent drawdown of American forces to Iraq (Biddle, Friedman and Shapiro, 2012).

To explore the possibility that airstrike effects hinge on the presence of armed forces, we also use a subnational dataset of the location of US and UK military units in Iraq (Van Wie and Walden, 2022b). This source provides weekly district-level data on the dismount ratio (soldiers per armed vehicles), troop density (soldiers per 1,000 district residents), and indicator variables denoting the presence of US Marines or the UK Army instead of US Army units (the bulk of deployed forces). We supplement these measures with declassified data on the location of US and UK military bases across Iraq as an alternative indicator of troop presence.

Figure 1 illustrates the spatial distribution of airstrikes and insurgent attacks in Iraq between February 2007 and July 2008. Both airstrikes and insurgent attacks exhibit significant spatial variation, being present in nearly every administrative unit but with clear spatial clustering within them, often mapping closely with population centers and roadways. These patterns suggest that aggregating our data to the administrative unit level would not only lead to the loss of valuable spatial information but also introduce bias in our analysis.

Moreover, while airstrikes are often concentrated near (and within) more urban areas, insurgent attacks tend to cluster not just in populated areas but in the roads that connect them. As a result, the effects of airstrikes, especially those that harm civilians, are likely not just confined to the immediate targeted location but have multiple pathways for spatial spillover, including via social and road networks. We therefore need a methodology that can account for potential spatial spillover and temporal carryover effects while also recognizing the influence of possible mediators such as civilian harm in these complex wartime environments.

⁴Given chronic underreporting of civilian casualties, we find that only 3.5% of US airstrikes (112 of 3,159) are associated with civilian casualties during our study period. By contrast, our satellite imagery indicates that civilian structures comprised more than 15% of targets struck. We therefore rely on estimates derived from imagery in our main analysis and replicate our findings using IBC estimates as a secondary measure.

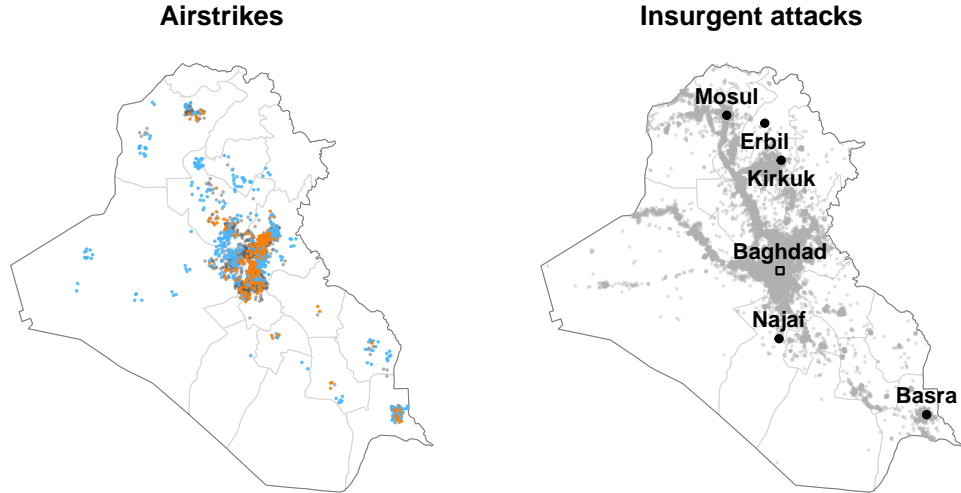


Figure 1: **Spatial distribution of airstrikes (left panel) and insurgent attacks (right) in Iraq from February 2007 to July 2008.** For airstrikes (left), the orange, blue, and gray points represent airstrikes that struck civilian, military, and unclassifiable locations, respectively, based on satellite image classification.

3 Methodological Framework

In this section, we introduce our proposed methodology for spatiotemporal causal inference. We first detail the twin concepts of spatial point processes and stochastic interventions that are central to our framework. We then formally define the estimands for the analysis of average and heterogenous causal effects as well as for causal mediation analysis.

3.1 Overview

Our methodology is flexible by design: it allows researchers to design granular spatiotemporal interventions and to make causal inferences about causal effects with arbitrary spillover and carryover effects. As illustrated in Figure 2 (left panel), the proposed framework asks the researcher to move through three steps: spatiotemporal data collection, modeling the spatial distribution of treatments, and then designing counterfactual stochastic interventions of interest by specifying their frequency, distribution, and duration. We use a spatial point process to model the treatment’s geographic distribution. More specifically, we use spatial and temporal covariates (including lags) to model treatment locations as an inhomogeneous Poisson point process that allows treatment intensity to vary across locations (this is a standard spatial modeling technique) (Baddeley, 2015). The expectation of this Poisson point process in a given region of interest is the average number of treatment events occurring in that region.⁵

Our stochastic intervention represents a hypothetical user-specified *distribution* of treatment events.

⁵Our methodological framework can accommodate propensity score models and stochastic interventions other than the Poisson process, such as those that specify dependence in treatment occurrence across space.

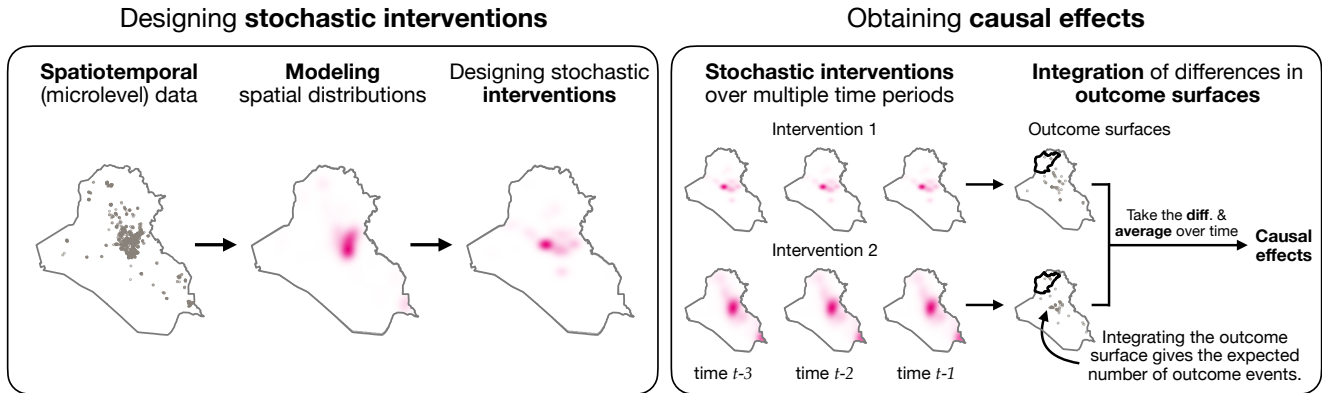


Figure 2: **Our spatiotemporal causal inference framework.** Stochastic interventions are designed based on the spatial distribution of the treatment. We then use them to estimate the causal effects of one intervention compared to another. We obtain the effect on the expected number of outcome events in any arbitrary areas (the bounded area in black) by taking the difference of integrated outcome surfaces, averaged across time.

At its core, the primary goal of our methodology is to help researchers estimate counterfactual outcomes given the distribution of this hypothetical stochastic intervention. In our application below, we use a counterfactual probability distribution of US airstrikes across Iraq over multiple time periods as our stochastic intervention. Researchers using our approach are free to define any intervention distribution of interest and to do so across multiple time periods. We caution, however, that setting a distribution that varies too dramatically from the actual distribution of realized treatment events will lead to a high variance of resulting estimates and, in extreme cases, a violation of identification assumptions.

Once counterfactual interventions have been constructed, we can investigate how behavioral outcomes would manifest given the hypothetical distribution of the treatment. We view treatments here as a time-series of consecutive maps (or a single map if the stochastic intervention is specified for a single period) that represent spatial distributions of treatment events. For example, we employ a hypothetical distribution of airstrikes concentrated around Baghdad and apply it over three time periods (see Intervention 1 in the right panel of Figure 2). We might also consider an alternative hypothetical intervention with a wider geographic distribution across the entire country (Intervention 2 of the same figure) and then compare outcomes (here, insurgent attacks) resulting from the two interventions.

As illustrated in the right panel of Figure 2, the proposed methodology estimates a counterfactual “outcome surface,” which represents a probability density of observing outcome events at every location in the space under the specified hypothetical stochastic intervention, thereby allowing for arbitrary spillover and carryover effects. We can obtain the causal effects by taking the difference of outcome surfaces at each time period under different stochastic interventions and averaging it over time (Figure 2, right). This procedure yields a variety of counterfactual quantities. For example, one can estimate the

expected number of outcome events in a certain region (Figure 2, right, depicted as the bounded area in black) under a counterfactual intervention of interest. Computing the differences in these counterfactual quantities under two stochastic interventions of interest lead to causal effect estimates.

Our approach does not require assumptions about spillover or carryover effects. We avoid segmenting the entire geographical area of interest into specific regions (i.e. districts or grid cells) when we design hypothetical interventions. Instead, we define interventions as probability distributions of treatment effects across the entire geographic space over as many time periods as needed.

3.2 Setup

We now formally present our methodology.⁶ Let Ω represent the entire geographical region of interest. We denote time periods with $t = 1, 2, \dots, T$ where T represents the total number of time periods. In our application, Ω is the entire country of Iraq and $T = 499$ (in days). We use daily level data to best capture the immediate nature of insurgent planning and targeting, dynamics that are obscured if we adopt more aggregate units like weeks or months. At each time period, the treatment assignment is a spatial point pattern over Ω .

We define the binary treatment variable at each location $s \in \Omega$ as $W_t(s)$, which indicates whether the location received the treatment ($W_t(s) = 1$) or not ($W_t(s) = 0$) at time period t . The collection of $W_t(s)$ at all locations fully represents the treatment point pattern at time period t and is denoted by the random variable $W_t = \{W_t(s), s \in \Omega\}$ with its realization w_t . Alternatively, the treatment point pattern can be fully represented through the locations that received the treatment, referred to as the *treatment active locations* and denoted by $S_{W_t} = \{s \in \Omega : W_t = 1\}$. In our setting, S_{W_t} represents the airstrike locations in Iraq on the t th day. Lastly, we denote the treatment history by $\overline{W}_t = (W_1, W_2, \dots, W_t)$ and its realization by $\overline{w}_t = (w_1, \dots, w_t)$. Since W_t captures which locations receive treatment at time t as a point pattern, its history \overline{W}_t encodes all past treatment information for all locations up to time t .

Next, let Y_t denote the observed outcome point pattern at time t where $Y_t(s) = 1$ if location s experiences the outcome event at that time and $Y_t(s) = 0$ if it does not. In our application, $Y_t(s) = 1$ if location s observes insurgent attacks at time t . For a given treatment history \overline{w}_t , we denote the corresponding potential outcome by $Y_t(\overline{w}_t)$ and the observed outcome by $Y_t = Y_t(\overline{W}_t)$, respectively. Thus, $Y_t(\overline{w}_t)$ and Y_t corresponds to the potential and observed outcomes in all locations. The potential outcomes $Y_t(\overline{w}_t)$ are not restricted in how they can be affected by treatment spatially or temporally. This unrestricted formulation allows all previous treatments to influence future outcomes, and treatments at any location to affect outcomes at any location. We use $\mathcal{Y}_{\mathcal{T}} = \{Y_t(\overline{w}_t), \text{ for all } t \text{ and } \overline{w}_t\}$ to denote the collection of all potential outcomes under any treatment path and for any time point. We use $\overline{Y}_t = \{Y_1, Y_2, \dots, Y_t\}$ to represent the observed outcomes up to time t .

⁶See SI Section B for a schematic overview of the notation.

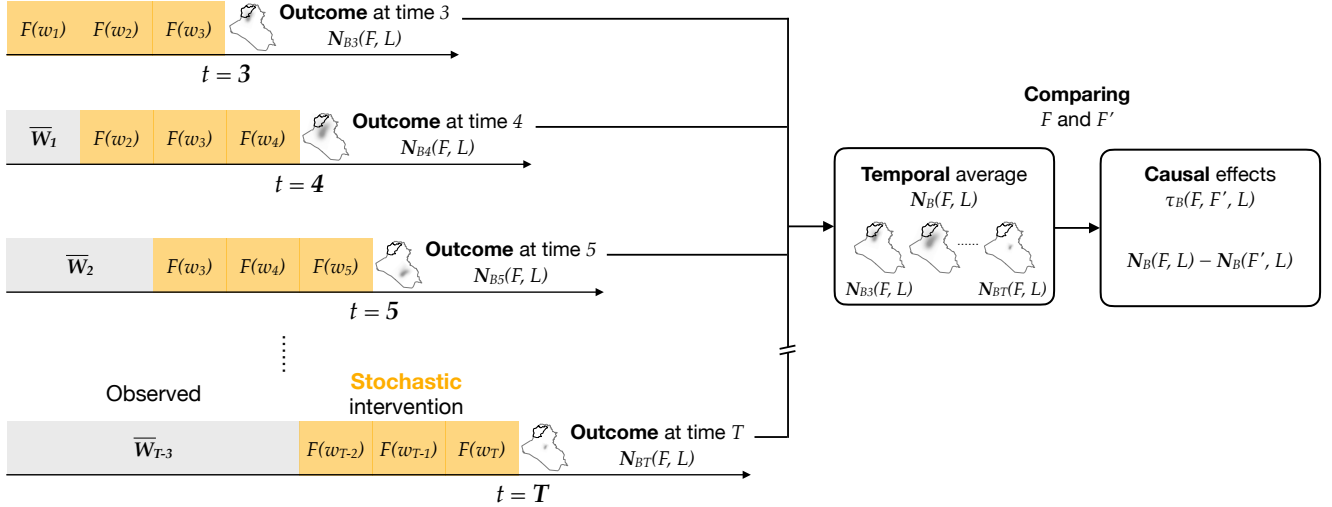


Figure 3: **Schematic representation of the causal estimands.** The estimand $N_{Bt}(F, L)$ represents the expected number of outcome active locations given a stochastic intervention F over preceding L time periods (shown in orange). For illustrative purposes, we set $L = 3$. Treatment histories are fixed prior to intervention F (shown in gray). The estimand $N_B(F, L)$ represents the temporal average of $N_{Bt}(F, L)$ across $t = 3, \dots, T$. The difference between $N_B(F, L)$ and $N_B(F', L)$ represents the temporal average effects of switching from intervention F' to F .

Finally, we use \mathbf{X}_t to denote a collection of spatiotemporal confounders at time t that are causally prior to the realized treatment for the same time period, i.e., W_t . These potential confounders can be either time-varying or time-invariant, and may or may not vary across space. Furthermore, the confounders may be arbitrarily affected by the past treatment history. Therefore, we let $\mathbf{X}_t(\bar{w}_{t-1})$ denote the potential value of the confounders at time period t that would result for a given treatment history. Then, the observed confounders are represented by $\mathbf{X}_t = \mathbf{X}_t(\bar{W}_{t-1})$, and the history of observed confounders are represented by $\bar{\mathbf{X}}_t = (\mathbf{X}_1, \mathbf{X}_2, \dots, \mathbf{X}_t)$. We use \mathcal{X}_T to denote the collection of all potential confounder values for all time points, similarly to \mathcal{Y}_T . We use $\bar{H}_t = \{\bar{W}_t, \bar{Y}_t, \bar{\mathbf{X}}_{t+1}\}$ to denote the observed random variables that have occurred up until the treatment assignment at time period $t + 1$.

3.3 Average treatment effects

Our causal estimands are based on the expected number of outcome events at each time period t in a certain region $B \subset \Omega$ under a specified stochastic intervention F that lasts during L time periods with $L \geq 1$. Our causal estimands therefore differ from conventional static comparisons of uniformly treated and untreated areas. Instead, we evaluate more nuanced and realistic intervention effects that account for the spatial distribution of treatment. Since we treat the data as a time-series of maps, the causal estimand is defined by averaging the expected number of outcome events over the $T - L + 1$ time periods (we set aside the first $L - 1$ time periods, which correspond to the periods of stochastic intervention).

Figure 3 provides a schematic summary of how we define the average treatment effects. For illus-

trative purposes, we consider a stochastic intervention F that lasts for $L = 3$ time periods (shown in orange). For each time period $t = 3, \dots, T$, we compute the expected number of outcome events under this intervention in region B , conditional on observed airstrikes up to time $t - L$, i.e., $\overline{\mathbf{W}}_{t-L}$ (shown in gray), which we will use to obtain the temporal average. In the current example, we generate a total of $T - L + 1 = T - 2$ expected outcomes: $\mathbf{N}_{B3}(F, L), \dots, \mathbf{N}_{BT}(F, L)$. We then take the temporal average of all $\mathbf{N}_{Bt}(F, L)$ for $t = 3, \dots, L$ and obtain a spatially and temporally averaged outcome, $\mathbf{N}_B(F, L)$ (the center box in the figure). Finally, to compare the effects of intervention F relative to another intervention F' , we take the difference between $\mathbf{N}_B(F, L)$ and $\mathbf{N}_B(F', L)$, resulting in the average treatment effect $\tau_B(F, F', L)$ shown in the right box.

Formally, we follow [Papadogeorgou et al. \(2022\)](#) and define the expected number of outcome events in region B at time period t under stochastic intervention F as follows:

$$\mathbf{N}_{Bt}(F, L) = \int_{\mathcal{W}} \dots \int_{\mathcal{W}} N_B(Y_t(\overline{\mathbf{W}}_{t-L}, w_{t-L+1}, \dots, w_t)) dF(w_{t-L+1}) \dots dF(w_t), \quad (1)$$

where $N_B(\cdot)$ counts the number of outcome events within B , and \mathcal{W} denotes the set of all possible treatment active locations at each period. Equation (1) integrates the counterfactual outcome surface with respect to the stochastic intervention F over L time periods. In our application, $\mathbf{N}_{Bt}(F, L)$ represents the expected number of insurgent attacks under a stochastic intervention of airstrikes F over L time periods.

Once $\mathbf{N}_{Bt}(F, L)$ is defined for each time period, we further average it over time to obtain the expected number of outcome events in region B . Averaging over time (as well as space, which we achieve by taking the expected outcome counts over the space) is essential because the uncertainty of a single observation $\mathbf{N}_{Bt}(F, L)$ cannot be directly assessed. Formally, our primary causal estimand is given by:

$$\mathbf{N}_B(F, L) = \frac{1}{T - L + 1} \sum_{t=L}^T \mathbf{N}_{Bt}(F, L) \quad (2)$$

where temporal averaging starts from $t = L$ given that the stochastic intervention F is defined over L time periods. Finally, we can define the average effect of a stochastic intervention F' relative to another intervention F'' (i.e., average treatment effect or ATE) as,

$$\tau_B(F', F'', L) = \mathbf{N}_B(F', L) - \mathbf{N}_B(F'', L). \quad (3)$$

3.4 Heterogeneous treatment effects

In addition to the ATE, researchers are often interested in how treatment effects vary across locations (heterogeneous treatment effects). To analyze heterogeneous treatment effects, we characterize treatment effects as functions of certain moderators. Here, we examine how the treatment effect at each small

geographical area, which we refer to as a “pixel”, varies as a function of its spatial or spatiotemporal characteristics. Specifically, we first partition Ω into p disjoint regions and then define the pixel-level conditional average treatment effect (CATE) using its spatial or temporal characteristics. We then compute the average of these pixel-level CATEs across pixels with the same moderator value (Zhou et al., 2024). Since the moderator may take many different values, we use linear projection to summarize the relationship between pixel-level CATEs and the moderator variable.

Formally, let $\mathcal{Q} = \{Q_1, \dots, Q_p\}$ be the set of p non-overlapping small geographical regions (i.e., pixels) that comprise Ω , where $\Omega = \cup_{i=1}^p Q_i$ and $Q_i \cap Q_{i'} = \emptyset$ for $i \neq i'$. We use $\mathbf{R}_{it} \in \mathcal{R}$ to denote the vector-value of the potential moderator in pixel Q_i at time t , with \mathcal{R} representing the support of the moderator. The value \mathbf{R}_{it} should be constant within Q_i at time t . If the moderator is not constant within each pixel at any given time period, then we can use a summary statistic such as the mean. In our application, \mathbf{R}_{it} represents troop characteristics, including mechanization and binary indicators denoting the presence of US bases.

Given this setup, we first define the pixel-level CATE by applying Equation (1) to pixel Q_i as follows:

$$\mathbf{N}_{it}(F, L) = \int_{\mathcal{W}} \cdots \int_{\mathcal{W}} N_{Q_i} \left(Y_t(\overline{\mathbf{W}}_{t-L}, w_{t-L+1}, \dots, w_t) \right) dF(w_{t-L+1}) \cdots dF(w_t).$$

Then, the difference in the pixel-level CATE between two stochastic interventions is given by:

$$\tau_{it}(F', F'', L) = \mathbf{N}_{it}(F', L) - \mathbf{N}_{it}(F'', L). \quad (4)$$

We can now define the overall CATE by taking the average of Equation (4) over all pixels with the same moderator value $\mathbf{r} \in \mathcal{R}$:

$$\tau_t(F', F'', L; \mathbf{r}) = \frac{1}{\sum_{i=1}^p I(\mathbf{R}_{i,t-L+1} = \mathbf{r})} \sum_{i=1}^p \tau_{it}(F', F'', L) I(\mathbf{R}_{i,t-L+1} = \mathbf{r}), \quad (5)$$

where I represents the indicator function. In our application, Equation 5 represents the causal effect of airstrikes for pixels with a given level of mechanization or with a US base presence, averaged over all such pixels. In Equation (5), we use the moderator value measured at time $t-L+1$, which is immediately before the application of stochastic interventions. This ensures that the moderator is unaffected by the treatment, avoiding post-treatment bias.

An important limitation of the CATE defined in Equation (5) is that the moderator may take many values, resulting in a small number of observations for each unique value of $\mathbf{R}_{i,t-L+1}$. This results in an imprecise estimate of the CATE function. To address this problem, we summarize the relationship between the treatment effects and the moderator values by projecting the former onto the latter. One simple example of such projection is linear regression where we regress $\tau_t(F', F'', L; \mathbf{R}_{i,t-L+1})$ on $\mathbf{R}_{i,t-L+1}$. In

this way, we obtain the coefficient on the moderator in each time period and then average these coefficients across periods to characterize how the treatment effect varies with the moderator. We can also use a nonparametric method such as local linear regression.

Formally, we define the time-specific projection estimand $\tilde{\tau}_t(F', F'', L; \mathbf{R}_{t-L+1}, \boldsymbol{\beta}_t^*)$, where

$$\boldsymbol{\beta}_t^* = \arg \min_{\boldsymbol{\beta}_t} \sum_{i=1}^p (\tau_t(F', F'', L; \mathbf{R}_{i,t-L+1}) - \tilde{\tau}_t(F', F'', L; \mathbf{R}_{i,t-L+1}, \boldsymbol{\beta}_t))^2 \quad (6)$$

with the following projection model that minimizes the mean square error,

$$\tilde{\tau}_t(F', F'', L; \mathbf{r}, \boldsymbol{\beta}_t) = \sum_{k=1}^K \beta_{tk} z_k(\mathbf{r}) = \mathbf{z}(\mathbf{r})^\top \boldsymbol{\beta}_t$$

with known functions $\mathbf{z}(\mathbf{r}) = [z_1(\mathbf{r}), \dots, z_K(\mathbf{r})]^\top$. Therefore, the above projection model represents the best approximation of the CATE using the moderator. Finally, the overall CATE is defined as the average of time-specific CATEs over time periods $L, L+1, \dots, T$,

$$\tilde{\tau}(F', F'', L; \mathbf{r}, \boldsymbol{\beta}_L^*, \dots, \boldsymbol{\beta}_T^*) = \frac{1}{T-L+1} \sum_{t=L}^T \tilde{\tau}_t(F', F'', L; \mathbf{R}_{i,t-L+1} = \mathbf{r}, \boldsymbol{\beta}_t^*).$$

3.5 Causal mediation analysis

Researchers often explore causal mechanisms and examine how the treatment affects an outcome through certain mediators (Imai et al., 2011). Below, we develop a methodology for causal mediation analysis with spatiotemporal data. Like the treatment variable, our mediator variable follows a stochastic intervention based on point patterns.⁷ We first modify notation to incorporate a mediator. Let $M_t(s) \in \mathcal{M}$ represent the mediating variable at location $s \in \Omega$ where \mathcal{M} is its support. In our application, $M_t(s)$ is a categorical variable since it represents the different types of airstrike locations (e.g., residential, farm land). For the sake of simplicity, we consider a binary mediator $M_t(s) \in \mathcal{M} = \{0, 1\}$ that indicates the presence of civilian harm; later we will consider a more nuanced, categorical mediator.

As with the treatment variable, we use M_t to represent the collection of mediator values at all locations, $M_t = \{M_t(s), s \in \Omega\}$ with its realization denoted by m_t . In addition, the collection of *mediator active locations* is denoted by $S_{M_t} = \{s \in \Omega : M_t(s) \neq 0\}$, while the mediator history is represented by $\overline{\mathbf{M}}_t = (M_1, M_2, \dots, M_t)$ with its realization $\overline{\mathbf{m}}_t$. Hence, airstrike locations with civilian harm are both *treatment active* and *mediator active* locations. In contrast, locations with airstrikes that did not kill civilians are *treatment active* but not *mediator active* locations.

We next define the potential and observed values of the mediators. In its full generality, let $M_t(\overline{\mathbf{w}}_t, \overline{\mathbf{m}}_{t-1})$

⁷See SI Section B for a schematic overview of the notation.

denote the value of the mediator we would observe at time period t , had previous treatment and mediator histories been equal to \bar{w}_t and \bar{m}_{t-1} , respectively.⁸ In addition, let $M_t(\bar{w}_t, \bar{m}_{t-1}; s)$ be its value at location $s \in \Omega$. This definition allows for the mediator to be affected by all past treatments and mediator values at any location, highlighting the fact that our methodology allow for arbitrary spillover and carryover effects. Lastly, we assume that the observed mediator equals its potential value for the observed path, i.e., $M_t = M_t(\bar{W}_t, \bar{M}_{t-1})$.

Although our methodology can handle more general cases, here we focus on the setting, in which all mediator active locations are also treatment active locations, i.e., $\{s \in \Omega : M_t(\bar{w}_t, \bar{m}_{t-1}; s) \neq 0\} \subset \{s \in \Omega : w_t(s) \neq 0\}$ for all \bar{w}_t and \bar{m}_{t-1} . In our application, this restriction holds because airstrike-caused civilian harm are our mediator, and civilian harm can occur only at airstrike locations.

We can now define the potential and observed values of outcomes and confounders. For a given treatment and mediator history, $(\bar{w}_t, \bar{m}_t) = (w_1, m_1, \dots, w_t, m_t)$, we denote the corresponding potential outcome by $Y_t(\bar{w}_t, \bar{m}_t)$ and the observed outcome by $Y_t = Y_t(\bar{W}_t, \bar{M}_t)$, respectively. We use $\mathcal{Y}_{\mathcal{T}} = \{Y_t(\bar{w}_t, \bar{m}_t), \text{ for all } t, \bar{w}_t, \text{ and } \bar{m}_t\}$ to denote the collection of all potential outcomes under any treatment and mediator path and for any time point.

Additionally, we let $X_t(\bar{w}_{t-1}, \bar{m}_{t-1})$ denote the potential value of the confounders at time period t that would result for a given treatment and mediator history. Then, the observed confounders are represented by $X_t = X_t(\bar{W}_{t-1}, \bar{M}_{t-1})$, while the history of observed confounders is denoted by $\bar{X}_t = (X_1, X_2, \dots, X_t)$. We use $\mathcal{X}_{\mathcal{T}}$ to denote the collection of all potential confounder values for all time points, similarly to $\mathcal{Y}_{\mathcal{T}}$. We use $\bar{H}_t = \{\bar{W}_t, \bar{M}_t, \bar{Y}_t, \bar{X}_{t+1}\}$ to denote the observed random variables that have occurred up until the treatment assignment at time period $t + 1$.

Given this new setup with a mediator, we now define our causal estimands. To do so, we specify the conditional distribution of the mediator given the treatment as another stochastic intervention in addition to a stochastic intervention of the treatment variable. Formally, let F_W denote an intervention distribution that generates the treatment variable W_t independently in each of L subsequent time periods. We also specify the conditional distribution of mediator given the treatment, $F_{M|w}$, which would be applied over the same L time periods. We now refer to the pair $F = (F_W, F_{M|w})$ as the stochastic intervention over (W, M) , and use $F(w, m)$ to denote the joint distribution $F_W(w)F_{M|w}(m)$.

We can then redefine the expected number of outcome events given in Equation (1) by incorporating mediators as follows:

$$\begin{aligned} N_{Bt}^{\text{med}}(F, L) = & \int_{(\mathcal{W}, \mathcal{M})} \cdots \int_{(\mathcal{W}, \mathcal{M})} N_B \left(Y_t(\bar{W}_{t-L}, \bar{M}_{t-L}, w_{t-L+1}, m_{t-L+1}, \dots, w_t, m_t) \right) \\ & dF(w_{t-L+1}, m_{t-L+1}) \cdots dF(w_t, m_t). \end{aligned} \quad (7)$$

⁸Since the mediator value is realized after the treatment at time t , M_t is a function of \bar{w}_t rather than \bar{w}_{t-1} .

Similarly to Equation (1), the distributions of both the treatment and mediator are fixed until time $t - L$ to their observed values, i.e., $\overline{\mathbf{W}}_{t-L}$ and $\overline{\mathbf{M}}_{t-L}$. For the remaining time periods from $t - L + 1$ to t , we employ stochastic intervention $F(w, m)$ for the treatment and mediator variables.

Just like $\mathbf{N}_{Bt}(F, L)$ in Equation (1), the estimand $\mathbf{N}_{Bt}^{\text{med}}(F, L)$ needs to be averaged over time:

$$\mathbf{N}_B^{\text{med}}(F, L) = \frac{1}{T - L + 1} \sum_{t=L}^T \mathbf{N}_{Bt}^{\text{med}}(F, L).$$

To compare the effects of stochastic interventions $F' = (F'_W, F'_{M|w})$ and $F'' = (F''_W, F''_{M|w})$, we consider the difference between the two stochastic interventions by,

$$\tau_B^{\text{med}}(F', F'', L) = \mathbf{N}_B^{\text{med}}(F', L) - \mathbf{N}_B^{\text{med}}(F'', L).$$

A key benefit of causal mediation analysis is its ability to decompose total effects into direct and indirect treatment effects (Imai et al., 2011). In the current setup, direct effects capture the effects of changing the treatment distribution while fixing the mediator distribution, whereas indirect effects represent the effects of changing the mediator distribution while holding the treatment distribution constant. Formally, we define the *direct effect* of altering the treatment intervention distribution from F'_W to F''_W while keeping the mediator distribution unchanged as $F'_{M|w}$ by,

$$\tau_B^{\text{DE,med}}(F'_W, F''_W; L, F'_{M|w}) = \tau_B^{\text{med}}\left((F'_W, F'_{M|w}), (F''_W, F'_{M|w}), L\right). \quad (8)$$

Similarly, the corresponding *indirect effect* is defined by fixing the treatment intervention as F''_W and changing the mediator distribution from $F'_{M|w}$ to $F''_{M|w}$:

$$\tau_B^{\text{IE,med}}(F'_{M|w}, F''_{M|w}; L, F''_W) = \tau_B^{\text{med}}\left((F''_W, F'_{M|w}), (F''_W, F''_{M|w}), L\right). \quad (9)$$

In our application, direct effects represent the effects of altering the distribution of airstrikes while holding the conditional distribution of civilian harm fixed. By extension, indirect effects represent the effects of changing civilian harm while fixing the airstrike distribution. In keeping with standard causal mediation analysis, these direct and indirect effects sum to the total effect. That is, there are two decompositions, depending on which intervention distribution is held constant. The difference here is that total

effects represent the effects of changing *both* the treatment and mediator stochastic interventions.⁹

$$\begin{aligned}\tau_B^{\text{med}}(F', F'', L) &= \tau_B^{\text{IE,med}}(F'_{M|w}, F''_{M|w}; L, F'_W) + \tau_B^{\text{DE,med}}(F'_W, F''_W; L, F''_{M|w}) \\ &= \tau_B^{\text{IE,med}}(F'_{M|w}, F''_{M|w}; L, F''_W) + \tau_B^{\text{DE,med}}(F'_W, F''_W; L, F'_{M|w}).\end{aligned}$$

Distinguishing between direct and indirect effects facilitates the investigation of both causal mechanisms and complex spillover effects. For example, some theories anticipate that insurgent attacks will increase in the wake of airstrikes that harm civilians. We can test this hypothesis by estimating the indirect effect $\tau_B^{\text{IE,med}}(F'_{M|w}, F''_{M|w}; L, F'_W)$ where we specify $F''_{M|w}$ such that it generates a greater amount of civilian harm than $F'_{M|w}$.

4 Estimation

In this section, we introduce estimators for the ATE, heterogeneous effects, and causal mediation effects. We first discuss the two core assumptions required for estimating ATE and heterogeneous treatment effects: (1) unconfoundedness and (2) overlap. We demonstrate that under these assumptions, which are common features of standard causal inference, the proposed estimators are consistent and asymptotically normal. Finally, we extend our causal assumptions to accommodate the presence of mediators, develop the estimators for direct, indirect, and total effects in causal mediation analysis, and derive their asymptotic properties.

4.1 Average treatment effects

We begin by introducing two causal assumptions. We first consider the unconfoundedness assumption, which ensures that the treatment assignment is random given the observed covariates (Papadogeorgou et al., 2022; Bojinov and Shephard, 2019). Formally, let f denote the density of intervention F . The unconfoundedness assumption in our context is stated as follows.

Assumption 1 (Unconfoundedness). *The treatment assignment at time t does not depend on any unobserved potential outcomes or potential values for the time-varying confounders given the observed history:*

$$f(W_t | \overline{\mathbf{W}}_{t-1}, \overline{\mathcal{Y}}_T, \overline{\mathcal{X}}_T) = f(W_t | \overline{H}_{t-1}).$$

Assumption 1 states that the realized assignment of the treatment point patterns at time period t is conditionally independent of *both past and future* potential outcomes and confounders, given the observed history. Therefore, Assumption 1 is more restrictive than the standard sequential ignorability

⁹Our mediation framework aligns with the literature on interventional mediation effects (e.g., Didelez, Dawid and Geneletti, 2006; Lok, 2016; Vansteelandt and Daniel, 2017), which considers stochastic interventions on the mediator. As shown by Didelez, Dawid and Geneletti (2006) and Geneletti (2007), generalized intervention effects permit any plausible mediator distribution. Our empirical application corresponds to a special case where the overall effect (Vanderweele, Vansteelandt and Robins, 2014) equals the total effect, as no intermediate confounder exists between treatment (airstrikes) and mediator (civilian harm).

assumption (Robins, Hernan and Brumback, 2000), which requires the conditional independence with respect to future potential outcomes alone.

We next consider the overlap assumption. We need the overlap assumption because the hypothetical treatment patterns under the stochastic intervention should be sufficiently likely to be observed with non-zero probabilities. Formally, let $e_t(w) = f(W_t = w \mid \bar{H}_{t-1})$ be the propensity score at time t , and the overlap assumption in our context is given as follows.

Assumption 2 (Bounded relative overlap). *The density ratio between the treatment point pattern of the realized data and that of the hypothetical intervention is bounded, i.e., there exists a positive constant δ such that*

$$\frac{f(w \mid \bar{H}_{t-1})}{e_t(w)} > \delta$$

for all $w \in \mathcal{W}$.

Under these assumptions, we now introduce the ATE estimator by extending the inverse probability of treatment weighting estimator to spatiotemporal point pattern data. Intuitively, our estimator represents a *weighted average of spatially-smoothed outcomes*. The weights represent the ratio of the intervention density over the propensity score evaluated at the observed treatment. In other words, the weights show how likely it is to observe the realized treatment events under the stochastic intervention relative to the propensity score. This approach avoids direct outcome modeling, thereby circumventing the need to accurately specify spillover or carryover effects.

Formally, we define the weight of time period t according to intervention F as

$$\zeta_t(F, L) = \prod_{t'=t-L+1}^t \frac{f(W_{t'})}{e_{t'}(W_{t'})}, \quad (10)$$

where the weight is the product of L ratios because the stochastic intervention is defined over L time periods. Each ratio in the product represents the relative likelihood of observing the realized treatment at each time period under the hypothetical intervention over the propensity score. Therefore, the numerator $f(W_{t'})$ varies with the specified stochastic intervention, whereas the denominator $e_{t'}(W_{t'})$ is estimated from the observed data and thus remains the same.

Second, we define a spatially-smoothed version of the outcome response. Smoothing is often necessary because spatiotemporal data tend to be sparse. We use kernel smoothing on the observed point pattern and obtain the smoothed outcome surface at time point t ,

$$\tilde{Y}_t(\omega) = \sum_{s \in S_{Y_t}} K_b(\|\omega - s\|), \quad \omega \in \Omega, \quad (11)$$

where $K_b(u) = b^{-1}K(u/b)$ is a kernel with bandwidth parameter b and $\|\cdot\|$ is the Euclidean norm (i.e.,

spatial distance). Intuitively, the value of the smoothed outcome surface at a point ω is the weighted sum of densities evaluated at all outcome active locations with the weights inversely proportional to their distance from ω . The bandwidth b controls the degree of smoothing with a greater value indicating a more smooth surface.¹⁰

We now combine the weights $\zeta_t(F, L)$ and the smoothed outcome surface $\tilde{Y}_t(\omega)$ to define the weighted smoothed outcome surface $\hat{Y}_t : \Omega \rightarrow \mathbb{R}^+$ as

$$\hat{Y}_t(F, L; \omega) = \zeta_t(F, L) \tilde{Y}_t(\omega). \quad (12)$$

The integral of this weighted smoothed outcome surface over a region of interest B estimates the expected number of points within that region under the stochastic intervention. Specifically, we define the estimator of $N_{Bt}(F, L)$ (see Equation (1)) and its temporal average $N_B(F, L)$ (see Equation (2)) as,

$$\widehat{N}_{Bt}(F, L) = \int_B \hat{Y}_t(F, L; \omega) d\omega, \quad (13)$$

$$\widehat{N}_B(F, L) = \frac{1}{T - L + 1} \sum_{t=L}^T \widehat{N}_{Bt}(F, L). \quad (14)$$

Then, the estimator of the ATE $\tau_B(F', F'', L)$ (see Equation (3)) is defined as

$$\hat{\tau}(F', F'', L) = \widehat{N}_B(F', L) - \widehat{N}_B(F'', L). \quad (15)$$

Papadogeorgou et al. (2022) shows that these estimators are consistent and asymptotically normal.

As we have shown in Equation (10), our estimators are inverse probability weighting (IPW) estimators because we divide the stochastic intervention density $f(W_{t'})$ by the propensity score $e_{t'}(W_{t'})$. These IPW estimators become unstable if the propensity scores are too small. To address this issue, we also employ the Hájek estimator, which stabilizes the weights $\zeta_t(F, L)$ through normalization (so that the sum of weights is one). To employ the Hájek estimator, we can replace Equation (14) with,

$$\widehat{N}_B(F, L) = \sum_{t=L}^T \widehat{N}_{Bt}(F, L) / \sum_{t=L}^T \zeta_t(F, L).$$

Zhou et al. (2024) shows that this Hájek estimator is consistent and asymptotically normal.

Our framework builds on the time-series causal inference approach (Bojinov and Shephard, 2019) and exploits temporal variation in a time series of maps to construct estimators that are robust to arbitrary

¹⁰We can think of K_b as a scaled version of a kernel $K : [0, \infty) \rightarrow [0, \infty)$ with $\int K(u) du = 1$, where K is a smooth function used to estimate the spatial spread patterns of insurgent attacks. Therefore, $K_b(u)$ adjusts the spread of outcomes based on the bandwidth b .

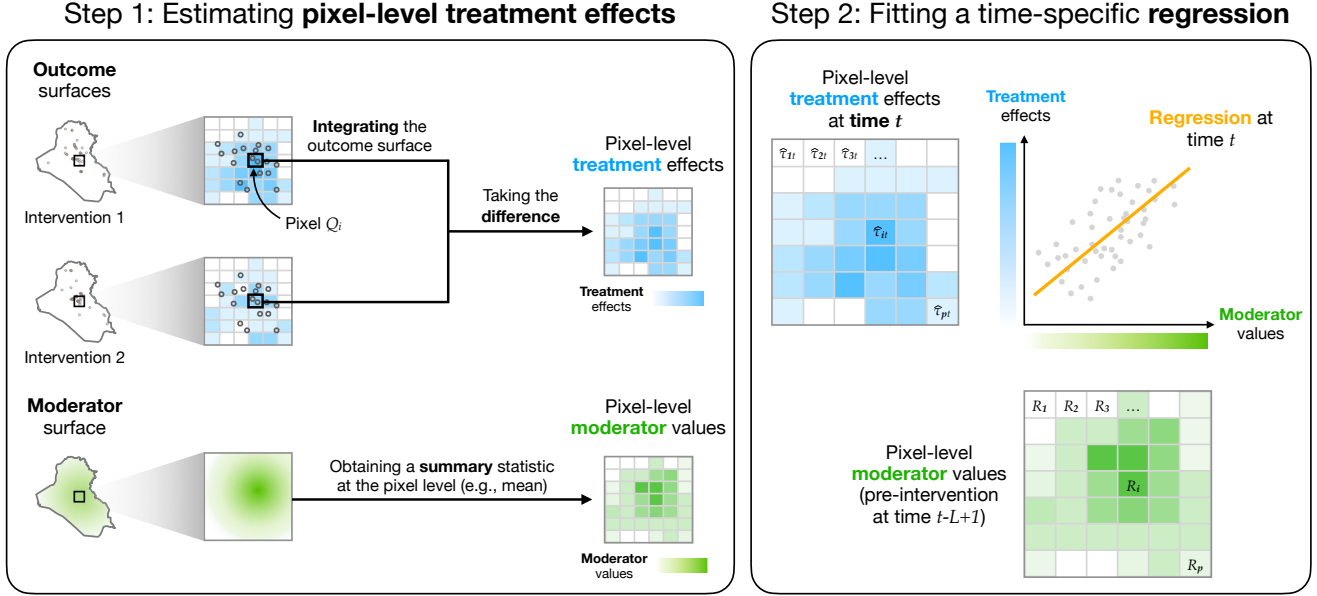


Figure 4: **Schematic representation of heterogeneous treatment effect estimation procedures.** To estimate heterogeneous treatment effects, we first estimate pixel-level treatment effects (left). We then regress pixel-level treatment effects on pixel-level moderator values to summarize the relationship between moderator values and treatment effects (right).

spillover and carryover effects. Although this strategy may result in some efficiency loss by not exploiting spatial variation, the resulting robustness to spillover and carryover effects has broader theoretical and practical importance.

4.2 Heterogeneous treatment effects

The intuition behind the estimation strategy for heterogeneous treatment effects is illustrated in Figure 4. The estimation strategy consists of two steps. In the first step, we estimate the causal effects in each pixel (Figure 4, left, shown as blue pixel-level grid cells). This procedure follows the estimation of the ATE with the set B equal to each pixel. We then consider the value of the moderator in each pixel (Figure 4, left, shown as green pixel-level grid cells). Spatially continuous moderators (e.g., population density, terrain features) need to be summarized at the pixel level to ensure that each pixel has a single moderator value. For discrete moderators that already have one value per pixel, this step can be omitted.

In the second step, we fit a time-specific regression for each time period (Figure 4, right). Specifically, for each time period t , we regress pixel-level treatment effects on pixel-level moderator values from the pre-intervention period (time $t - L + 1$). By performing this image-to-image regression, we project treatment effects onto moderator values. This projection step is crucial because, given the wide range of possible moderator values, simply averaging pixel-level treatment effects by moderator values could lead to imprecise estimates. Finally, we take the average of the time-specific coefficients across time to obtain the relationship between moderators and treatment effects.

To estimate heterogeneous treatment effects, we continue to rely on Assumptions 1 and 2. Formally, we apply Equations (13) and (15) to pixel Q_i and obtain a pixel-level causal effect estimate as follows,

$$\widehat{\mathbf{N}}_{it}(F, L) = \int_{Q_i} \widehat{Y}_t(F, L; \omega) d\omega, \quad \text{and} \quad \widehat{\tau}_{it}(F', F'', L) = \widehat{\mathbf{N}}_{it}(F', L) - \widehat{\mathbf{N}}_{it}(F'', L).$$

Next we obtain the coefficient estimates in Equation (6) by fitting a time-specific least squares regression,

$$\widehat{\boldsymbol{\beta}}_t = \arg \min_{\boldsymbol{\beta}_t} (\widehat{\boldsymbol{\tau}}_t - \mathbf{Z}_t \boldsymbol{\beta}_t)^\top (\widehat{\boldsymbol{\tau}}_t - \mathbf{Z}_t \boldsymbol{\beta}_t)$$

where $\widehat{\boldsymbol{\tau}}_t = (\widehat{\tau}_{1t}(F', F'', L), \dots, \widehat{\tau}_{pt}(F', F'', L))^\top$ is the vector of causal effect estimators for all pixels at time t , and $\mathbf{Z}_t = [\mathbf{z}(\mathbf{R}_{1,t-L+1}), \dots, \mathbf{z}(\mathbf{R}_{p,t-L+1})]^\top$ is the matrix of p moderators across all pixels. The functional form \mathbf{z} is determined by researchers or can be made flexible, using spline basis functions.

Finally, using the estimated coefficients, we can obtain the projection CATE estimator as follows:

$$\widehat{\tau}_{F', F''}^{\text{Proj.}}(\mathbf{r}; \boldsymbol{\beta}_L^*, \dots, \boldsymbol{\beta}_T^*) = \mathbf{z}(\mathbf{r})^\top \left(\frac{1}{T - L + 1} \sum_{t=L}^T \widehat{\boldsymbol{\beta}}_t \right). \quad (16)$$

While the estimator in Equation (16) is based on IPW, Hájek estimators can also be obtained by normalizing the weights. Zhou et al. (2024) show that this estimator is consistent and asymptotically normal.

4.3 Causal mediation analysis

We now turn to causal mediation analysis, which is a core methodological contribution of this paper. We first extend Assumptions 1 and 2 by incorporating mediators. Formally, let $F = (F_W, F_{M|w})$ be an intervention on the treatment and mediator, where f_W and $f_{M|w}$ denote the densities of F_W and $F_{M|w}$, respectively. In addition to the unconfoundedness for the treatment assignment, we also require that the realized mediator point patterns are conditionally independent of *both past and future* potential outcomes and confounders, given the observed history.

Assumption 3 (Unconfoundedness with mediators). *The treatment assignment at time t does not depend on any unobserved potential outcomes or potential values for the time-varying confounders given the observed history:*

$$f(W_t | \overline{\mathbf{W}}_{t-1}, \overline{\mathbf{M}}_{t-1}, \overline{\mathcal{Y}}_T, \overline{\mathcal{X}}_T) = f(W_t | \overline{\mathbf{H}}_{t-1}).$$

In addition, the mediator assignment at time t does not depend on any unobserved potential values given the history including the treatment assignment:

$$f(M_t | \overline{\mathbf{W}}_t, \overline{\mathbf{M}}_{t-1}, \overline{\mathcal{Y}}_T, \overline{\mathcal{X}}_T) = f(M_t | W_t, \overline{\mathbf{H}}_{t-1}).$$

We refer to $\rho_t(m) = f(m | \overline{\mathbf{H}}_{t-1}, W_t)$ as the mediator score.

We should note that Assumption 3 rules out the presence of (observed or unobserved) post-treatment

confounders that can be affected by the contemporaneous treatment W_t and confound the mediator-outcome relationship (Imai et al., 2011; Acharya, Blackwell and Sen, 2016). In our application, this assumption is reasonable since civilian harm occurs almost instantaneously after an airstrike. The assumption may not be credible in other settings, in which much longer time passes after the treatment assignment and before the realization of mediator. Finally, as before, we make the overlap assumption.

Assumption 4 (Bounded relative overlap with mediators). *The density ratio between the treatment and mediator point patterns of the realized data and those of the hypothetical intervention is bounded, i.e., there exist positive constants δ_W, δ_M such that*

$$\frac{f(w | \bar{H}_{t-1})}{e_t(w)} > \delta_W \quad \text{and} \quad \frac{f(m | \bar{H}_{t-1}, W_t = w)}{\rho_t(m)} > \delta_M.$$

for all $w \in \mathcal{W}$ and $m \in \mathcal{M}$.

With the restated assumptions, we now extend general causal estimators to account for the presence of mediators. We can achieve this by incorporating the density ratio of mediators into the weights. For intervention $F = (F_W, F_{M|w})$ with corresponding densities $f_W, f_{M|w}$, define the weight of time period t according to intervention F ,

$$\xi_t(F, L) = \prod_{t'=t-L+1}^t \frac{f_W(W_{t'})f_{M|W_{t'}}(M_{t'})}{e_{t'}(W_{t'})\rho_{t'}(M_{t'})}.$$

Then we can define analogs of Equations (12), (13), and (14) by replacing $\zeta_t(F, L)$ by $\xi_t(F, L)$ as follows:

$$\begin{aligned} \hat{Y}_t^{\text{med}}(F, L; \omega) &= \xi_t(F, L)\tilde{Y}_t(\omega), & \hat{\mathbf{N}}_{Bt}^{\text{med}}(F, L) &= \int_B \hat{Y}_t^{\text{med}}(F, L; \omega)d\omega, \\ \hat{\mathbf{N}}_B^{\text{med}}(F, L) &= \frac{1}{T-L+1} \sum_{t=L}^T \hat{\mathbf{N}}_{Bt}^{\text{med}}(F, L). \end{aligned}$$

Finally, the estimators of the total, direct, and indirect effects of a fixed region B are defined as

$$\begin{aligned} \hat{\tau}_B^{\text{med}}(F', F'', L) &= \hat{\mathbf{N}}_B^{\text{med}}(F', L) - \hat{\mathbf{N}}_B^{\text{med}}(F'', L), \\ \hat{\tau}_B^{\text{DE,med}}(F'_W, F''_W; L, F_{M|w}) &= \hat{\tau}_B^{\text{med}}((F'_W, F_{M|w}), (F''_W, F_{M|w}), L), \\ \hat{\tau}_B^{\text{IE,med}}(F'_{M|w}, F''_{M|w}; L, F_W) &= \hat{\tau}_B^{\text{med}}((F_W, F'_{M|w}), (F_W, F''_{M|w}), L). \end{aligned}$$

While these estimators are based on IPW, we employ Hájek estimators by normalizing weights, which we find to be much more stable in practice. In SI Sections C and D, we show that the estimators are consistent and asymptotically normal.

5 Empirical Analysis of Airstrikes and Insurgent Violence in Iraq

To illustrate the versatility of our approach, we apply it to several intertwined debates in the study of political violence and, in particular, counterinsurgency. We first explore the ATE of airstrikes on insurgent violence. We then test heterogeneous effects by examining whether the traits of deployed soldiers — including their level of mechanization, density per capita, and base locations — moderate airstrike effects. We also explore the oft-cited role of civilian harm as a causal mechanism linking airstrike effects to subsequent insurgent attacks.

To preview our main results, we find substantial evidence that US airstrikes increased short-term insurgent violence. Much of this evidence is consistent with a resolve-based theory of insurgent violence. Post-airstrike insurgent retaliation, including the use of both improvised explosive devices (IEDs) and small arms, is typically concentrated near (and on) paved roads, suggesting an emphasis on targeting American forces. Similarly, we find that airstrikes have the most pronounced effect on insurgent attacks where highly mechanized forces are present and near US bases.

Moreover, we find that these effects take some time to unfold, with statistically significant increases in attacks usually observed about a week after intensified aerial bombardment. This timing suggests that insurgents use their violence to signal resolve to local audiences and counterinsurgent foes quickly, before reputational damage for inaction sets in. Finally, contrary to existing studies, we find little evidence that civilian harm mediates the causal effects of airstrikes. Taken together, these results suggest that insurgent violence in Iraq was driven at least partly by a desire to demonstrate resolve rather than seek revenge.

5.1 Average Treatment Effects

We assess the ATE of airstrikes in two ways. First, we design a counterfactual intervention where we increase the average daily number of airstrikes from one to six while holding their spatial distribution constant and evaluate how these changes affect the amount and location of subsequent insurgent attacks (*intensification*). The choice of shifting from one to up to six daily airstrikes reflects the actual frequency from our in-sample data. This intervention also permits us to capture the spatiotemporal distribution of these intensified airstrikes. We begin by focusing on Iraq-wide effects but also concentrate on major road networks and adjacent areas to detect changes in the frequency of insurgent retaliation as well as the nature of their intended targets.

Second, we test whether the *targeting* of airstrikes leads to increased insurgent violence. We design a separate counterfactual intervention where we concentrate airstrikes on urban centers (e.g., small cities) without US bases while holding the number of airstrikes fixed. This counterfactual helps isolate whether insurgents are quickly but deliberately seeking out and targeting US bases (as expected by a resolve explanation) or are confining their attacks to the bombed areas, a pattern more consistent with theories

that emphasize revenge motives by either aggrieved individuals or sympathetic rebels nearby.

In each scenario, we concentrate on the immediate aftermath of airstrikes. We use relatively brief time lags of one to fourteen days (that is, up to two weeks after the airstrike) to capture the initial dynamics of post-strike insurgent behavior.¹¹

Estimation procedures. Estimating ATE involves two key steps: (1) estimating propensity scores and then (2) estimating causal effects. Estimation of propensity scores requires modeling the spatiotemporal distribution of airstrikes across Iraq. Once these scores are estimated, we can design counterfactual stochastic interventions and then estimate causal effects.

We estimate propensity scores by modeling the locations of airstrikes as an inhomogeneous Poisson process. Airstrike locations are influenced by their demographic and political characteristics, aid flows, distance from bases and roads, and prior histories of both airstrikes and insurgent attacks. We therefore adjust for district-level populations and aid levels; distance from major roads, cities, other populated settlements, and rivers; and 1-day, 7-day, and 30-day histories of airstrikes, non-lethal shows of force, and insurgent violence. Given that prior airstrikes and insurgent violence likely influences the density and location of future airstrikes, we transform the historical point pattern data into distance maps using an exponential decay function (see SI Section E.1 for details). We also include time splines and an indicator for the “surge” of American troops to Baghdad and its environs (25 March 2007-1 January 2008).

By controlling for these confounders and prior histories, we incorporate covariates that shape treatment assignment. To validate our approach, we examine its out-of-sample predictive performance and find that our model captures airstrike time trends well (see SI Figure S4).

Our intensification counterfactual intervention uses normalized airstrike density from 2006 (hereafter, “baseline density”) by multiplying it by the target daily airstrike count. Since the baseline density is normalized to integrate to one, this multiplication yields the desired counterfactual scenarios. As Figure 5a illustrates, this approach increases airstrike density while preserving its spatial distribution. In our application, we consider cases in which airstrike intensity ranges from one to six airstrikes per day, which reflects the observed daily distribution of airstrike counts. Combined with the use of the out-of-sample spatial distribution of airstrikes, our estimation procedure strengthens the validity of Assumption 2.

For our targeting hypothesis, we use fine-grained location data for US bases to design a counterfactual intervention that allows us to shift their location. We create a “power density” that is formally defined as $d_\alpha(\omega) = \prod_{i=1}^k d_i(\omega)^{\alpha_i} / \int_{\Omega} \prod_{i=1}^k d_i(\omega)^{\alpha_i}$, where $d_i(\omega)$ denotes distributions of spatial objects of interest (e.g., the bases) and α_i represents their precision parameters. In our application, we let $k = 1$ and use the distance from small and medium-sized cities without US bases to construct a power density across a range of their precision parameter values. We convert the distance metrics (in kilometers) using an exponential decay function with a coefficient of -20 . Small and medium-sized cities are defined by their

¹¹We leave the issue of causal inference with longer time periods to future work.

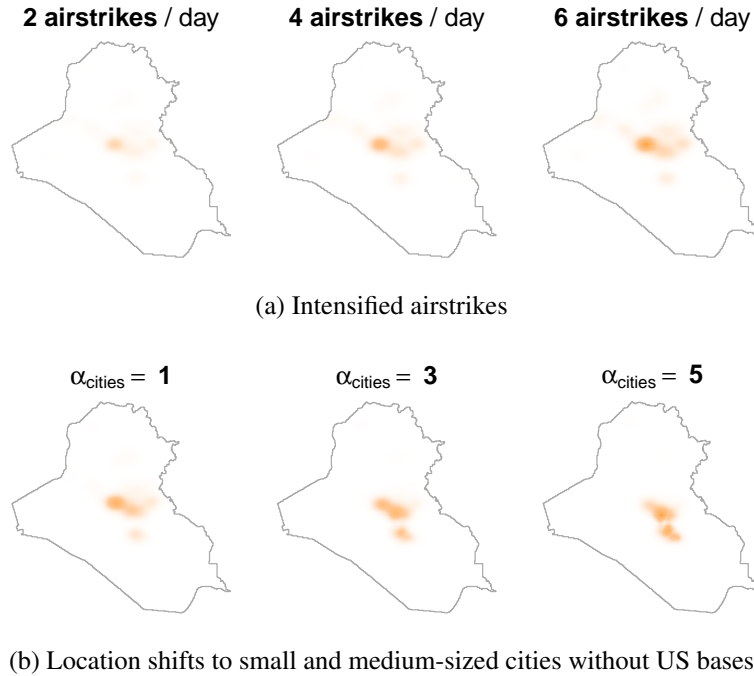


Figure 5: **Counterfactual interventions.** In Panels 5a and 5b, dark orange indicates areas with high airstrike densities. Panel 5a shows counterfactual interventions with intensified airstrikes of 2, 4, and 6 daily airstrikes. Panel 5b shows counterfactual interventions with location shifts. For the location-shift interventions, the average daily airstrikes is set to be five, while changing the prioritization of small and medium-sized cities without US bases (α_{cities}).

population sizes (50,000–200,000 and 200,000–500,000, respectively).

Intuitively, this approach considers several scenarios with different levels of precision applied to small and medium-sized cities without US bases. The counterfactual density is then defined as the product of the baseline density and the power density (Papadogeorgou et al., 2022; Mukaigawara et al., 2024), which is equivalent to reweighting the out-of-sample treatment pattern with the weights based on target locations. As Figure 5b illustrates, this intervention concentrates on small and medium-sized cities without US bases as the prioritization parameter increases (by raising the value of α_{cities}).

Results. We find that shifting the distribution of airstrikes from one to 2–6 per day for 7–14 days increases the number of insurgent small arms attacks (SAFs). Figure 6 summarizes the point estimates along with 95% confidence intervals. In substantive terms, increasing the number of airstrikes for 7–14 days results in an average expected number of SAFs ranging from 7.5 to 26 per day. These increases in small arms fire by insurgents is statistically significant during treatment windows from 9–14 days after anywhere between three and six airstrikes. Simply put, the greater the number of airstrikes, the greater the amount of insurgent small arms fire, with the largest increases associated with the upper range of daily airstrikes observed in our sample. We observe similar effects for improvised explosive devices (IED), where statistically significant increases in these attacks are noted with between three and six daily

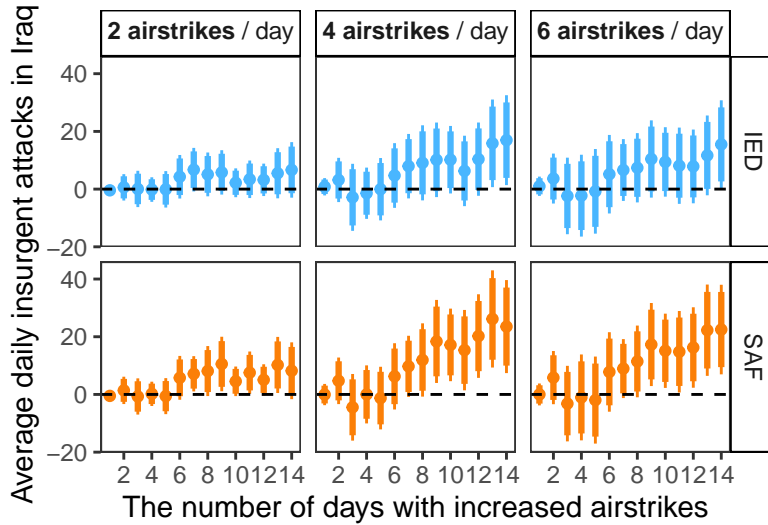


Figure 6: **Average treatment effects of intensifying airstrikes.** The figure summarizes the effects of increasing the number of daily airstrikes from 1 per day to 2, 4, and 6 per day without changing their spatial distributions. The x-axis represents the number of days with stochastic interventions. Thick and thin lines indicate 95% and 90% confidence intervals, respectively. We found similar effects when both IED and SAF cases are combined (See SI Figure S7).

airstrikes by the 14 day post-airstrike mark.

The apparent delay in retaliatory attacks observed in Figure 6 is consistent with the claim that insurgents carefully plan their attacks to maximize their chances of enhancing their resolve rather than lashing out at the nearest (and earliest available) target. The delay is a relatively brief one, however; insurgents do not postpone their retaliation for (many) weeks or even months later. The slightly longer delay associated with IEDs can be explained by the greater degree of planning and logistics that are required to emplace these devices. The existing research rarely documents this level of granular detail on insurgent planning and targeting cycles because the data are often bundled at temporal and spatial levels that are too aggregate to trace these action-reaction cycles.

Where do these insurgent attacks occur? The flexibility of our methodology in measuring causal effects across arbitrary areas offers insights. Consistent with a resolve-based explanation, post-strike insurgent attacks cluster along major roadways, precisely where mechanized American and UK patrols are most likely to be found. Figure 7 summarizes these results. The left panel displays the locations of major road networks (in gray) in Iraq along with the estimated causal effects, with dark orange color representing increased insurgent attacks. Areas near Baghdad and Mosul are magnified for visualization purposes. The overlap between orange shaded areas and gray lines implies that most small arms attacks occur in near road networks. To examine this further, we estimate the proportion of causal effects for SAF attacks near major highways. (Figure 7, top right). We find that approximately 70% of the causal effects occur within 10 kilometers of major roads.

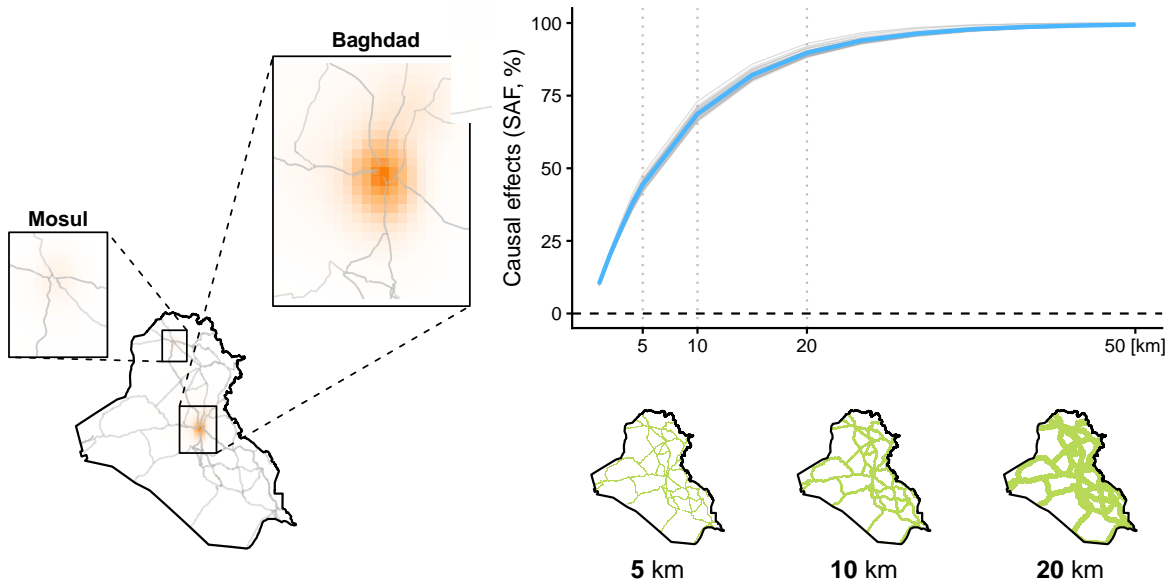


Figure 7: **Roadways and spatial causal effects.** The left panel shows the outcome surface (SAF, $L = 14$) comparing areas with 1 versus 6 airstrikes, with densities in orange and major road networks in gray. The top-right panel plots the share of overall causal effects by distance from major roads; each light gray line represents a different comparison of $L \geq 6$ to 2–6 airstrikes, and the blue line shows their average. The bottom-right panels highlight areas within 5, 10, and 20 kilometers of major road networks (in green).

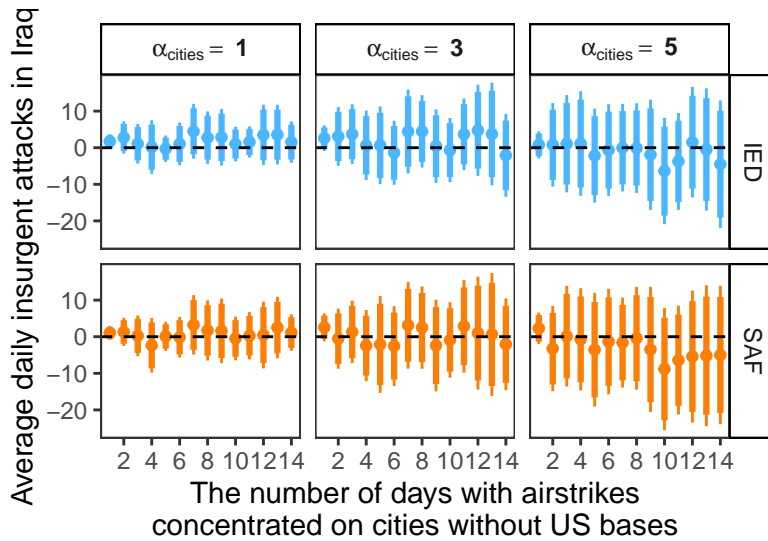


Figure 8: **Average treatment effects of targeting cities without US bases.** The figure summarizes the effects of focusing airstrikes on small and medium-sized cities without US bases, with different values of α_{cities} . The number of airstrikes is set to five per day. The x-axis represents the number of days with stochastic interventions. Thick and thin lines indicate 95% and 90% confidence intervals, respectively. We found similar effects when both IED and SAF cases are combined (See SI Figure S7).

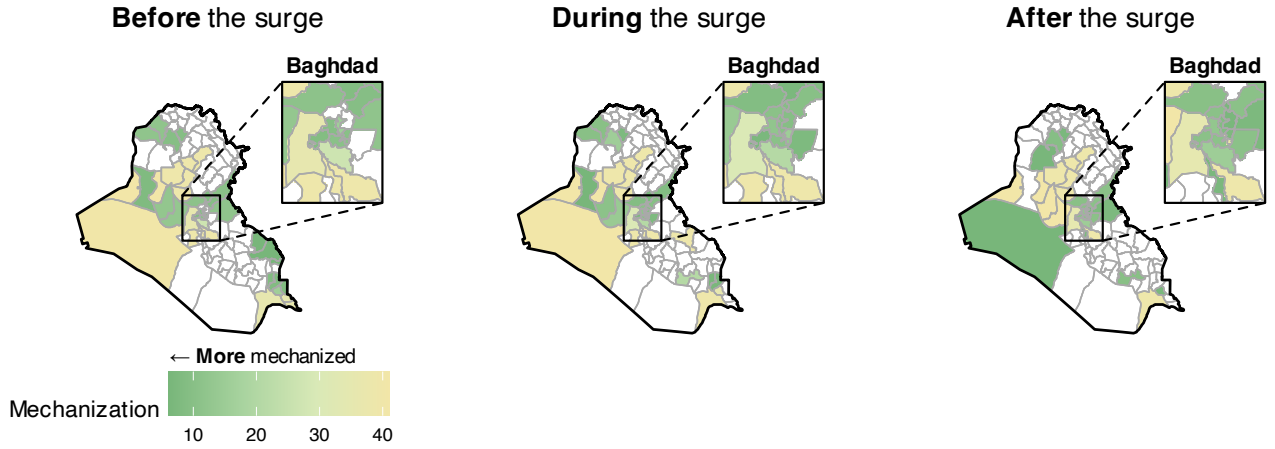


Figure 9: **District-level mechanization.** Before, during, and after the surge correspond to 23 February 2007, 1 September 2007, and 5 July 2008. Higher values indicate lower mechanization; NA areas (white) denote locations with no data. Mechanization exhibits marked temporal and spatial variation across Iraq. See SI Figure S8 for the full time series.

We find a similar spatial pattern when analyzing the effect of shifting airstrike locations to small- and medium-sized cities without US bases. As anticipated by our resolve-based explanation, shifting locations does not produce statistically significant effects in attacks (Figure 8). Contrary to the intensification scenarios above (Figure 6), increased targeting of small- and medium-sized cities without US bases (corresponding to higher values of α_{cities}) does not increase insurgent attacks. Point estimates remain weakly negative, with no substantive changes in response to higher values of α_{cities} even after 14 days of increased targeting. Taken together, intensification of airstrikes generates increased insurgent attacks, particularly near highways and in cities with military bases, and does so quite quickly, typically within 7–10 days of the initial airstrikes.

5.2 Heterogeneous Treatment Effects

Having identified a positive relationship between an increased distribution of daily airstrikes and increased insurgent violence, we now test heterogeneous treatment effects to help distinguish between grievance- and resolve-based explanations. Resolve-based explanations suggest that (1) post-strike insurgent retaliation should be highest in areas that are marked by high concentrations of soldiers and, in particular, visible and symbolic targets such as mechanized units; and (2) these post-strike responses should cluster around areas and locations marked by one or more US military bases. By contrast, according to grievance-based theories, retaliation should be concentrated spatially around the targeted location, with no clear pattern to its timing given the possibility that revenge (or tip-sharing) could unfold opportunistically over both the short- and long-term.

We draw on existing data to denote the weekly level of troop mechanization (the number of soldiers

in a unit per armored vehicle) and the presence of US bases (a binary indicator) in a given district. Each exhibits substantial temporal and spatial variation. For example, Figure 9 illustrates the substantial spatiotemporal variation in mechanization levels within the relative confines of the modest-sized Baghdad Governorate.

Estimation procedures. We continue to rely on the estimated propensity score and the counterfactual intervention used for estimating ATE. We examine whether mechanization levels and the presence of bases predict treatment effects when the frequency of airstrikes increases from one to 2–6 per day. For binary moderators, we consider the following linear regression model, $\tau_{t,F',F''}^{\text{Proj.}}(\mathbf{r}; \boldsymbol{\beta}_t^*) = \beta_{t,0} + \beta_{t,1}r$, and for continuous moderators, we employ, $\tau_{t,F',F''}^{\text{Proj.}}(\mathbf{r}; \boldsymbol{\beta}_t^*) = \sum_{l=0}^5 \beta_{t,l}z_l(r)$, where z_l is a natural cubic spline basis of troop mechanization and troop density.

Results. As Figure 10 shows, both mechanization levels and the presence of US bases predict the nature of insurgent violence. As Figure 10a reveals, we witness insurgent violence unfolding in a two-step pattern, with small arms fire being deployed first against units with lower mechanization levels (Figure 10a, bottom right) before improvised explosive devices are brought to bear against more heavily mechanized units (Figure 10a, top center and right). Consistent with our theoretical expectations, we observe a near-immediate response to airstrikes, with statistically significant increases observed 9-14 days and 13-14 days after intensified airstrikes for small arms fire and IEDs, respectively. The presence of US bases also predicts the frequency of these attacks. Areas with US bases observe far more small arms fire, for example, than areas without bases (Figure 10b).¹²

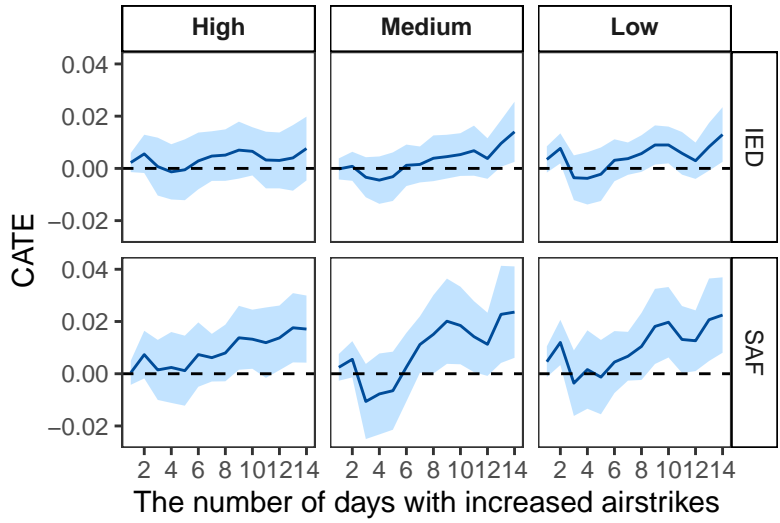
Our approach helps move us beyond simple ATE calculations (“do airstrikes work?”) to more nuanced questions about how airstrike effects hinge on the nature of the strategic environment. This causal heterogeneity is typically masked by too-aggregate data, especially for the intervention and outcomes, as well as the inability of existing approaches to capture spillover and carryover effects. Moreover, this approach could be extended even further if daily patrol data were made available or, alternatively, could be used to study how economic aid programs condition the causal effects of airstrikes.¹³ These results provide additional evidence that airstrikes create incentives for insurgents to demonstrate their continued resolve and military capabilities to local and counterinsurgent audiences by quickly seeking out and attacking US forces, including heavily mechanized forces, at or near their fortified bases.

5.3 Causal Mediation Analysis

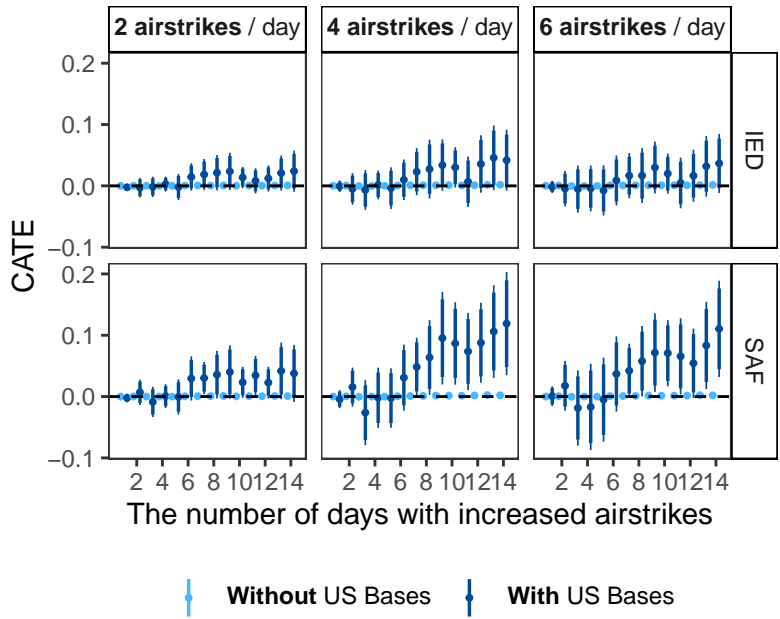
Building on these prior analyses, we now turn to the question of how civilian harm mediates the causal relationship between airstrikes and insurgent violence. We use the more expansive term “civilian harm” here to indicate our measure records target type and property damage, not just fatalities. We estimate

¹²Intriguingly, we find no evidence that the sectarian nature of the population (Sunni/Shia) moderates the causal effects of airstrikes. See SI Figure S9.

¹³For one such example, see Zhou et al. (2024).



(a) Mechanization



(b) US bases

Figure 10: **Heterogeneous treatment effects (mechanization and the presence of US bases)**. Heterogeneous treatment effects with respect to the degree of mechanization (Panel 10a) and the presence of the US bases (Panel 10b) are shown. For mechanization, lines indicate point estimates and shades display the 95% confidence intervals. High, medium, and low levels of mechanization correspond to 10, 25, and 35 soldiers per armored vehicle, given that the mechanization variable in our data ranges from 6 to 41. For the presence of US bases, dark and light colors indicate the average treatment effects in areas with and without bases, respectively. Thick and thin lines indicate 95% and 90% confidence intervals, respectively.

the *indirect* effects of civilian harm by modifying its intensity while keeping the number of airstrikes constant (see Equation (9)). Specifically, we examine whether increased civilian harm from airstrikes in Baghdad City mediates the causal effects across Iraq. We focus on Baghdad because it was the site of the highest number of civilian harm from airstrikes, had resulting property damage across its neighborhoods and semi-urban outskirts, and was the epicenter of the “surge” effort in 2007–08 (Petersen, 2024, pp. 246–259).

Estimation procedures. Our estimation procedures has four steps: (1) estimating propensity scores, (2) designing counterfactual stochastic interventions for airstrikes, (3) estimating mediator scores, and (4) designing counterfactual stochastic interventions for civilian harm given these airstrikes. Similar to propensity scores, mediator score estimation is equivalent to modeling the conditional distribution of civilian harm.

We use the propensity scores estimated for the ATE. To design a stochastic intervention of airstrikes, we concentrate them in Baghdad. This adjustment addresses the low frequency of airstrikes in Baghdad in the 2006 out-of-sample data used to generate the baseline density (0.02 average daily airstrikes), which limits meaningful analysis of the mediation effect of civilian harm. We set the expected number of airstrikes across Iraq to six per day but concentrate them around Baghdad. This procedure adjusts the daily expected number of airstrikes in the city itself to four, a level of airstrikes that was actually observed in Baghdad City in the 2007 in-sample data.

Our primary mediator is a categorical variable derived from satellite imagery that distinguishes among civilian, military, and unclassified locations. We therefore estimate mediator scores by adopting a two-stage approach. In the first stage, we model the conditional distribution of airstrikes hitting targets *either* civilians or military targets given airstrikes. In the second stage, conditional on the results of the first stage, we model the distribution of airstrikes hitting military targets. Since civilian harm is expected to be higher in densely populated areas, we consider population density along with distance from roads, cities, residential and other buildings, and settlements as covariates. We use an exponential decay function (see SI Section G.2 for details) to create distance maps of buildings from exact airstrike locations (in kilometers). To avoid a strong functional form assumption, we then employ a generalized additive model to estimate mediator scores. Model fit is evaluated using accuracy based on the area under the receiver operating characteristic curve (ROC). The area under the curve (AUC) for the first stage is 0.80, and the AUCs for the second stage are 0.78 (civilians) and 0.85 (military targets) (see Figure S10).

To design a counterfactual distribution of the mediator, we employ the incremental propensity score intervention approach proposed by Kennedy (2019). The incremental propensity score intervention allows us to avoid positivity assumptions and directly modify the conditional mediator probability with a single increment parameter $\delta \in (0, \infty)$ (Kennedy, 2019). Specifically, this approach replaces the media-

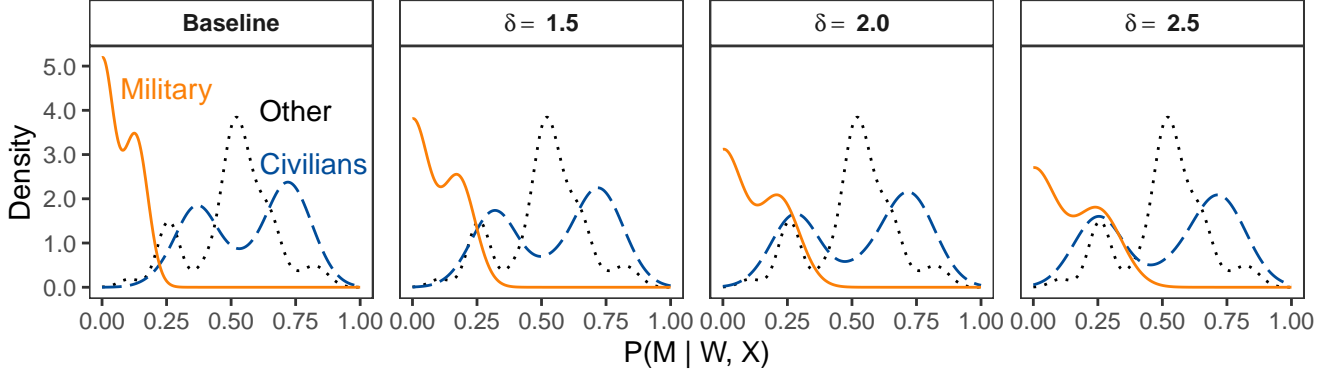


Figure 11: **Counterfactual conditional mediator densities.** The plot shows changes in the densities of conditional mediator probabilities in response to various values of δ . The conditional probabilities of hitting military targets, civilian locations, and other targets, given airstrike locations and covariates, are shown in red, blue, and black, respectively.

tor score $\Pr(M_t = m_t | W_t, \mathbf{X}_t)$ in the second stage with the following new counterfactual distribution:

$$\Pr_{\text{new}}(M_t = m_t | W_t, \mathbf{X}_t) = \frac{\delta \Pr(M_t = m_t | W_t, \mathbf{X}_t)}{\delta \Pr(M_t = m_t | W_t, \mathbf{X}_t) + 1 - \Pr(M_t = m_t | W_t, \mathbf{X}_t)}. \quad (17)$$

where $\Pr(M_t = m_t | W_t, \mathbf{X}_t)$ represents the probability of hitting civilians (or military targets) given covariates and airstrike locations. This counterfactual probability can be modified by changing the parameter $\delta > 0$, with a higher value of δ resulting in a greater updated probability $\Pr_{\text{new}}(M_t = m_t | W_t, \mathbf{X}_t)$. For example, if $\delta = 0$, then $\Pr_{\text{new}}(M_t = m_t | W_t, \mathbf{X}_t)$ equals 0. As δ tends to infinity, the updated probability tends to 1.

We construct counterfactual conditional distributions of civilian harm given airstrikes by setting $\delta \in \{1.5, 2, 2.5\}$. Figure 11 summarizes the changes in the densities of conditional probabilities in response to δ . The density of the conditional probability of hitting other targets (black) remains unchanged. As δ increases, the density for military targets (red) shifts right, while the density for civilians (blue) shifts left.

Results. We find little evidence that altering the probability of civilian harm in Baghdad City affects the number of insurgent attacks in Iraq at any point up to 10 days after the airstrike. As summarized in Figure 12, civilian harm has no statistically significant impact on insurgent attacks, regardless of the values of δ (see Equation (17)) and L in Baghdad (see panel (a)). Nor do we find evidence that civilian harm mediates airstrike effects on insurgent violence in other strategically salient areas (Figure S12). As a robustness check, we conducted a series of additional tests on these areas and found no evidence of indirect effects (SI Section G.4). Similarly, replacing our preferred satellite imagery measure with the more conventional binary indicator of civilian fatalities does not change our results (see SI Section G.5).

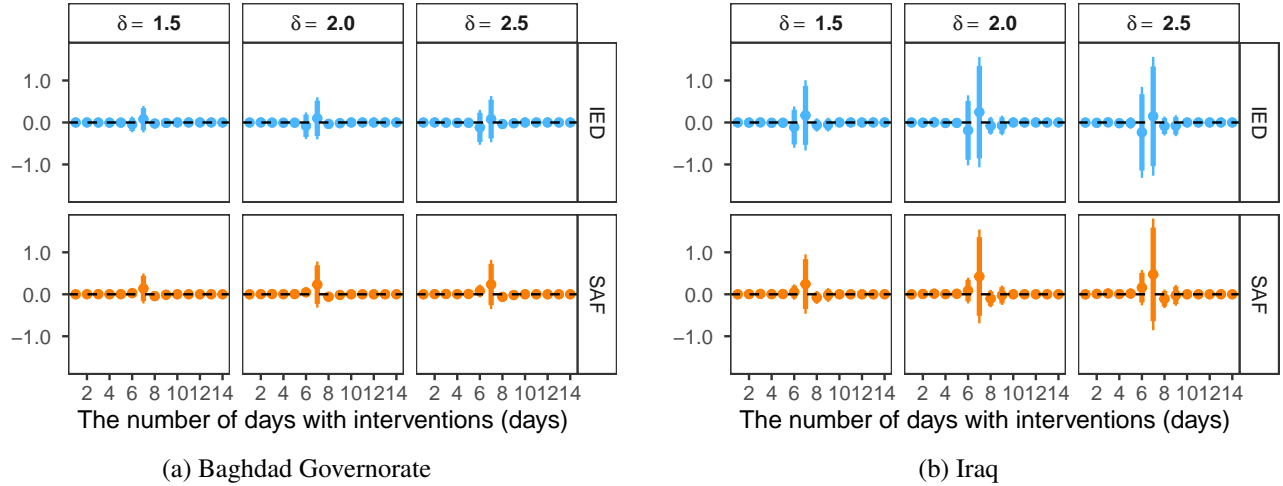


Figure 12: **Indirect effects of civilian harm on the number of insurgent attacks.** The dots represent point estimates while thick and thin bars represent the 90% and 95% confidence intervals, respectively. The x-axis represents the number of days with stochastic interventions.

In short, airstrikes that harm civilians do not appear to increase insurgent violence or have significant spillover effects even after we increase the airstrike distribution. While we cannot rule out the possibility that grievances fuel increased violence in the long-term, it appears that civilian harm does not elicit an immediate armed response from either aggrieved individuals or those claiming to act on their behalf.

6 Concluding Remarks

We offer a new spatiotemporal framework that allows investigators to conduct causal inference with microlevel data in the presence of spatial spillover and temporal carryover effects. Our flexible approach can estimate ATE, explore heterogeneous treatment effects, and conduct causal mediation analysis all within the same unified framework that preserves the granular nature of microlevel data. In doing so, we avoid the inferential pitfalls that arise from data overaggregation.

Our framework also helps uncover new insights about wartime dynamics, including the spatial and temporal dimensions of airstrike effects, that are typically neglected in studies of political violence. We find that airstrikes increased insurgent violence in Iraq, that rebels typically retaliated quickly, and that they targeted American units — even highly mechanized ones — and their bases to establish a reputation for resolve. Drawing on a new, more expansive, measure of civilian harm, we find little evidence that airstrikes led to short-term increases in attacks or displaced violence to new locations.

Together, our methodological approach and findings suggest new avenues for research on counterinsurgency and, more broadly, political violence. Perhaps most importantly, our microlevel theories of political violence leave their spatial and temporal implications implicit, if they are acknowledged at all. Where we should expect to observe effects, why they should appear in these locations (and not else-

where), and when we should expect them to appear are all questions typically ignored or otherwise obscured by too-aggregate research designs. Explicitly offering and testing spatial and temporal hypotheses, rather than simply estimating average treatment effects, would represent an important advance for existing theories.

Adopting our spatiotemporal framework would similarly expand our theoretical understanding of civil war dynamics, counterinsurgency, mass repression, and other settings where we suspect that microlevel interventions have broader effects. We note, too, the policy relevance of these investigations. To date, we have undercounted civilian harm in wartime because existing approaches ignore, or cannot account for, spillover and carryover effects. Understanding the extent of spillover, for example, not only helps improve accounting for the full extent of harm inflicted but also underscores the wider consequences of relying on airpower as a tool of counterinsurgency. Capturing these spillover effects also opens the possibility of designing post-harm aid interventions that better reflect the location(s) of harmed populations beyond a narrow focus on where the bombs fell.

While we chose a single case to highlight our method, our method could be applied to host of different empirical domains. Disease outbreaks, the downstream consequences of pollution, the effects of development aid and humanitarian assistance in fragile settings, and local policing initiatives are all marked by spillover and carryover effects that could be examined using our approach and statistical package. Our approach could also help investigate how the local effects of these interventions and programs “scale-up” spatially and temporally to produce general equilibrium effects. By directly engaging questions of spillover and interference, our framework offers a bridge between estimating local effects and understanding how these effects collectively produce more macrolevel outcomes. In short, our geospatial framework helps answers difficult empirical puzzles while opening new opportunities to advance our theories across a wide range of disciplines and domains.

References

- Acharya, Avidit, Matthew Blackwell and Maya Sen. 2016. "Explaining Causal Findings Without Bias: Detecting and Assessing Direct Effects." *American Political Science Review* 110(3):512–529.
- Aiken, Emily, Suzanne Bellue, Dean Karlan, Christopher Udry and Joshua Blumenstock. 2022. "Machine Learning and Phone Data can Improve Targeting of Humanitarian Aid." *Nature* 603(864-870).
- Alkhuzai, Amir H., Ihsan J. Ahmad, Mohammed J. Hweel, Thakir W. Ismail, Hanan H. Hasan, Abdul Rahman Younis, Osman Shawani, Vian M. Al-Jaf, Mahdi M. Al-Alak, Louay H. Rasheed, Suham M. Hamid, Naeema Al-Gasseer, Fazia A. Majeed, Naira A. Al Awqati, Mohamed M. Ali, J. Ties Boerma and Colin Mathers. 2008. "Violence-Related Mortality in Iraq from 2002 to 2006." *New England Journal of Medicine* 358(5):484–493.
- Allen, Susan, Sam Bell and Carla Machain. 2021. "Air Power, NGOs, and Collateral Killings." *Foreign Policy Analysis* 17(2):1–17.
- Baddeley, Adrian. 2015. *Spatial point patterns : methodology and applications with R*. Interdisciplinary statistics first edition. ed. Boca Raton, FL: Chapman and Hall/CRC, an imprint of Taylor and Francis.
- Balcells, Laia. 2017. *Rivalry and Revenge: The Politics of Violence during Civil War*. Cambridge: Cambridge University Press.
- Berman, Eli, Jacob Shapiro and Joseph Felter. 2011. "Can Hearts and Minds Be Bought? The Economics of Counterinsurgency in Iraq." *Journal of Political Economy* 119:766–819.
- Biddle, Stephen. 2006. "Allies, Airpower, and Modern Warfare: The Afghan Model in Afghanistan and Iraq." *International Security* 30(3):161–176.
- Biddle, Stephen, Jeffrey Friedman and Jacob Shapiro. 2012. "Testing the Surge: Why Did Violence Decline in Iraq in 2017?" *International Security* 37(1):7–40.
- Binetti, Marco. 2025. "Assessing the impact of non-military aid on tactical military effectiveness: The case of Iraq between 2004 and 2014." *International Interactions* .
- Bojinov, Iavor and Neil Shephard. 2019. "Time Series Experiments and Causal Estimands: Exact Randomization Tests and Trading." *Journal of the American Statistical Association* 114(528):1665–1682.
- Chenoweth, Erica, Jonathan Pinckney and Orion Lewis. 2018. "Days of Rage: Introducing the NAVCO 3.0 Dataset." *Journal of Peace Research* 55(4):524–534.

- Condra, Luke, Joseph Felter, Radha Iyengar and Jacob Shapiro. 2011. "The Effects of Civilian Casualties in Afghanistan and Iraq." *NBER Working Paper 16152*.
- Condra, Luke N. and Jacob N. Shapiro. 2012. "Who Takes the Blame? The Strategic Effects of Collateral Damage." *American Journal of Political Science* 56(1):167–187.
- Corum, James and Wray Johnson. 2003. *Airpower in Small Wars: Fighting Insurgents and Terrorists*. Lawrence, KS: University Press of Kansas.
- Crost, Benjamin, Joseph Felter and Patrick Johnston. 2014. "Aid Under Fire: Development Projects and Civil Conflict." *American Economic Review* 104(6):1833–1856.
- Csörgö, Miklós. 1968. "On the Strong Law of Large Numbers and the Central Limit Theorem for Martingales." *Transactions of the American Mathematical Society* 131(1):259–275.
- Dasgupta, Aditya, Kishore Gawande and Devesh Kapur. 2017. "(When) Do Antipoverty Programs Reduce Violence? India's Rural Employment Guarantee and Maoist Conflict." *International Organization* 71(3):605–632.
- Dell, Melissa and Pablo Querubin. 2018. "Nation Building Through Foreign Intervention: Evidence from Discontinuities in Military Strategies." *American Economic Review* 133(2):701–64.
- Didelez, Vanessa, Philip Dawid and Sara Geneletti. 2006. Direct and indirect effects of sequential treatments. In *Proceedings of the Twenty-Second Conference on Uncertainty in Artificial Intelligence (UAI 06)*. pp. 138–146.
- Empirical Studies of Conflict. 2012. "Iraq Ethnicity Dataset."
- Findley, Michael, Joseph Young, Daniel Strandow and Olgahan Cat. 2023. "Aiding War: Foreign Aid and the Intensity of Violent Armed Conflict." *International Studies Quarterly* 67(3):1–15.
- Foster, W.F. 1928. "Air Power and its Application." *RUSI* 73(490):247–261.
- Geneletti, Sara. 2007. "Identifying direct and indirect effects in a non-counterfactual framework." *Journal of the Royal Statistical Society, Series B* 69(2):199–215.
- Gordon, Michael. 2022. *Degrade and Destroy: The Inside Story of the War Against the Islamic State, From Barack Obama to Donald Trump*. New York: Farrar, Straus, and Giroux.
- Hamilton, Eric. 2008. Developments Fighting Al Qaeda in Iraq. In *Institute for the Study of War, Jan 2008*, 8 pp.

- Huang, Wei, Hongbing Xu, Jing Wu, Minghui Ren, Yang Ke and Jie Qiao. 2024. “Toward Cleaner Air and Better Health: Current State, Challenges, and Priorities.” *Science* 385:386–390.
- Hızlı, Çağlar, ST John, Anne Juuti, Tuure Saarinen, Kirsi Pietiläinen and Pekka Marttinen. 2023. “Temporal Causal Mediation through a Point Process: Direct and Indirect Effects of Healthcare Interventions.”
URL: <https://arxiv.org/abs/2306.09656>
- Imai, Kosuke, Luke Keele, Dustin Tingley and Teppei Yamamoto. 2011. “Unpacking the Black Box of Causality: Learning about Causal Mechanisms from Experimental and Observational Studies.” *American Political Science Review* 105(4):765–789.
- Johnston, Patrick and Anoop Sarbahi. 2016. “The Impact of US Drone Strikes on Terrorism in Pakistan.” *International Studies Quarterly* 60(2):203–219.
- Kalyvas, Stathis. 2006. *The Logic of Violence in Civil War*. Cambridge: Cambridge University Press.
- Kennedy, Edward H. 2019. “Nonparametric Causal Effects Based on Incremental Propensity Score Interventions.” *Journal of the American Statistical Association* 114(526):645–656.
- Keremoglu, Eda, Sebastian Hellmeier and Nils Weidmann. 2022. “Thin-Skinned Leaders: Regime Legitimation, Protest Issues, and Repression in Autocracies.” *Political Science Research and Methods* 10(1):136–152.
- Khan, Azmat and Anand Gopal. 2017. “The Uncounted.” *The New York Times* .
- Kocher, Matthew, Thomas Pepinsky and Stathis Kalyvas. 2011. “Aerial Bombing and Counterinsurgency in the Vietnam War.” *American Journal of Political Science* 55(2):201–218.
- Kotsadam, Andreas, Gudrun Østby, Siri Rustad, Andreas Tollefsen and Hendrik Urdal. 2018. “Development aid and infant mortality. Micro-level evidence from Nigeria.” *World Development* 105:59–69.
- Krick, Benjamin, Jonathan Petkun and Mara Revkin. 2025. “Civilian Harm and Military Legitimacy: Evidence from the Battle of Mosul.” *International Organization* 79(2):332–357.
- Lok, Judith J. 2016. “Defining and estimating causal direct and indirect effects when setting the mediator to specific values is not feasible.” *Statistics in Medicine* 35(22):4008–4020.
- Lyall, Jason. 2019. “Bombing to Lose? Airpower and the Dynamics of Coercion in Counterinsurgency Wars.” *Unpublished Manuscript* .

- Lyall, Jason and Isaiah Wilson. 2009. “Rage Against the Machines: Explaining Outcomes in Counterinsurgency War.” *International Organization* 63:67–106.
- Mukaigawara, Mitsuru, Lingxiao Zhou, Georgia Papadogeorgou, Jason Lyall and Kosuke Imai. 2024. “geocausal: An R Package for Spatio-Temporal Causal Inference.”
URL: <https://doi.org/10.31219/osf.io/5kc6f>
- Newton, Richard. 2019. *The RAF and Tribal Control: Airpower and Irregular Warfare Between the World Wars*. Lawrence, KS: University of Kansas Press.
- Papadogeorgou, Georgia, Kosuke Imai, Jason Lyall and Fan Li. 2022. “Causal inference with spatio-temporal data: Estimating the effects of airstrikes on insurgent violence in Iraq.” *Journal of the Royal Statistical Society. Series B, Statistical methodology* 84(5):1969–1999.
- Petersen, Roger. 2024. *Death, Dominance, and State-Building: The US in Iraq and the Future of American Military Intervention*. Oxford: Oxford University Press.
- Raleigh, Clionadh, Andrew Linke Håvard Hegre and Joakim Karlsen. 2010. “Introducing ACLED-Armed Conflict Location and Event Data.” *Journal of Peace Research* 47(5):651–660.
- Rigterink, Anouk. 2021. “The Wane of Command: Evidence on Drone Strikes and Control within Terrorist Organizations.” *American Political Science Review* 115(1):31–50.
- Robins, James M, Miguel Angel Hernan and Babette Brumback. 2000. “Marginal structural models and causal inference in epidemiology.” *Epidemiology* pp. 550–560.
- Rozenas, Arturas and Yuri Zhukov. 2019. “Mass Repression and Political Loyalty: Evidence from Stalin’s ‘Terror by Hunger’.” *American Political Science Review* 113(2):569–583.
- Runge, Jakob, Vladimir Petoukhov, Jonathan F. Donges, Jaroslav Hlinka, Nikola Jajcay, Martin Vejmelka, David Hartman, Norbert Marwan, Milan Paluš and Jürgen Kurths. 2015. “Identifying causal gateways and mediators in complex spatio-temporal systems.” *Nature Communications* 6(1):8502–8502.
- Schon, Justin and Ore Koren. 2022. “Introducing AfroGrid, a unified framework for environmental conflict research in Africa.” *Scientific Data* 9(116):1–11.
- Schwab, Regina, Werner Krause and Samer Massoud. 2023. “The Bombing of Hospitals and Local Violence Dynamics in Civil Wars: Evidence from Syria (2017-2020).” HiCN Working Paper 403.
- Sexton, Renard. 2016. “Aid as a Tool against Insurgency: Evidence from Contested and Controlled Territory in Afghanistan.” *American Political Science Review* 110(4):731–749.

- Sexton, Renard and Christoph Zurcher. 2024. “Aid, Attitudes, and Insurgency: Evidence from Development Projects in Northern Afghanistan.” *American Journal of Political Science* 68(3):1168–1182.
- Shaver, Andrew and Jacob Shapiro. 2021. “The Effect of Civilian Casualties on Wartime Informing: Evidence from the Iraq War.” *Journal of Conflict Resolution* 65(7-8):1337–1377.
- Silverman, Daniel. 2020. “Too Late to Apologize? Collateral Damage, Post-Harm Compensation, and Insurgent Violence in Iraq.” *International Organization* 74(4):853–871.
- Tchetgen Tchetgen, Eric J., Isabel R. Fulcher and Ilya Shpitser. 2021. “Auto-G-Computation of Causal Effects on a Network.” *Journal of the American Statistical Association* 116(534):833–844.
- U.S. Army Field Manual No.3-24*. 2007. Chicago: University of Chicago Press.
- van der Vaart, Aad W. 2010. “TIME SERIES.” *VU University Amsterdam, lecture notes* .
- Van Wie, Ryan C. and Jacob A. Walden. 2022a. “Troops or Tanks? Rethinking COIN mechanization and force employment.” *Small wars & insurgencies* 33(6):1032–1058.
- Van Wie, Ryan and Jacob Walden. 2022b. “Replication Data for: “Troops or Tanks: Rethinking Mechanization in Iraq”.”
URL: <https://doi.org/10.7910/DVN/E9NX1Y>
- Van Wie, Ryan and Jacob Walden. 2023. “Excessive Force or Armored Restraint: Government Mechanization and Civilian Casualties in Civil Conflict.” *Journal of Conflict Resolution* 67(10):2058–2084.
- VanderWeele, Tyler. 2015. *Explanation in causal inference : methods for mediation and interaction*. 1st ed. ed. New York: Oxford University Press.
- Vanderweele, Tyler J., Stijn Vansteelandt and James M. Robins. 2014. “Effect Decomposition in the Presence of an Exposure-Induced Mediator–Outcome Confounder.” *Epidemiology* 25(2):300–306.
- Vansteelandt, Stijn and Rhian M. Daniel. 2017. “Interventional Effects for Mediation Analysis with Multiple Mediators.” *Epidemiology* 28(2):258–265.
- Wang, Ye, Cyrus Samii, Haoge Chang and Peter M. Aronow. 2020. “Design-Based Inference for Spatial Experiments under Unknown Interference.” *arXiv preprint arXiv:2010.13599* .
URL: <https://arxiv.org/abs/2010.13599>
- Weintraub, Michael. 2016. “Do All Good Things Go Together? Development Assistance and Insurgent Violence in Civil War.” *Journal of Politics* 78(4):1468–2508.

- Xu, Jia, Liangdong Lu and Jiuchang Wei. 2025. “The Impact of Geographic, Mobility and Social Media Ties on Massive-Scale Regional Public Emotional Interaction.” *Humanities and Social Sciences Communications* 12:1–12.
- Young, Rachel and Solomon Hsiang. 2024. “Mortality Caused by Tropical Cyclones in the United States.” *Nature* 635:121–28.
- Zhang, Wenjia and Kexin Ning. 2023. “Spatiotemporal Heterogeneities in the Causal Effects of Mobility Intervention Policies during the COVID-19 Outbreak: A Spatially Interrupted Time-Series (SITS) Analysis.” *Annals of the American Association of Geographers* 113(5):1112–1134.
- Zhou, Lingxiao, Kosuke Imai, Jason Lyall and Georgia Papadogeorgou. 2024. “Estimating Heterogeneous Treatment Effects for Spatio-Temporal Causal Inference: How Economic Assistance Moderates the Effects of Airstrikes on Insurgent Violence.”
URL: <https://arxiv.org/abs/2412.15128>
- Zhukov, Yuri M., Jason S. Byers, Marty A. Davidson and Ken Kollman. 2024. “Integrating Data Across Misaligned Spatial Units.” *Political Analysis* 32(1):17–33.
- Zürcher, Christoph. 2017. “What Do We (Not) Know About Development Aid and Violence? A Systematic Review.” *World Development* 98(10):506–522.

SUPPLEMENTARY INFORMATION FOR
 “SPATIOTEMPORAL CAUSAL INFERENCE WITH
 SPILLOVER AND CARRYOVER EFFECTS”

A	Satellite imagery data	2
B	Schematic overview of notation	3
C	Asymptotic properties: IPW estimator	4
	C.1 Definitions and assumptions	4
	C.2 Asymptotic normality	5
	C.3 Estimator of the upper bound of the asymptotic variance	8
D	Asymptotic properties: Hájek estimator	10
	D.1 Definitions and assumptions	10
	D.2 Asymptotic normality under the true weights	12
	D.3 Consistent estimation of the variance bound with the true weights	14
	D.4 Asymptotic normality and estimation of the variance bound under the estimated weights	15
E	Average treatment effects	16
	E.1 Covariates	16
	E.2 Estimation of propensity scores	17
	E.3 Outcome surfaces	18
	E.4 Combined outcomes	19
F	Heterogeneous treatment effects	20
	F.1 Troop characteristics	20
	F.2 Presence of Sunni and Shia	21
G	Causal mediation analysis	22
	G.1 Model fit	22
	G.2 Covariates	22
	G.3 Geographical areas	23
	G.4 Main results in other geographical areas	24
	G.5 Results using an indicator for civilian casualties	26

A Satellite imagery data

We used a small purpose-built program to assist human coders in classifying the targets of each airstrike. We first indexed each airstrike to the relevant historical DigitalGlobe satellite imagery using each event's date and precise geospatial coordinates (in Military Grid Reference System). We then superimposed a circle at the specified location to indicate the blast radius of the dropped ordnance. We calculated blast radius using the bomb or missile's weight (e.g., a 2,000-lb GBU-31/15 has an estimated blast radius of 39m). Two independent coders then classified the nature of the target(s) within the blast radius using an eight-fold framework. Possible target types included: residential compounds; buildings; farms; roads; other human settlements; unpopulated areas; other (which coders provided a brief description for); and unable to code (given poor quality satellite imagery). Given this typology, coders classified a primary and a secondary target based on location within the blast radius. To ensure accurate cataloguing of civilian harm, coders were instructed to assign codes with the following ranking:

1. Compound
2. Building
3. Farm
4. Road
5. Out-buildings/other settlement
6. Unpopulated

In doing so, the coders ensured that harm to civilian lives and property was captured across multiple dimensions (i.e. a house and farm damaged in the same airstrike) rather than a simply yes/no indicator of harm. Each coder rated his/her confidence in their assessment using a four-fold scale ranging from "totally confident" (100% certainty, no ambiguity) about the target to "not confident" ($\leq 25\%$ certainty, high ambiguity). Coding decisions were cross-validated by two coders. Given the fairly mechanical nature of the coding, intercoder reliability was high (95%). When disagreement arose, a third coder was used to adjudicate the coding discrepancy.

B Schematic overview of notation

The notation used in our methodological framework is summarized as follows.

First, consider the setting without mediators (Figure S1). As described in the main text, Ω denotes the full study region (Iraq), and suppose we are interested in estimating treatment effects within a particular subregion B (see Figure S1). Spatial point patterns represent the geographic locations of events. In this context, the point pattern of airstrikes in each time period constitutes the treatment pattern, and the point pattern of insurgent violence constitutes the outcome pattern.

The information encoded in each treatment pattern is whether each location $s \in \Omega$ had airstrikes. We introduce indicators for each location s to encode such information. The binary variable $W_t(s)$ represents whether each location s had airstrikes at time t , and we summarize all the binary variables $W_t(s)$ at time t as W_t (Figure S1, center). For simplicity, let us consider a situation where three locations s_1, s_2, s_3 received airstrikes. Then we have $W_t(s_1) = W_t(s_2) = W_t(s_3) = 1$, and for all other locations in Ω , we have $W_t(s) = 0$. The collection of all the $W_t(s)$ variables is W_t . Finally, we summarize all the treatment pattern from time 1 to t as $\overline{W}_t = (W_1, W_2, \dots, W_t)$. The realized values are $\overline{w}_t = (w_1, \dots, w_t)$. This represents a history of treatment, with locations of airstrikes from each time period. We do the same for the outcome pattern (Figure S1, left), with the potential outcome represented as $Y_t(\overline{w}_t)$ and the observed outcome as $Y_t = Y_t(\overline{W}_t)$.

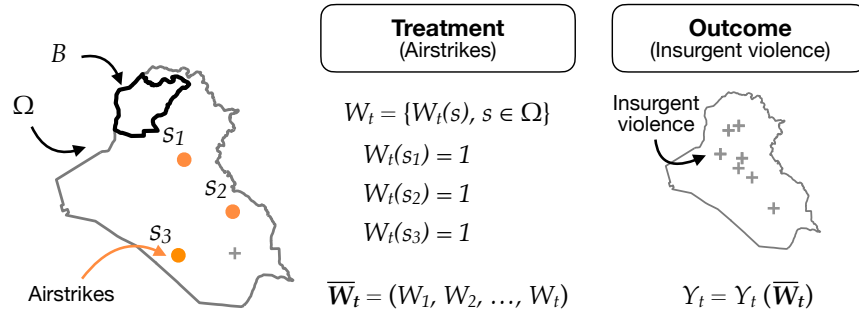


Figure S1: **Notation without mediators.** The left panel depicts the locations of airstrikes at time t . The treatment is summarized by a collection of indicators (center).

Next, we extend this notational framework to incorporate mediators (Figure S2). We do so by using indicator variables in the same way as the treatment. Suppose that two locations s_1 and s_2 experienced airstrikes without civilian casualties (shown in blue in Figure S2, left), while a third location s_3 experienced an airstrike with civilian casualties (orange). This additional information is encoded by an indicator $M_t(s)$, where in this illustration $M_t(s_1) = M_t(s_2) = 0$ and $M_t(s_3) = 1$ (Figure S2, center). The collection of mediator indicators over all locations forms M_t , and the mediator history through time is given by $\overline{M}_t = (M_1, M_2, \dots, M_t)$ with realized history \overline{m}_t . The potential outcome is now indexed by both the treatment and the mediator (Figure S2, right). Although $M_t(s)$ is binary here, it can be

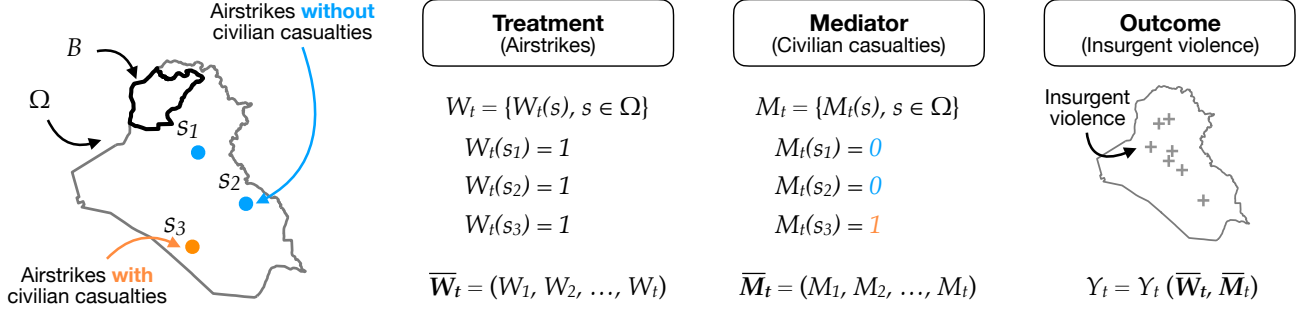


Figure S2: **Notation with mediators.** This time we also have information about the mediator (civilian casualties) encoded separately from the treatment (center).

generalized to categorical mediator values.

C Asymptotic properties: IPW estimator

In this section, we first derive the IPW estimators' asymptotic distributions. We show that they are consistent and asymptotically normal. We also discuss how estimators' asymptotic variance cannot be estimated without additional assumptions and derive an alternative, conservative, inferential approach. In Section D, we derive the Hájek estimator's asymptotic properties and its variance estimator.

C.1 Definitions and assumptions

Some useful definitions from the manuscript:

$$\begin{aligned} \xi_t(F, L) &= \prod_{t'=t-L+1}^t \frac{f_W(W_{t'})f_{M|W_{t'}}(M_{t'})}{e_{t'}(W_{t'})\rho_{t'}(M_{t'})} \\ \tilde{Y}_t(\omega) &= \sum_{s \in S_{Y_t}} K_b(\omega, s) \\ \hat{Y}_t(F, L; \omega) &= \xi_t(F, L)\tilde{Y}_t(\omega) \\ N(\tilde{Y}_t, B) &= \int_B \tilde{Y}_t(\omega)d\omega \\ N(Y_t, B) &= |S_{Y_t} \cap B| \end{aligned}$$

Some definitions that will be useful for the proofs:

- For $\epsilon > 0$, we use $\mathcal{N}_\epsilon(A)$ to denote the ϵ -neighborhood of a set A : $\mathcal{N}_\epsilon(A) = \{\omega \in \Omega : \text{there exists } a \in A \text{ with } \text{dist}(\omega, a) < \epsilon\}$.
- We use ∂B to denote the boundary of B (its closure excluding the interior points), $\partial B = \bar{B} \setminus B^\circ$.

C.2 Asymptotic normality

Assumption S.1 (Regularity conditions). *For each theoretical result, we require a subset of the following regularity conditions:*

- (a) *There exists $\delta_Y > 0$ such that $|S_{Y_t(\bar{\mathbf{w}}_t)}| < \delta_Y$ for all $t \in \mathcal{T}$ and $\bar{\mathbf{w}}_t \in \mathcal{W}^T$.*
- (b) *Let $\eta_t = \text{Var}\{\xi_t(F'', L) - \xi_t(F', L)\}N(Y_t, B) | \bar{H}_{t-L}^*$ for $t \geq L$. Then, there exists $\eta \in \mathbb{R}^+$ such that $(T - L + 1)^{-1} \sum_{t=L}^T \eta_t \xrightarrow{p} \eta$ as $T \rightarrow \infty$.*
- (c) *There exists a neighborhood of set B 's boundary over which outcome active locations are observed during at most T^{1-Q^*} time periods, for some $Q^* \in (1/2, 1)$ and as $T \rightarrow \infty$, i.e. there exists $\delta_B > 0$ such that*

$$P \left(\sum_{t=L}^T I \left(\exists s \in S_{Y_t} \cap \mathcal{N}_{\delta_B}(\partial B) \right) > T^{1-Q^*} \right) \rightarrow 0, \text{ as } T \rightarrow \infty.$$

Theorem 1 (Asymptotic normality of estimator over a fixed region B). *If Assumption 4 and the regularity conditions in the appendix hold, and the kernel bandwidth $b_T \rightarrow 0$, then*

$$\sqrt{T} \left(\widehat{\tau}_B(F', F'', L) - \tau_B(F', F'', L) \right) \xrightarrow[T \rightarrow \infty]{d} N(0, \eta).$$

Furthermore, $(T - L + 1)^{-1} \sum_{t=L}^T [\widehat{\tau}_{Bt}(F', F'', L)]^2$ is a consistent estimator of an upper bound of the asymptotic variance η .

Theorem 1 states that the estimator is asymptotically normally distributed, and allows us to estimate a bound for the estimator's variance assuming a long enough time series. Therefore, this result allows us to make inference on the effect for a change in the intervention of the treatment and mediator assignment on the outcome process over a region B . Since direct and indirect effects can be written in this form for carefully defined stochastic interventions (see (9) and (8)), Theorem 1 also implies that our estimators of the direct and indirect effect in (15) are consistent and asymptotically normal, which allows us to make inference on the causal pathways of the spatio-temporal point pattern treatment within a region B . We can similarly show that the estimator for the expected number of outcome active locations $\widehat{N}_B(F, L)$ is consistent for $N_B(F, L)$ and asymptotically normal, but the proof is omitted here for clarity.

Proof of Theorem 1. The proof of this theorem follows closely the proof of (Theorem 1 in Papadoggeorgou et al., 2022). The main difference lies in the fact that the stochastic interventions take place over both the treatment and mediator assignment, and the causal assumptions and proof below have to be altered to accommodate that.

In what follows, we write K_{b_T} instead of K_b to reflect the dependence of the bandwidth parameter on the time series length T . The variables temporally precedent to the treatment assignment at time period t , W_t , is the expanded history $\overline{H}_{t-1}^* = \{\overline{W}_{t-1}, \overline{M}_{t-1}, \overline{Y}_T, \overline{X}_T\} \supset \overline{H}_{t-1}$. Since $\overline{H}_{t-1}^* \subset \overline{H}_t^*$, the expanded history is a filtration generated by the collection of potential values of confounders and outcomes, \overline{X}_T and \overline{Y}_T , and the previous treatments and mediator values, \overline{W}_{t-1} and \overline{M}_{t-1} . Let

$$\begin{aligned}
e_{Bt} &= \widehat{\tau}_{Bt}(F', F'', L) - \tau_{Bt}(F', F'', L) \\
&= [\xi_t(F'', L) - \xi_t(F', L)]N(\tilde{Y}_t, B) - \left\{ \mathbf{N}_{Bt}(F'', L) - \mathbf{N}_{Bt}(F', L) \right\} \\
&= \underbrace{[\xi_t(F'', L) - \xi_t(F', L)]N(Y_t, B) - \left\{ \mathbf{N}_{Bt}(F'', L) - \mathbf{N}_{Bt}(F', L) \right\}}_{q_{1Bt}} - \underbrace{[\xi_t(F'', L) - \xi_t(F', L)]N(\tilde{Y}_t, B)}_{q_{2Bt}}
\end{aligned} \tag{18}$$

We show that

1. $\sqrt{T} \left(\frac{1}{T-L+1} \sum_{t=L}^T q_{1Bt} \right)$ is asymptotically normal, and
2. $\sqrt{T} \left(\frac{1}{T-L+1} \sum_{t=L}^T q_{2Bt} \right)$ converges to zero in probability.

Showing asymptotic normality of q_{1Bt} : We use (van der Vaart, 2010, Theorem 4.16). Let $\mathcal{F}_t = \overline{H}_{t-L+1}^*$. We show that

- (1) q_{1Bt} is a martingale difference series with respect to the filtration \mathcal{F}_{t-1} , and
- (2) for every $\epsilon > 0$, $(T-L+1)^{-1} \sum_{t=L}^T E\{q_{1Bt}^2 I(|q_{1Bt}| > \epsilon\sqrt{T-L+1}) \mid \mathcal{F}_{t-1}\} \xrightarrow{p} 0$.

To prove that q_{1Bt} is a martingale difference series, we show that $E(|q_{1Bt}|) < \infty$ and $E(q_{1Bt} \mid \mathcal{F}_{t-1}) = 0$. For the first part, Assumption 4 and Assumption S.1(a) imply that:

$$\begin{aligned}
|q_{1Bt}| &= |[\xi_t(F'', L) - \xi_t(F', L)]N(Y_t, B) - \{\mathbf{N}_{Bt}(F'', L) - \mathbf{N}_{Bt}(F', L)\}| \\
&\leq [\xi_1(F, L) + \xi_2(F, L)]N(Y_t, B) + \mathbf{N}_{Bt}(F', L) + \mathbf{N}_{Bt}(F'', L) \\
&\leq 2\delta_Y(\delta_W^L \delta_M^L + 1),
\end{aligned} \tag{19}$$

hence $E[|q_{1Bt}|] < \infty$. For the second part, it suffices to show that

$$E[\xi_t(F, L)N(Y_t, B) \mid \mathcal{F}_{t-1}] = \mathbf{N}_{Bt}(F, L),$$

where the expectation is taken with respect to treatments and mediators $(W_{t-L+1}, M_{t-L+1}, \dots, W_t, M_t)$:

$$\begin{aligned}
& E[\xi_t(F, L)N(Y_t, B) \mid \mathcal{F}_{t-1}] \tag{20} \\
&= \int \left[\prod_{t'=t-L+1}^t \frac{f_W(w_{t'})f_{M|w_{t'}}(m_{t'})}{e_{t'}(w_{t'})\rho_{t'}(m_{t'})} \right] N_B(Y_t(W_1, M_1, \dots, W_{t-L}, M_{t-L}, w_{t-L+1}, m_{t-L+1}, \dots, w_t, m_t)) \times \\
&\quad f(w_{t-L+1} \mid \mathcal{F}_{t-1})f(m_{t-L+1} \mid \mathcal{F}_{t-1}, W_{t-L+1}) \times \\
&\quad f(w_{t-L+2} \mid \mathcal{F}_{t-1}, W_{t-L+1}, M_{t-L+1}) \times \\
&\quad \dots \times \\
&\quad f(w_t \mid \mathcal{F}_{t-1}, W_{t-L+1}, M_{t-L+1}, \dots, W_{t-1}, M_{t-1})f(m_t \mid \mathcal{F}_{t-1}, W_{t-L+1}, M_{t-L+1}, \dots, M_{t-1}, W_t) \\
&\quad d(w_{t-L+1}, m_{t-L+1}, \dots, w_t, m_t) \\
&= \int \left[\prod_{t'=t-L+1}^t \frac{f_W(w_{t'})f_{M|w_{t'}}(m_{t'})}{e_{t'}(w_{t'})\rho_{t'}(m_{t'})} \right] N_B(Y_t(W_1, M_1, \dots, W_{t-L}, M_{t-L}, w_{t-L+1}, m_{t-L+1}, \dots, w_t, m_t)) \times \\
&\quad f(w_{t-L+1} \mid \bar{H}_{t-L}^*)f(m_{t-L+1} \mid \bar{H}_{t-L}^*, W_{t-L+1})f(w_{t-L+2} \mid \bar{H}_{t-L+1}^*)f(m_{t-L+2} \mid \bar{H}_{t-L+1}^*, W_{t-L+2}) \dots \\
&\quad f(w_t \mid \bar{H}_{t-1}^*)f(m_t \mid \bar{H}_{t-1}^*, W_t) \\
&\quad d(w_{t-L+1}, m_{t-L+1}, \dots, w_t, m_t) \tag{because $\bar{H}_t^* = \bar{H}_{t-1}^* \cup \{W_t, M_t\}$ } \\
&= \int N_B(Y_t(W_1, M_1, \dots, W_{t-L}, M_{t-L}, w_{t-L+1}, m_{t-L+1}, \dots, w_t, m_t)) \prod_{t'=t-L+1}^t f_W(w_{t'})f_{M|w_{t'}}(m_{t'}) \\
&\quad d(w_{t-L+1}, m_{t-L+1}, \dots, w_t, m_t) \tag{By Assumption 2} \\
&= \mathbf{N}_{Bt}(F, L).
\end{aligned}$$

This establishes the claim that q_{1Bt} is a martingale difference series with respect to filtration \bar{H}_{t-L}^* .

Next, let $\epsilon > 0$. Since q_{1Bt} is bounded by (19), choose T_0 as

$$\begin{aligned}
T_0 &= \operatorname{argmin}_{t \in \mathbb{N}^+} \{ \epsilon \sqrt{t-L+1} > 2\delta_Y(\delta_W^L \delta_M^L + 1) \} \\
&= \operatorname{argmin}_{t \in \mathbb{N}^+} \left\{ t > L-1 + \left[\frac{2\delta_Y(\delta_W^L \delta_M^L + 1)}{\epsilon} \right]^2 \right\} \tag{21} \\
&= \left\lceil L-1 + \left[\frac{2\delta_Y(\delta_W^L \delta_M^L + 1)}{\epsilon} \right]^2 \right\rceil
\end{aligned}$$

Then, for $T > T_0$, $I(|q_{1Bt}| > \epsilon \sqrt{T-L+1}) = 0$ and $E(q_{1Bt}^2 I(|q_{1Bt}| > \epsilon \sqrt{T-L+1}) \mid \bar{H}_{t-L}^*) = 0$.

Combining the previous results to show asymptotic normality of the first error: Since q_{1Bt} has mean zero, $E(q_{1Bt}^2 \mid \mathcal{F}_{t-1}) = \operatorname{Var}(q_{1Bt} \mid \mathcal{F}_{t-1})$, and since $\tau_{Bt}(F', F'', L)$ is fixed, $\operatorname{Var}(q_{1Bt} \mid \mathcal{F}_{t-1}) =$

$\text{Var}\{[\xi_t(F'', L) - \xi_t(F', L)]N(Y_t, B) \mid \mathcal{F}_{t-1}\} = \eta_t$. This gives us that

$$\frac{1}{T-L+1} \sum_{t=L}^T E(q_{1Bt}^2 \mid \mathcal{F}_{t-1}) = \frac{1}{T-L+1} \sum_{t=L}^T \eta_t \xrightarrow{p} \eta,$$

from Assumption S.1(b). From Theorem 4.16 of [van der Vaart \(2010\)](#),

$$\sqrt{T} \left(\frac{1}{T-L+1} \sum_{t=L}^T q_{1Bt} \right) \xrightarrow{d} N(0, \eta).$$

Showing convergence to zero of q_{2Bt} : We want to show that for $T \rightarrow \infty$ and $b_T \rightarrow 0$ as $T \rightarrow \infty$,

$$\sqrt{T} \left(\frac{1}{T-L+1} \sum_{t=L}^T q_{2Bt} \right) \xrightarrow{p} 0.$$

To do so, we note that the error q_{2Bt} is a weighted comparison of the outcome active locations within set B based on the observed data $N(Y_t, B)$ and the smoothed observed outcome surface $N(\tilde{Y}_t, B)$

$$\frac{1}{T-L+1} \sum_{t=L}^T q_{2Bt} = \frac{1}{T-L+1} \sum_{t=L}^T (\xi_t(F'', L) - \xi_t(F', L)) \left[\int_B \sum_{s \in S_{Y_t}} K_{b_T}(\omega; s) d\omega - N_B(Y_t) \right].$$

Since $|\xi_t(F'', L) - \xi_t(F', L)| \leq 2(\delta_W^L \delta_M^L + 1)$ from Assumption 2, and using Assumption S.1(c) the result can be acquired following the steps of the proof of Theorem 1 in [Papadogeorgou et al. \(2022\)](#), since the treatment and mediator assignment are nuisances in showing that this error converges to zero, and it is only required that they lead to bounded weights $\xi_t(F, L)$.

C.3 Estimator of the upper bound of the asymptotic variance

Since η is the limit of

$$(T-L+1)^{-1} \sum_{t=L}^T \text{Var}\{[\xi_t(F'', L) - \xi_t(F', L)]N(Y_t, B) \mid \bar{H}_{t-L}^*\},$$

we cannot directly estimate η from the data without additional assumptions (available data are on a single time series and we do not have access to replicates of the world with respect to $W_{t-L+1}, M_{t-L+1}, \dots, W_t$ given \bar{H}_{t-L}^*). Instead, we consider

$$\eta_t^* = E\left\{ \left\{ [\xi_t(F'', L) - \xi_t(F', L)]N(Y_t, B) \right\}^2 \mid \bar{H}_{t-L}^* \right\} \geq \eta_t$$

for which

$$(T - L + 1)^{-1} \sum_{t=L}^T \eta_t^* \rightarrow \eta^* \geq \eta.$$

We show that $\widehat{\eta}^* = (T - L + 1)^{-1} \sum_{t=L}^T \left[\widehat{\tau}_{Bt}(F', F'', L) \right]^2$ is a consistent estimator for η^* , by showing that

1. $\widetilde{\eta}^* = (T - L + 1)^{-1} \sum_{t=L}^T \left\{ [\xi_t(F'', L) - \xi_t(F', L)] N(Y_t, B) \right\}^2$ is consistent for η^* , and
2. $\widehat{\eta}^* - \widetilde{\eta}^* \xrightarrow{p} 0$.

Define $\Psi_t = \left\{ [\xi_t(F'', L) - \xi_t(F', L)] N(Y_t, B) \right\}^2 - \eta_t^*$. Then, Ψ_t is a martingale difference series with respect to \overline{H}_{t-L+1}^* since the following two hold:

- $E(|\Psi_t|) < \infty$ since Ψ_t is bounded (derived using Assumption 2 and Assumption S.1(a)), and
- $E(\Psi_t \mid \overline{H}_{t-L+1}^*) = E\left\{ [\xi_t(F'', L) - \xi_t(F', L)] N(Y_t, B) \mid \overline{H}_{t-L}^* \right\} - \eta_t^* = 0$.

Also, since $[\xi_t(F'', L) - \xi_t(F', L)] N(Y_t, B)$ is bounded we have that $\sum_{t=L}^{\infty} t^{-2} E(\Psi_t^2) < \infty$. From Theorem 1 in Csörgö (1968) we have that

$$\frac{1}{T - L + 1} \sum_{t=L}^T \Psi_t = \frac{1}{T - L + 1} \sum_{t=L}^T \left\{ [\xi_t(F'', L) - \xi_t(F', L)] N(Y_t, B) \right\}^2 - \frac{1}{T - L + 1} \sum_{t=L}^T \eta_t^* \xrightarrow{p} 0,$$

showing that $\widetilde{\eta}^*$ consistently estimates the asymptotic variance bound η^* . Next, write

$$\begin{aligned} \widehat{\eta}^* - \widetilde{\eta}^* &= (T - L + 1)^{-1} \sum_{t=L}^T [\xi_t(F'', L) - \xi_t(F', L)]^2 \{ N(\widetilde{Y}_t, B)^2 - N(Y_t, B)^2 \} \\ &= (T - L + 1)^{-1} \sum_{t=L}^T [\xi_t(F'', L) - \xi_t(F', L)]^2 \{ N(\widetilde{Y}_t, B) + N(Y_t, B) \} \{ N(\widetilde{Y}_t, B) - N(Y_t, B) \} \\ &= (T - L + 1)^{-1} \sum_{t=L}^T c_t \{ N(\widetilde{Y}_t, B) - N(Y_t, B) \} \end{aligned}$$

for $c_t = [\xi_t(F'', L) - \xi_t(F', L)]^2 \{ N(\widetilde{Y}_t, B) + N(Y_t, B) \}$. Note that since $\xi_t(F, L)$ is bounded (using Assumption 2) and since $N(\widetilde{Y}_t, B), N(Y_t, B)$ are bounded (using Assumption S.1(a)), the constants c_t are also bounded. Therefore, following the proof for convergence to zero of the second error q_{2Bt} , we can show that $\sqrt{T}(\widehat{\eta}^* - \widetilde{\eta}^*) \xrightarrow{p} 0$ which of course implies that $\widehat{\eta}^* - \widetilde{\eta}^* \xrightarrow{p} 0$. Therefore, $\widehat{\eta}^*$ is consistent for η^* . □

D Asymptotic properties: Hájek estimator

In this section, we derive asymptotic properties of the Hájek estimator and its variance upper bound. We follow and extend the proofs provided in [Zhou et al. \(2024\)](#). We state definitions and assumptions, derive asymptotic properties with the true propensity and mediator scores, and show asymptotic properties with the estimated propensity and mediator scores.

D.1 Definitions and assumptions

We use the following notation,

$$\begin{aligned}\xi_t(F, L) &= \prod_{t'=t-L+1}^t \frac{f_W(W_{t'})f_{M|W_{t'}}(M_{t'})}{e_{t'}(W_{t'})\rho_{t'}(M_{t'})} \\ \tilde{Y}_t(\omega) &= \sum_{s \in S_{Y_t}} K_b(\omega, s) \\ \hat{Y}_t^I(F, L; \omega) &= \xi_t(F, L)\tilde{Y}_t(\omega) \\ \hat{Y}_t^H(F, L; \omega) &= \frac{\xi_t(F, L)}{\frac{1}{T-L+1} \sum_{t=L}^T \xi_t(F, L)} \tilde{Y}_t(\omega) \\ \tilde{\tau}_t^I(F', F''; \gamma^*) &= \int_B \hat{Y}_t^I(F', L; \omega) d\omega - \int_B \hat{Y}_t^I(F'', L; \omega) d\omega \\ \tilde{\tau}_t^H(F', F''; \gamma^*) &= \int_B \hat{Y}_t^H(F', L; \omega) d\omega - \int_B \hat{Y}_t^H(F'', L; \omega) d\omega,\end{aligned}$$

where I and H denote the IPW and Hájek estimators, respectively. We define intervention F as $F = (F_W, F_{M|W})$. Additionally, let $e_t(W_t; \gamma^P)$ be a parametric propensity score model and $\rho_t(M_t, W_t; \gamma^M)$ be a parametric mediator score model, with $\gamma = (\gamma^P, \gamma^M) \in \mathbb{R}^K$ be a K -dimensional vector of parameters, and $\hat{\gamma} = (\hat{\gamma}^P, \hat{\gamma}^M)$ be an estimate of γ .

We first restate the regularity conditions as follows. The first two assumptions are equivalent to Assumptions A.1 and A.2 in [Zhou et al. \(2024\)](#) without projection but with both propensity and mediator scores.

Assumption S.2 (Regularity conditions: IPW estimator with the true propensity and mediator scores). *The following two conditions hold.*

- (a) (Bounded outcome) *There exist a positive constant $\delta_Y < \infty$ such that $N_\Omega(Y_t) < \delta_Y$ for all $Y_t \in \overline{\mathcal{Y}}_T$.*
- (b) (Asymptotic variance) *For all t , there exists $\eta^I \in \mathbb{R}^+$ such that*

$$\frac{1}{T-L+1} \sum_{t=L}^T \text{Var} \left[\tilde{\tau}_t^I(F', F''; \gamma^*) \mid \overline{H}_{t-L}^* \right] \xrightarrow{p} \eta^I$$

as $T \rightarrow \infty$.

Assumption S.3 (Regularity conditions: the propensity and mediator score models). *Assume that the parametric form of the propensity and mediator scores indexed by $\gamma = (\gamma^P, \gamma^M)$,*

$$f_W (W_t = w_t \mid \bar{H}_{t-1}; \gamma^P) f_{M|w_t} (M_t = m_t \mid \bar{H}_{t-1}, W_t = w_t; \gamma^M),$$

is correctly specified and differentiable with respect to $\gamma \in \mathbb{R}^K$, and let the partial derivative,

$$\begin{aligned} & \psi (W_t, M_t, \bar{H}_{t-1}; \gamma) \\ &= \frac{\partial}{\partial \gamma} \log \{ f_W (W_t = w_t \mid \bar{H}_{t-1} = \bar{h}_{t-1}; \gamma^P) f_{M|w} (M_t = m_t \mid \bar{H}_{t-1} = \bar{h}_{t-1}, W_t = w_t; \gamma^M) \}, \end{aligned}$$

be twice continuously differentiable score functions. Let γ^ denote the true values of the parameters, where γ^* is in an open subset of the Euclidean space. Denote $\mathcal{F}_t = \bar{H}_{t-L+1}^*$. We assume that the following conditions hold:*

1. (a) $\mathbb{E}_{\gamma^*} \left[\|\psi (W_t, M_t, \bar{H}_{t-1}; \gamma^*)\|^2 \right] < \infty$,
- (b) *There exists a positive definite matrix \mathbf{V}_{pm} such that*

$$\frac{1}{T} \sum_{t=1}^T \mathbb{E}_{\gamma^*} \left(\psi (W_t, M_t, \bar{H}_{t-1}; \gamma^*) \psi (W_t, M_t, \bar{H}_{t-1}; \gamma^*)^\top \mid \mathcal{F}_{t-1} \right) \xrightarrow{p} \mathbf{V}_{pm}$$

- (c) $\frac{1}{T} \sum_{t=1}^T \mathbb{E}_{\gamma^*} \left[\|\psi (W_t, M_t, \bar{H}_{t-1}; \gamma^*)\|^2 I \left(\|\psi (W_t, M_t, \bar{H}_{t-1}; \gamma^*)\| > \epsilon \sqrt{T} \right) \mid \mathcal{F}_{t-1} \right] \xrightarrow{p} 0$,
for all $\epsilon > 0$, as $T \rightarrow \infty$.

2. *Let the k^{th} element of the $\psi (w_t, m_t, \bar{H}_{t-1}; \gamma)$ vector be $\psi_k (w_t, m_t, \bar{H}_{t-1}; \gamma)$ and denote $P_{kjt} = \frac{\partial}{\partial \gamma_j} \psi_k (W_t, M_t, \bar{H}_{t-1}; \gamma) \mid_{\gamma^*}$. Then, for all k, j , we have $\mathbb{E}_{\gamma^*} [|P_{kjt}|] < \infty$ and there exists $0 < r_{kj} \leq 2$ such that $\sum_{t=1}^T \frac{1}{t^{r_{kj}}} \mathbb{E}_{\gamma^*} (|P_{kjt} - \mathbb{E}_{\gamma^*} (P_{kjt} \mid \mathcal{F}_{t-1})|^{r_{kj}} \mid \mathcal{F}_{t-1}) \xrightarrow{p} 0$*
3. *There exists an integrable function $\ddot{\psi} (w_t, m_t, \bar{h}_{t-1})$ such that $\ddot{\psi} (w_t, m_t, \bar{h}_{t-1})$ dominates the second partial derivatives of $\psi (w_t, m_t, \bar{h}_{t-1}; \gamma)$ in a neighborhood of γ^* for all $(w_t, m_t, \bar{h}_{t-1})$*

Below, to clarify that $\xi_t(F, L)$ is a function of γ , we denote $\xi_t(F, L)$ as $\xi_t(F, L, \gamma)$. The two assumptions stated below are equivalent to Assumptions A.4 and A.5 in [Zhou et al. \(2024\)](#).

Assumption S.4. *Define*

$$\mathbf{A}_t = \begin{pmatrix} \widehat{Y}_t^I (F', L, \gamma^*; \omega) \\ \widehat{Y}_t^I (F'', L, \gamma^*; \omega) \\ \xi_t (F', L, \gamma^*) \\ \xi_t (F'', L, \gamma^*) \end{pmatrix}. \quad (22)$$

Then, there exists a positive definite matrix \mathbf{V}^H such that as $T \rightarrow \infty$,

$$\frac{1}{T-L+1} \sum_{t=L}^T \text{Var}[\mathbf{A}_t \mid \bar{H}_{t-L}^*] \xrightarrow{p} \tilde{\mathbf{V}}^H.$$

Assumption S.5 (Regularity conditions: Score function of the propensity and mediator score models).
Define

$$s(\bar{H}_{t-1}, W_t, M_t, Y_t; \gamma) = \begin{pmatrix} \hat{Y}_t^I(F', L, \gamma; \omega) - N_t(F') \\ \hat{Y}_t^I(F'', L, \gamma; \omega) - N_t(F'') \\ \xi_t(F', L, \gamma^*) - 1 \\ \xi_t(F'', L, \gamma^*) - 1 \end{pmatrix},$$

and propensity and mediator score functions $\psi(W_t, M_t, \bar{H}_{t-1}; \gamma)$ satisfying Assumption S.3, the following conditions hold.

(a) As defined in Section D.1, let $\gamma \in \mathbb{R}^K$. Then, there exists $\mathbf{U} \in \mathbb{R}^{K \times 2}$ such that

$$\frac{1}{T-L+1} \sum_{t=L}^T \mathbb{E}_{\gamma^*}[\psi(W_t, M_t, \bar{H}_{t-1}; \gamma^*) s(\bar{H}_{t-1}, W_t, M_t, Y_t; \gamma^*)^\top \mid \bar{H}_{t-L}^*] \xrightarrow{p} \mathbf{U}, \text{ and}$$

$$\mathbf{V}^* = \begin{bmatrix} \tilde{\mathbf{V}}^H & \mathbf{U}^\top \\ \mathbf{U} & \mathbf{V}_{pm} \end{bmatrix} \text{ is positive definite.}$$

(b) If $P_{jt} = \frac{\partial}{\partial \gamma_j} s(\bar{H}_{t-1}, W_t, M_t, Y_t; \gamma) \Big|_{\gamma^*}$, where γ_j is the j^{th} entry of γ , then there exists $r_j \in (0, 2]$ such that

$$\frac{1}{T-L+1} \sum_{t=L}^T \frac{1}{t^{r_j}} \left(|P_{jt} - \mathbb{E}_{\theta^*}[P_{jt} \mid \bar{H}_{t-L}^*]| \right) \xrightarrow{p} 0.$$

D.2 Asymptotic normality under the true weights

With the aforementioned assumptions, we now present the asymptotic normality of the Hájek estimator with the true propensity and mediator scores.

Theorem 2 (Asymptotic normality of the Hájek estimator using the true propensity and mediator scores).
Suppose that Assumptions 3, 4, S.2, and S.4 hold. Define \mathbf{A}_t as in Equation (22). Also, define \mathbf{J} as,

$$\mathbf{J} = \begin{bmatrix} \mathbf{I} & -\mathbf{I} & -\frac{1}{T-L+1} \sum_{t=L}^T N_t(F') & \frac{1}{T-L+1} \sum_{t=L}^T N_t(F'') \end{bmatrix}.$$

Then,

$$\frac{1}{\sqrt{T-L+1}} \sum_{t=L}^T \left(\tilde{\tau}_t^H(F', F''; \gamma^*) - \tau_t(F', F''; \gamma^*) \right) \xrightarrow{d} N(\mathbf{0}, \mathbf{J} \tilde{\mathbf{V}}^H \mathbf{J}^\top),$$

where $\tilde{\mathbf{V}}^H$ defined in Assumption S.4.

Proof of Theorem 2. The proof extends those of Theorem A.1 and Theorem A.4 in Zhou et al. (2024) by incorporating mediator scores. Let $\mathcal{F}_t = \overline{H}_{t-L+1}^*$, and $\mathbf{A}_t^* = \mathbf{A}_t - (N_t(F'), N_t(F''), \xi(F'), \xi(F''))^\top$ where $\xi(F') = \xi(F'') = 1$. Then, we apply Theorem A.2 of Papadogeorgou et al. (2022). The first step of the proof is to show that \mathbf{A}_t^* is a martingale difference sequence. Given Equation (20), we have $\mathbb{E}[\widehat{Y}_t^I(F') \mid \mathcal{F}_{t-1}] = N_t(F')$. Also, by Assumption 3,

$$\begin{aligned}
& \mathbb{E}[\xi_t(F', L, \gamma^*) \mid \mathcal{F}_{t-1}] \\
&= \int \prod_{t'=t-L+1}^t \frac{f_W(w_{t'}) f_{M|W_{t'}}(m_{t'})}{e_{t'}(w_{t'}) \rho_{t'}(m_{t'})} f_W(w_{t'} \mid \overline{H}_{t'-1}^*) f_{M|w}(m_{t'} \mid w_{t'}, \overline{H}_{t'-1}^*) \mathbf{d}(\mathbf{w}_{(t-L+1):t}, \mathbf{m}_{(t-L+1):t}) \\
&= \int \prod_{t'=t-L+1}^t \frac{f_W(w_{t'}) f_{M|W_{t'}}(m_{t'})}{e_{t'}(w_{t'}) \rho_{t'}(m_{t'})} e_{t'}(w_{t'}) \rho_{t'}(m_{t'}) \mathbf{d}(\mathbf{w}_{(t-L+1):t}, \mathbf{m}_{(t-L+1):t}) \\
&= \int \prod_{t'=t-L+1}^t f_W(w_{t'}) f_{M|W_{t'}}(m_{t'}) \mathbf{d}(\mathbf{w}_{(t-L+1):t}, \mathbf{m}_{(t-L+1):t}) \\
&= 1.
\end{aligned}$$

Since the similar results apply to F'' , we obtain $\mathbb{E}[\mathbf{A}_t^* \mid \mathcal{F}_{t-1}] = 0$. Additionally, by Assumptions 4 and S.2(a), $\|\mathbf{A}_t^*\|$ is bounded and $\mathbb{E}[\|\mathbf{A}_t^*\|] < \infty$. Therefore, for $\epsilon > 0$ and for large t , it follows that $I(\|\mathbf{A}_t^*\| > \epsilon\sqrt{T}) = 0$. Thus, as $T \rightarrow \infty$, for any $\epsilon > 0$,

$$\frac{1}{T-L+1} \sum_{t=L}^T E \left[\|\mathbf{A}_t^*\|^2 I(\|\mathbf{A}_t^*\| > \epsilon\sqrt{T}) \mid \mathcal{F}_{t-1} \right] \xrightarrow{p} 0.$$

Assumption S.4 ensures the remaining condition of the multivariate Martingale central limit theorem. Therefore, similarly to Theorem A.4 in Zhou et al. (2024), we have

$$\frac{1}{\sqrt{T-L+1}} \sum_{t=L}^T \mathbf{A}_t^* \xrightarrow{d} N(\mathbf{0}, \widetilde{\mathbf{V}}^H)$$

where

$$\frac{1}{T-L+1} \sum_{t=L}^T \mathbb{E}[\mathbf{A}_t^* \mathbf{A}_t^{*\top} \mid \mathcal{F}_{t-1}] \xrightarrow{p} \widetilde{\mathbf{V}}^H$$

and

$$\sqrt{T-L+1}(\hat{\boldsymbol{\theta}} - \boldsymbol{\theta}^*) \xrightarrow{d} N(\mathbf{0}, \widetilde{\mathbf{V}}^H),$$

where

$$\boldsymbol{\theta} = \frac{1}{T-L+1} \left(\sum_{t=L}^T N_t(F'), \sum_{t=L}^T N_t(F''), \xi(F'), \xi(F'') \right)^\top,$$

$$\hat{\boldsymbol{\theta}} = \frac{1}{T-L+1} \sum_{t=L}^T \left(\hat{Y}_t^I(F', L; \omega), \hat{Y}_t^I(F'', L; \omega), \xi_t(F', L), \xi_t(F'', L) \right)^\top.$$

The second step of the proof is to apply the Delta method. Define

$$h(\boldsymbol{\theta}) = \frac{\frac{1}{T-L+1} \sum_{t=L}^T N_t(F')}{\xi(F')} - \frac{\frac{1}{T-L+1} \sum_{t=L}^T N_t(F'')}{\xi(F'')}.$$

We know that the Jacobian matrix is

$$\mathbf{J}(\boldsymbol{\theta}) = \begin{bmatrix} \frac{1}{\xi(F')} \mathbf{I} & -\frac{1}{\xi(F'')} \mathbf{I} & -\frac{\frac{1}{T-L+1} \sum_{t=L}^T N_t(F')}{\xi(F')^2} & \frac{\frac{1}{T-L+1} \sum_{t=L}^T N_t(F'')}{\xi(F'')^2} \end{bmatrix}$$

where \mathbf{I} is the identity matrix. Now denote

$$\mathbf{J} = \mathbf{J}(\boldsymbol{\theta}^*) = \begin{bmatrix} \mathbf{I} & -\mathbf{I} & -\frac{1}{T-L+1} \sum_{t=L}^T N_t(F') & \frac{1}{T-L+1} \sum_{t=L}^T N_t(F'') \end{bmatrix}.$$

Then, we obtain,

$$\sqrt{T-L+1}(h(\hat{\boldsymbol{\theta}}) - h(\boldsymbol{\theta}^*)) \xrightarrow{d} N(\mathbf{0}, \mathbf{J} \tilde{\mathbf{V}}^H \mathbf{J}^\top)$$

as $T \rightarrow \infty$. Therefore,

$$\frac{1}{\sqrt{T-L+1}} \sum_{t=L}^T \left(\tilde{\tau}_t^H(F', F''; \gamma^*) - \tau_t(F', F''; \gamma^*) \right) \xrightarrow{d} N(\mathbf{0}, \mathbf{J} \tilde{\mathbf{V}}^H \mathbf{J}^\top).$$

□

D.3 Consistent estimation of the variance bound with the true weights

We next show consistent estimation of the variance bound with the true propensity and mediator scores.

This result corresponds to Proposition A.2 in [Zhou et al. \(2024\)](#).

Proposition S.1 (Consistent estimation of variance bound for the Hájek estimator with the true propensity and mediator scores). *Suppose that Assumptions 3, 4, S.2, and S.4 hold. Let*

$$\hat{\mathbf{V}}^H = \frac{1}{T-L+1} \sum_{t=L}^T \hat{\mathbf{V}}_t^H \text{ with } \hat{\mathbf{V}}_t^H = \mathbf{A}_t \mathbf{A}_t^\top \text{ and}$$

$$\hat{\mathbf{J}} = \begin{bmatrix} \mathbf{I} & -\mathbf{I} & -\frac{1}{T-L+1} \sum_{t=L}^T \hat{Y}_t^H(F', L, \gamma^*; \omega) & \frac{1}{T-L+1} \sum_{t=L}^T \hat{Y}_t^H(F'', L, \gamma^*; \omega) \end{bmatrix}$$

Then $\hat{\mathbf{J}}\hat{\mathbf{V}}^H\hat{\mathbf{J}}^\top$ is a consistent estimator for $\mathbf{J}\mathbf{V}^{H*}\mathbf{J}^\top$.

Proof of Proposition S.1. From Theorem 2, we have

$$\hat{\boldsymbol{\theta}} = \left[-\frac{1}{T-L+1} \sum_{t=L}^T \hat{Y}_t^H(F', L, \gamma^*; \omega), \frac{1}{T-L+1} \sum_{t=L}^T \hat{Y}_t^H(F', L, \gamma^*; \omega), 1, 1 \right]^\top$$

as a consistent estimator of $\boldsymbol{\theta}$. Therefore, $\hat{\mathbf{J}} = \mathbf{J}(\hat{\boldsymbol{\theta}})$ is also a consistent estimator of $\mathbf{J}(\boldsymbol{\theta})$, and by Proposition A.1 in Zhou et al. (2024), we have $\hat{\mathbf{J}}\hat{\mathbf{V}}^H\hat{\mathbf{J}}^\top \xrightarrow{p} \mathbf{J}\mathbf{V}^{H*}\mathbf{J}^\top$. \square

D.4 Asymptotic normality and estimation of the variance bound under the estimated weights

Finally, we show the asymptotic properties under the estimated propensity and mediator scores.

Theorem 3 (Asymptotic normality of the Hájek estimator using the estimated propensity and mediator scores). *Suppose that Assumptions 3 and 4 hold, as well as Assumptions S.2, S.3, S.4 and S.5. Let $\hat{\gamma}$ be the estimate of the parameters obtained by solving $\sum_{t=L}^T \psi(W_t, M_t, \bar{H}_{t-1}; \gamma) = 0$. Then as $T \rightarrow \infty$, we have*

$$\frac{1}{\sqrt{T-L+1}} \sum_{t=L}^T (\tilde{\tau}_t^H(F', F''; \hat{\gamma}) - \tau_t(F', F''; \hat{\gamma})) \xrightarrow{d} N(\mathbf{0}, \mathbf{J}\mathbf{V}^H\mathbf{J}^\top),$$

where $\mathbf{V}^H = \tilde{\mathbf{V}}^H - \mathbf{U}^\top \mathbf{V}_{pm}^{-1} \mathbf{U}$ for matrices \mathbf{J} , $\tilde{\mathbf{V}}^H$ defined in Theorem 2, \mathbf{V}_{pm} defined in Assumption S.3, and \mathbf{U} in Assumption S.5.

Proof of Theorem 3. The proof closely follows that of Theorem A.2 in Zhou et al. (2024) by redefining the score function as follows:

$$s(\bar{H}_{t-1}, W_t, M_t, Y_t; \boldsymbol{\theta}) = \begin{pmatrix} \hat{Y}_t^I(F', L, \hat{\gamma}; \omega) - N_t(F') - \mu_1 \\ \hat{Y}_t^I(F'', L, \hat{\gamma}; \omega) - N_t(F'') - \mu_2 \\ \rho_{th'}(\gamma) - 1 - \mu_3 \\ \rho_{th''}(\gamma) - 1 - \mu_4 \\ \psi(W_t, M_t, \bar{H}_{t-1}; \gamma) \end{pmatrix}.$$

\square

Then, Theorem 4, which corresponds to Theorem 2 in Zhou et al. (2024), states the asymptotic efficiency under the estimated propensity and mediator score models.

Theorem 4. *If the propensity and mediator score models are correctly specified, the estimator $\frac{1}{T-L+1} \sum_{t=L}^T \tilde{\tau}_t^H(F', F''; \hat{\gamma})$ based on the estimated propensity and mediator scores has asymptotic variance that is no larger than the asymptotic variance of the same estimator using the known propensity and mediator scores. That is, for $\tilde{\mathbf{J}}\tilde{\mathbf{V}}^H\tilde{\mathbf{J}}^\top$ in Theorem 2, and $\mathbf{J}\mathbf{V}^H\mathbf{J}^\top$ in Theorem 3, $\mathbf{J}(\tilde{\mathbf{V}}^H - \mathbf{V}^H)\mathbf{J}^\top$ is a positive semidefinite matrix.*

For the proof of Theorem 4, see Zhou et al. (2024). Finally, Corollary 1 shows the consistent estimation of the variance upper bound.

Corollary 1. *Suppose that the conditions of Theorem 3 hold. For $A_t(\gamma)$ defined in Assumption S.4, define $\hat{V}^H = \frac{1}{T-L+1} \sum_{t=L}^T \hat{V}_t^H$ where \hat{V}_t^H defined in Proposition S.1. Also let \hat{J} as defined in Proposition S.1. Then, if Q , which depends on T , converges to the identity matrix I in probability as $T \rightarrow \infty$, $\hat{J}Q\hat{V}^HQ^\top\hat{J}^\top$ is a consistent estimator for $JV^{H*}J^\top$.*

The proof of Corollary 1 follows directly from Proposition S.1 and the fact that $\hat{\gamma}$ is a consistent estimator of γ^* .

E Average treatment effects

E.1 Covariates

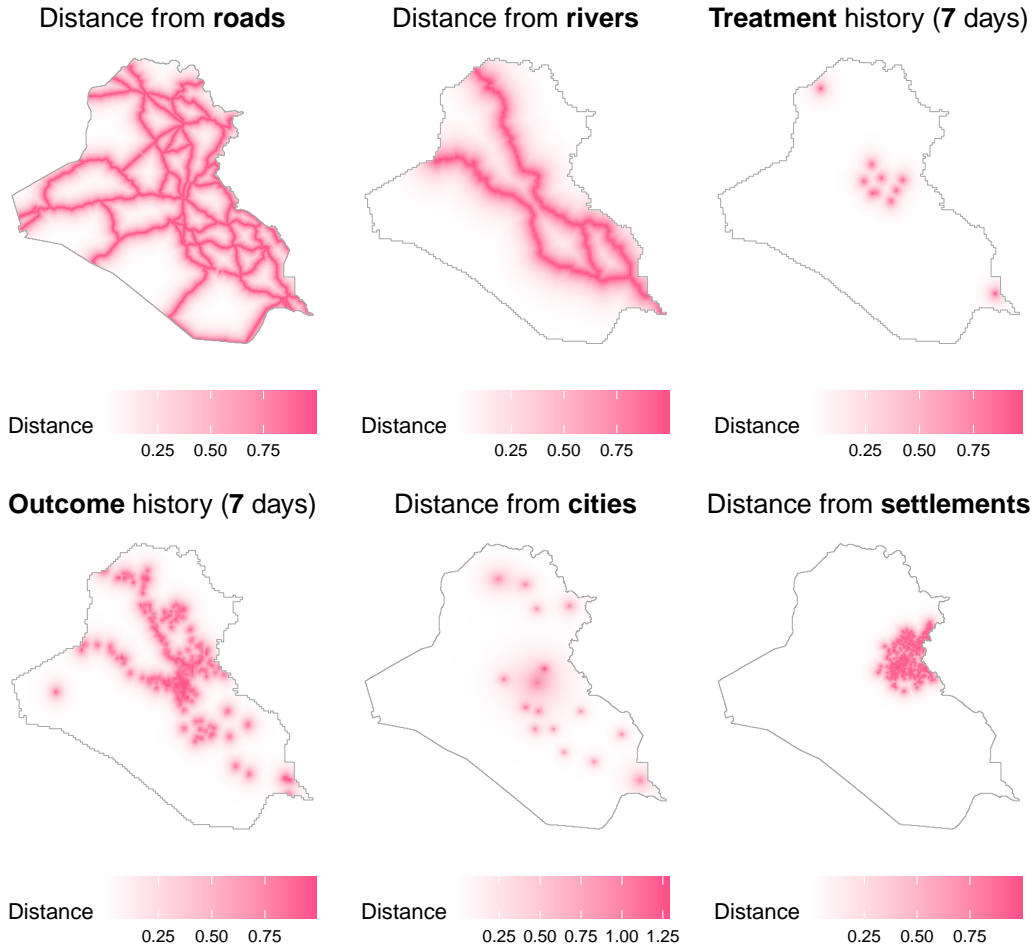


Figure S3: **Covariates (distance-based)**. The spatiotemporal covariates based on distance metrics are shown. For time-varying covariates (treatment and outcome history), data from day 100 are displayed. Distances from settlements are shown for one of the 18 Iraqi districts.

We transform raw distance metrics using exponential decay functions to make the covariates substantively interpretable. Following [Papadogeorgou et al. \(2022\)](#) and [Mukaigawara et al. \(2024\)](#), we apply a decay coefficient of -6 to treatment and outcome histories. For distances from roads and rivers, we use -3 , and for cities, we apply coefficients of -2 , -4 , -6 , -8 , and -10 to capture variation in population size. Finally, for settlements, we use -12 .

Figure S3 presents the transformed covariates. Objects are prioritized according to both their size and spatial influence. For example, larger cities exert greater spatial impact than smaller ones.

E.2 Estimation of propensity scores

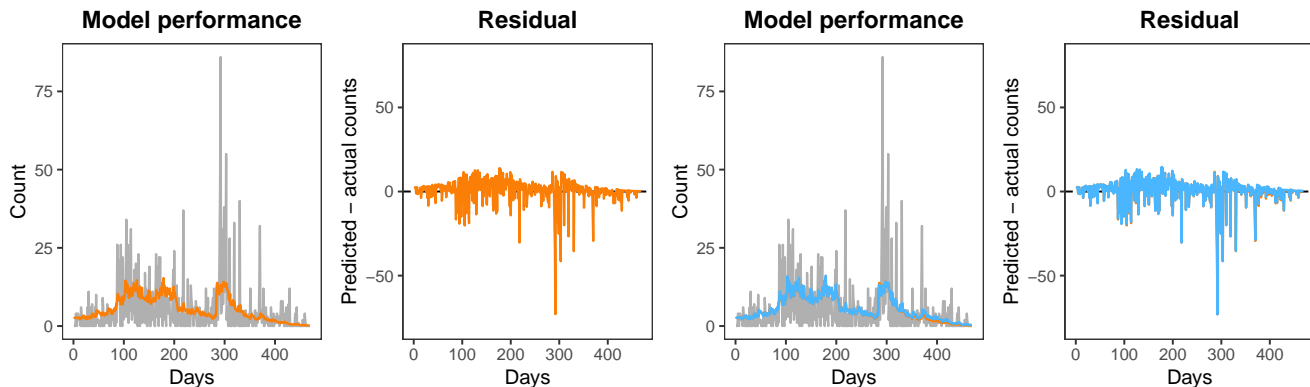


Figure S4: **Model performance.** The first panel (left) shows the actual and predicted counts (in gray and orange, respectively), and the second panel shows the residual plot. The third and fourth panels do the same with the first 80% of observations to examine out-of-sample prediction performance.

E.3 Outcome surfaces

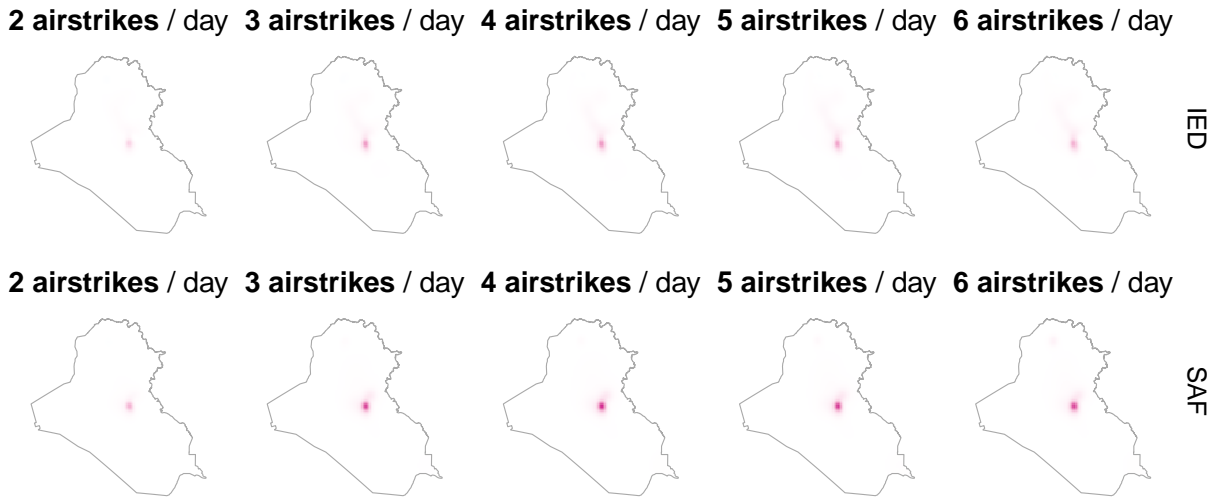


Figure S5: **Differences in outcome surfaces for intensity changes.** The first and second rows correspond to IED and SAF, respectively (with the treatment periods of 14 days). The areas in red and blue exhibit those with increased and decreased intensities of insurgent attacks, respectively.

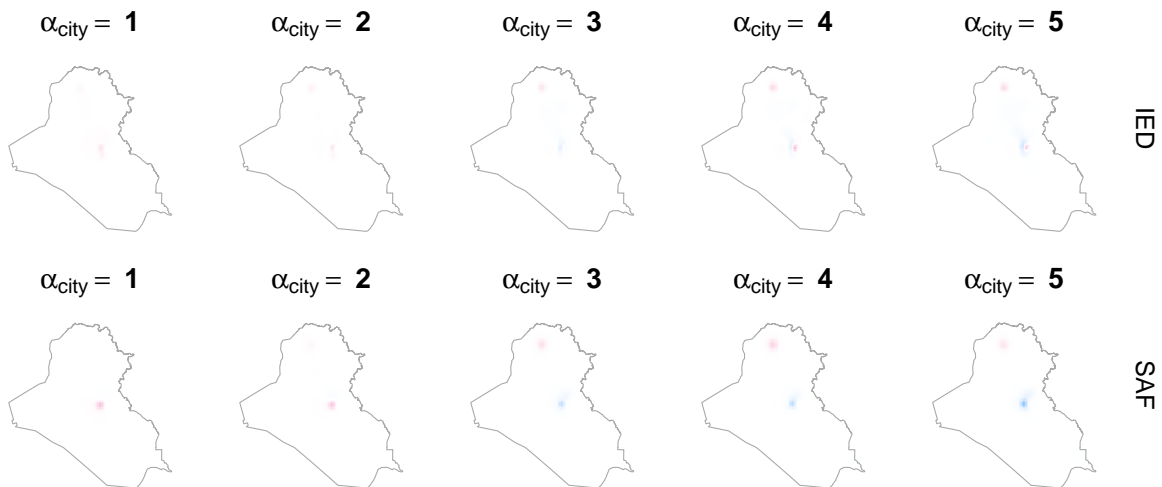
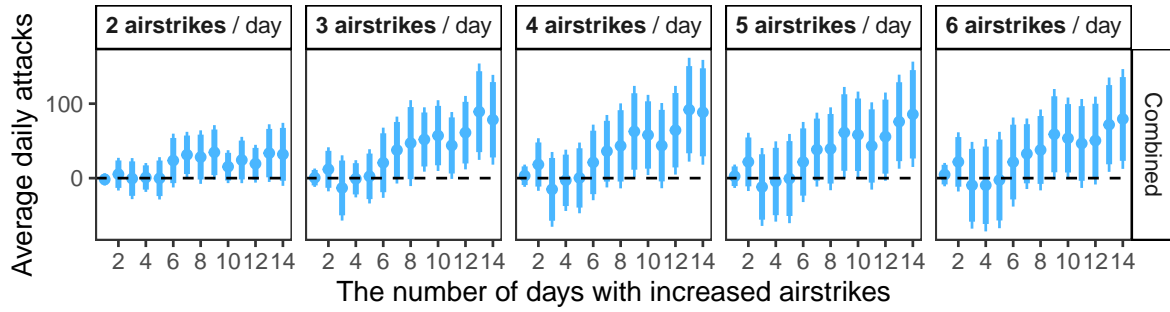
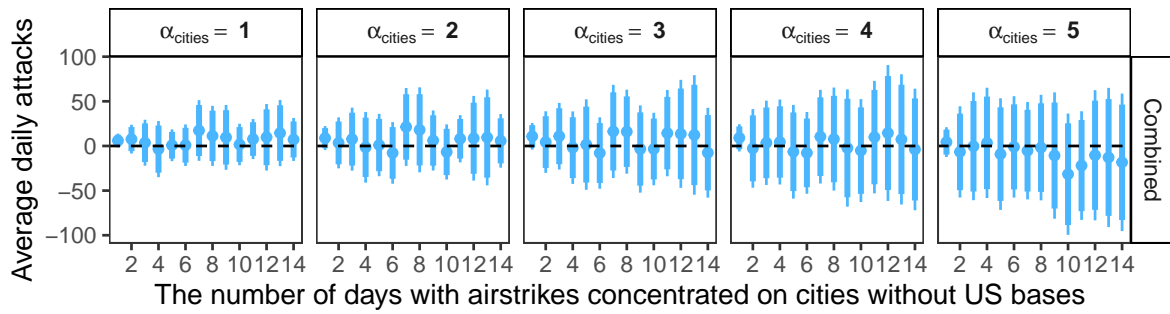


Figure S6: **Differences in outcome surfaces for location shifts.** The first and second rows correspond to IED and SAF, respectively (with the treatment periods of 14 days). The areas in red and blue exhibit those with increased and decreased intensities of insurgent attacks, respectively.

E.4 Combined outcomes



(a) Intensity



(b) Location shift

Figure S7: **Average treatment effects (both IED and SAF cases combined).** We find statistically significant effects for intensity changes (a) but not for location shifts (b).

F Heterogeneous treatment effects

F.1 Troop characteristics

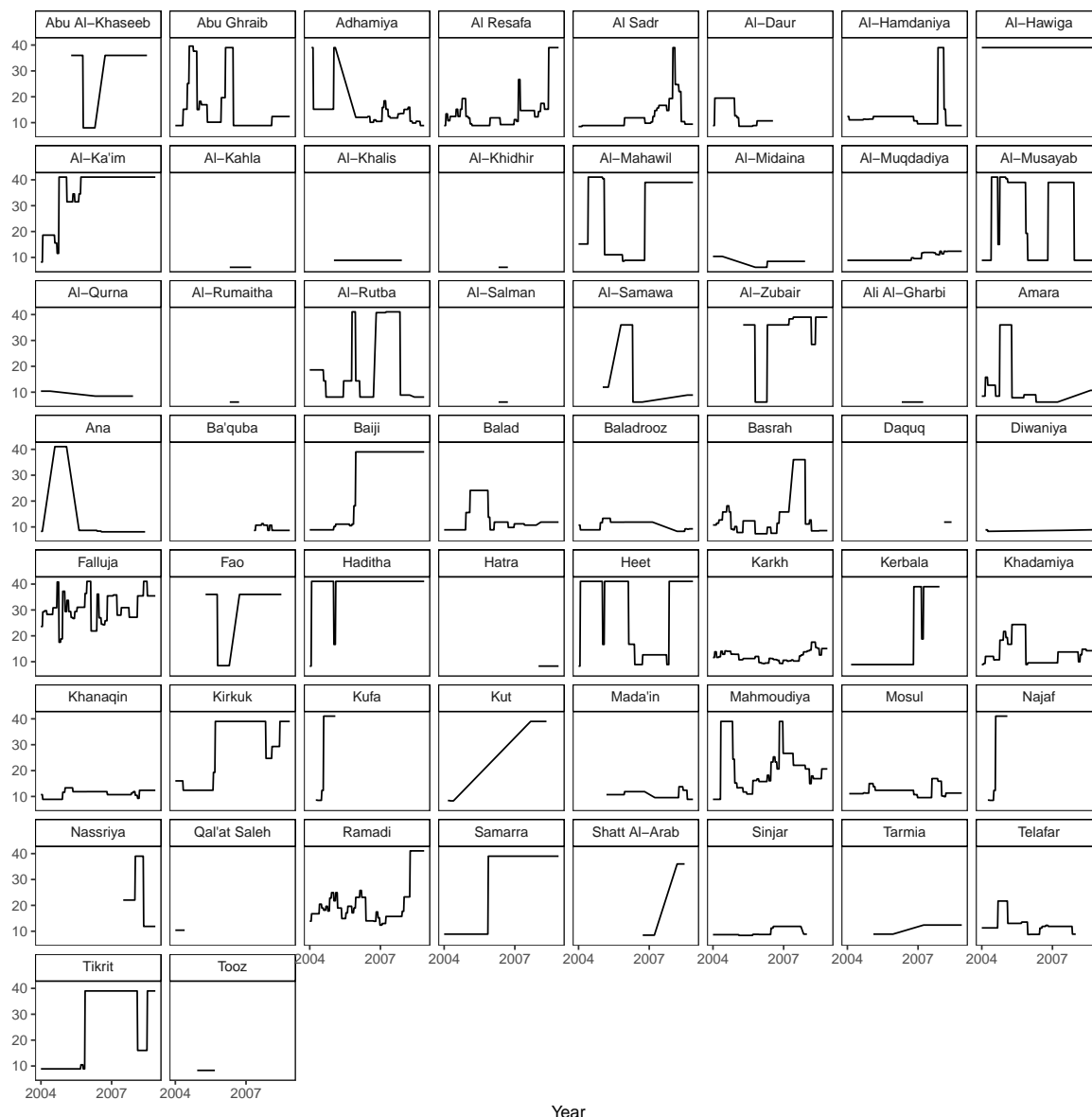
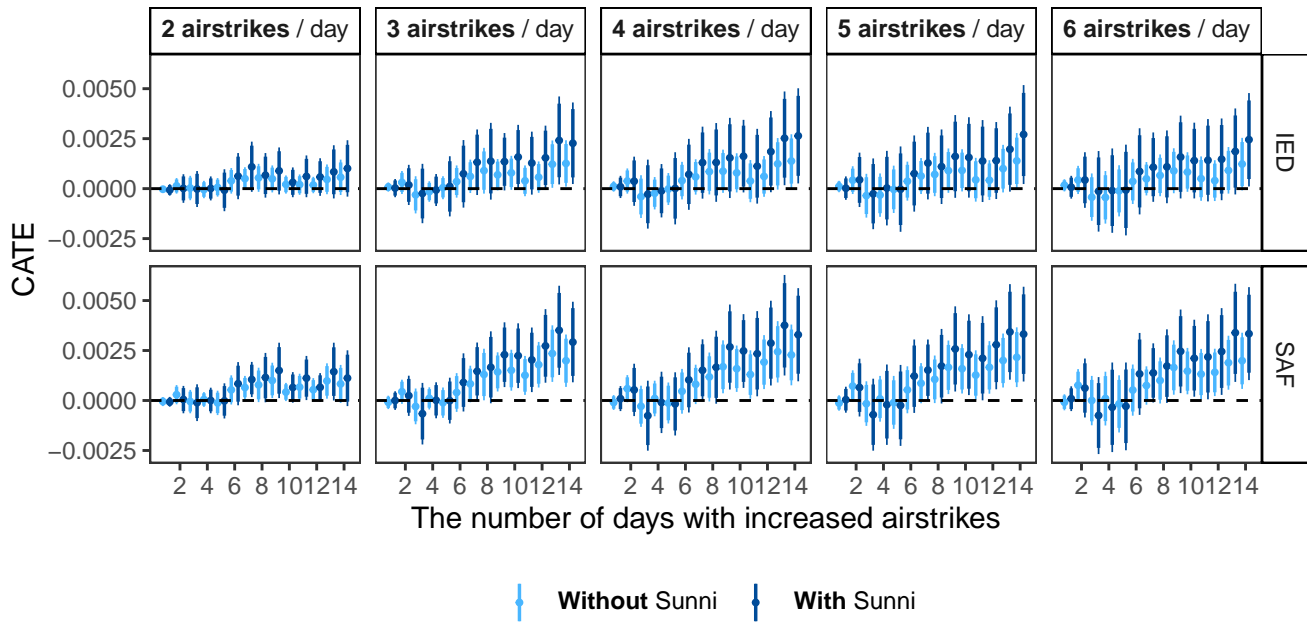
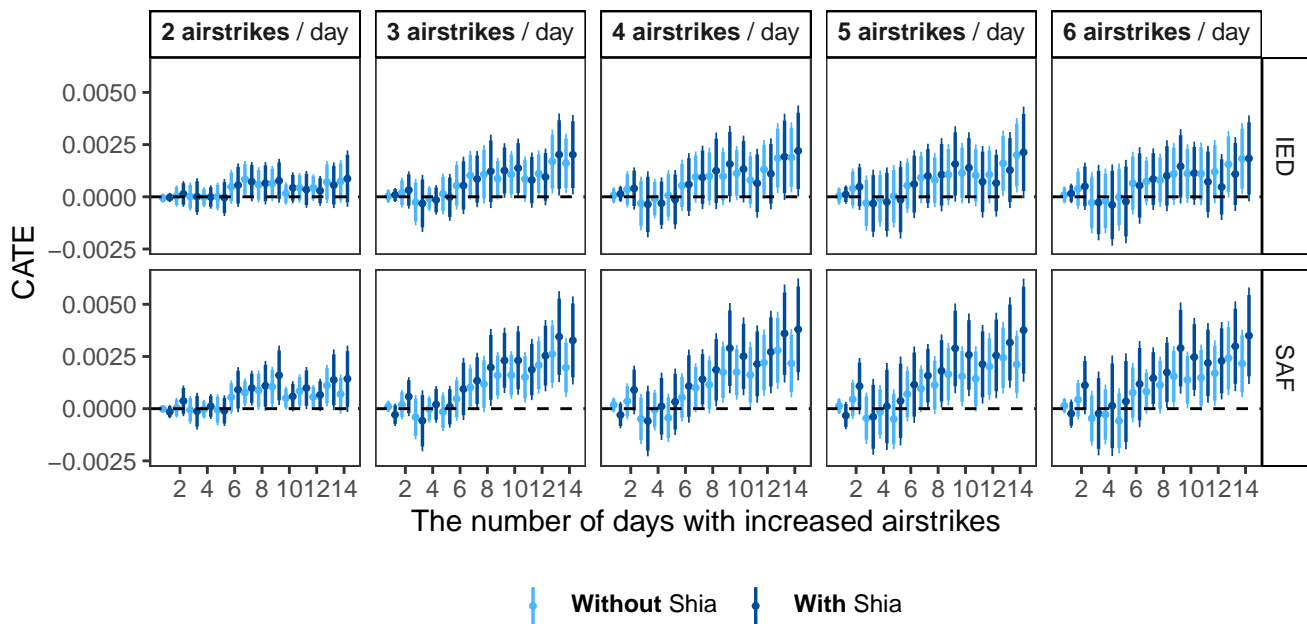


Figure S8: **Troop characteristics: Mechanization.** We display weekly data from 58 of Iraq’s 104 districts. Following (Van Wie and Walden, 2023, 2069), we treat the remaining “missing” districts as having no large-scale US or UK military presence for the given week/district. Given operational secrecy, we cannot rule out that small units (including Special Forces) may have been operating in these areas. But, as Van Wie and Walden note, their search methodology is a reasonable one to uncover the persistent presence of battalion-sized units and their level of mechanization. As a result, we assign a zero to these missing week-districts when performing our heterogeneity analysis.

F.2 Presence of Sunni and Shia



(a) Sunni



(b) Shia

Figure S9: **Heterogeneous treatment effects (the presence of Sunni and Shia)**. Heterogeneous treatment effects with respect to the presence of Sunni and Shia (Panels S9a and S9b, respectively) are shown. Thick and thin lines indicate 95% and 90% confidence intervals, respectively.

G Causal mediation analysis

G.1 Model fit

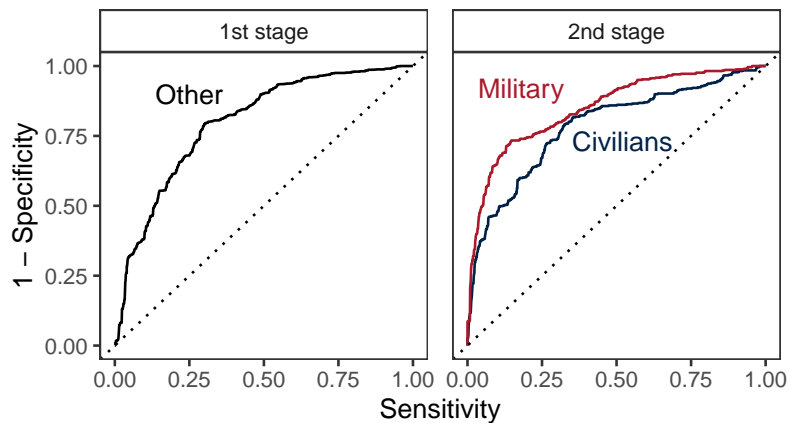


Figure S10: **Receiver operating characteristic curves (ROCs)**. The left panel shows the ROC curve for the first stage, and the right panel shows the ROC curves for the second stage (civilians and military targets in blue and red, respectively). The 45-degree lines are shown as dotted lines.

G.2 Covariates

Similarly to the propensity score model (see SI Section E.1), we use an exponential decay function to transform distance-based metrics. We apply a coefficient of -0.5 to transform distances from buildings (both residential and non-residential; see Figure S11), which reflects the relatively smaller size of buildings compared to other geospatial objects such as cities, roads, and rivers.

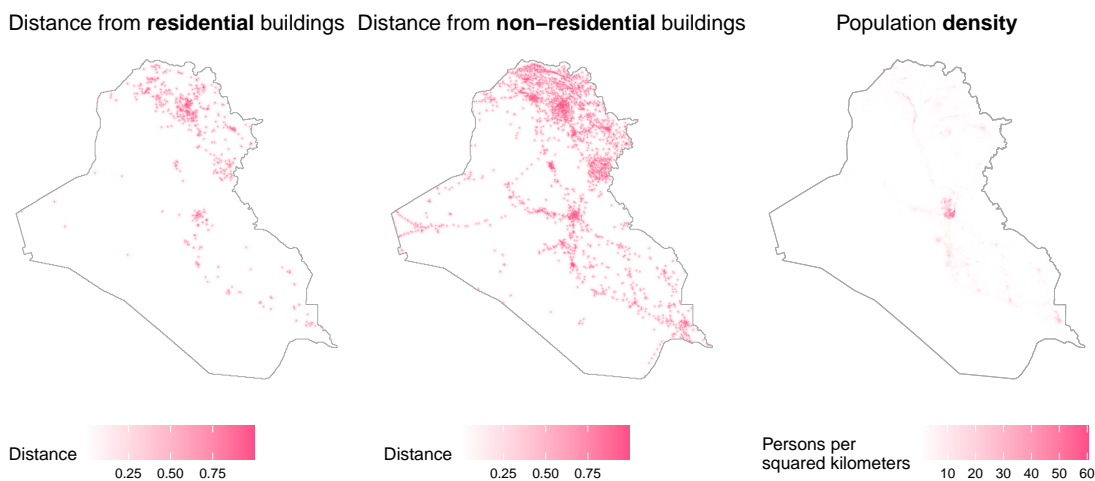


Figure S11: **Covariates (mediator)**. The additional covariates used to estimate the conditional mediator density are shown. The distances are converted by an exponential decay function.

G.3 Geographical areas

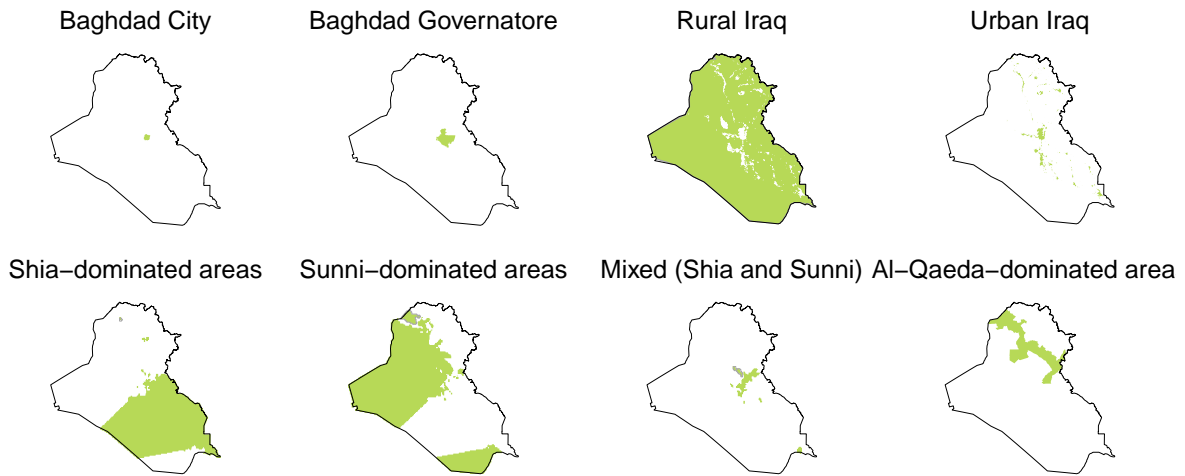


Figure S12: **Geographical areas.** Rural and urban areas are defined as areas with population count $< 300 / \text{km}^2$ and $\geq 300 / \text{km}^2$, respectively. Shia-Sunni demographic balance is provided by [Empirical Studies of Conflict \(2012\)](#). Al Qaeda territorial control is based on [Hamilton \(2008\)](#). We define “Rural Baghdad” as the entire Baghdad Governorate excluding Baghdad City.

G.4 Main results in other geographical areas

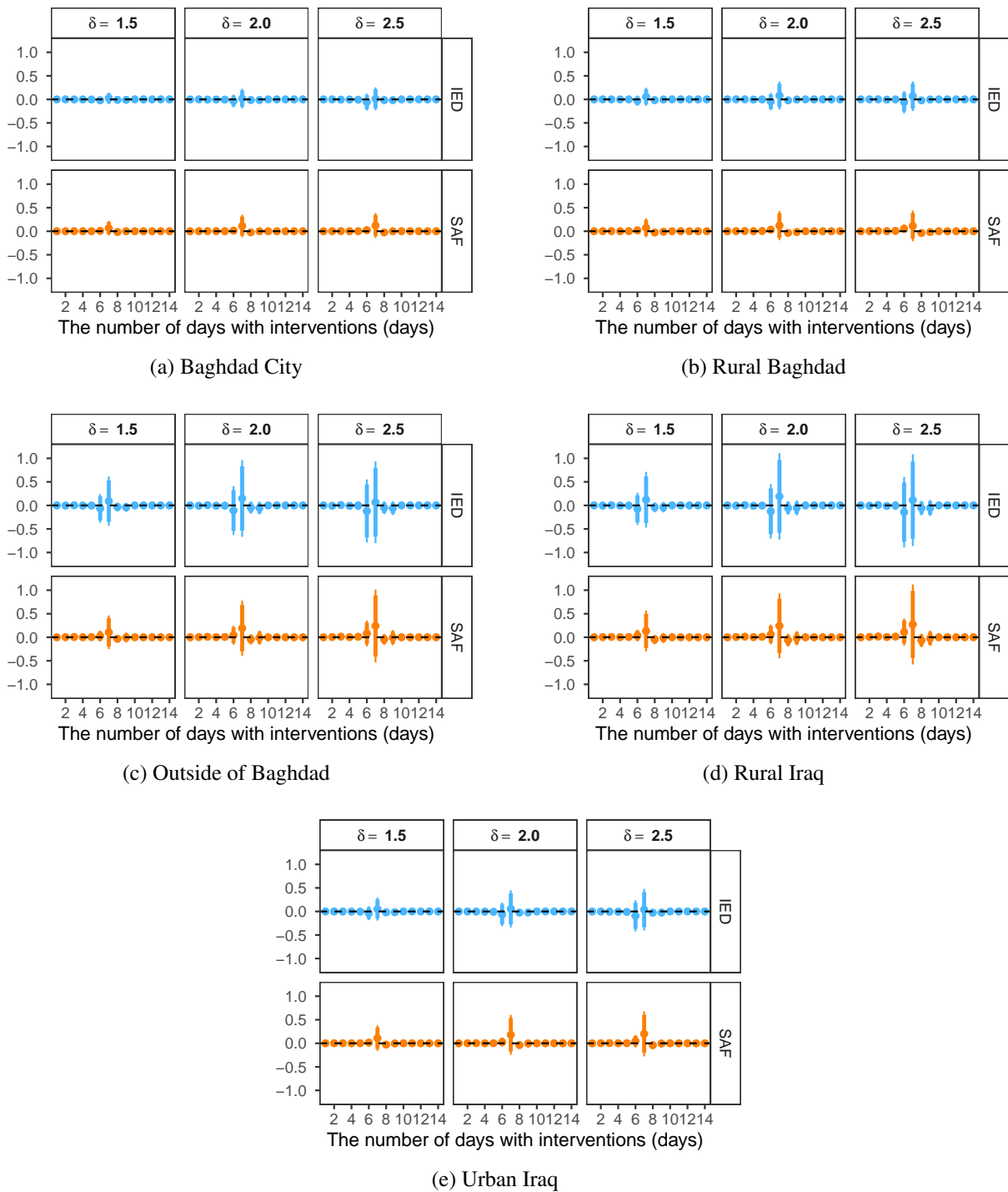
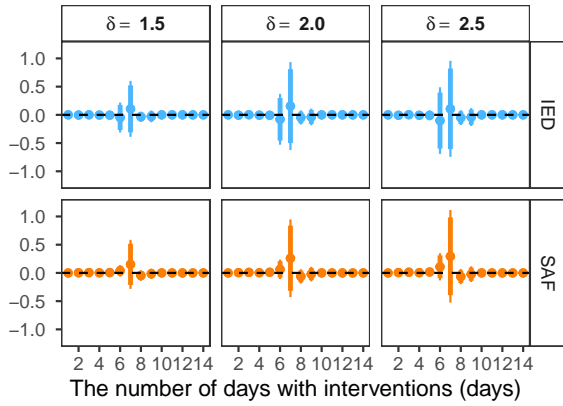
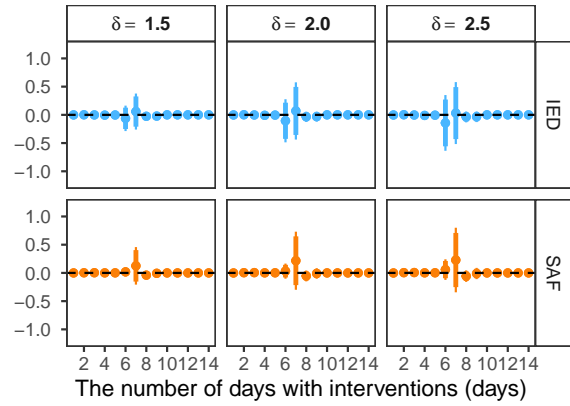


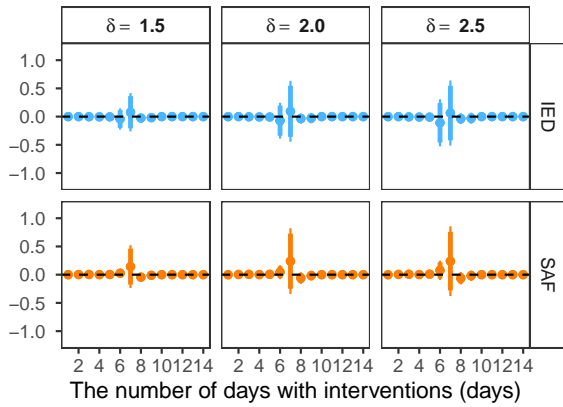
Figure S13: **Indirect effects of civilian harm in other areas, I.** Indirect effects in (a) Baghdad City, (b) rural Baghdad, (c) outside Baghdad, (d) rural Iraq, and (e) urban Iraq are shown.



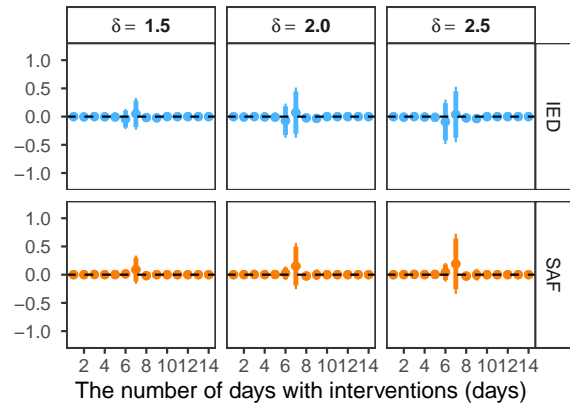
(a) Sunni-dominated area



(b) Shia-dominated area



(c) Mixed presence



(d) Al-Qaeda dominated area

Figure S14: **Indirect effects of civilian harm in other areas, II.** Indirect effects in (a) areas with Sunni dominance, (b) areas with Shia dominance, (c) areas with Sunni/Shia mixed presence, and (d) Al-Qaeda dominated areas are shown.

G.5 Results using an indicator for civilian casualties

To supplement our satellite imagery, we conduct mediation analyses using a binary variable for civilian casualties. We find that most airstrikes are recorded as having no civilian casualties (98.5% of in-sample airstrikes and 86.6% of out-of-sample airstrikes are coded as zero civilian casualties). Therefore, instead of changing the probability of airstrikes with civilian casualties in Baghdad City, we change the probability across Iraq. We check the model performance by the ROC (Figure S15). The area under the curve is 0.96.

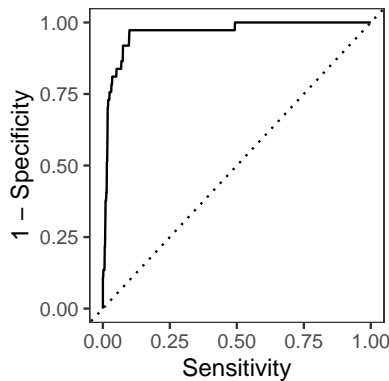


Figure S15: **Receiver operating characteristic curve (ROC)**. The area under the curve (AUCs) is 0.96. for the second stage (military targets). The 45-degree line is shown as a dotted line.

We construct counterfactual conditional distributions of civilian casualties given airstrikes by setting $\delta \in \{1.5, 2, 2.5\}$. As we increase the value of δ (from the left to right panels), the density of the conditional probability shifts to the left (a higher probability of hitting civilians; see Figure S16).

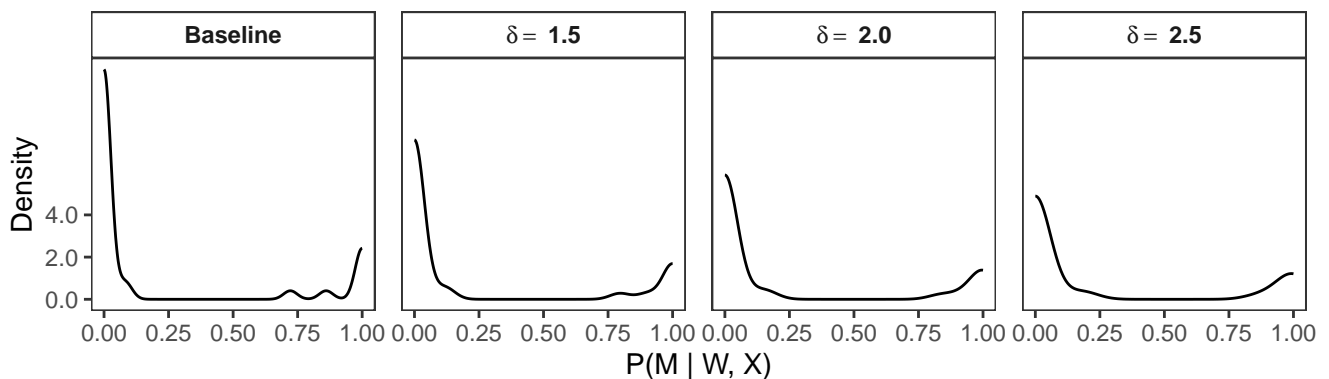


Figure S16: **Counterfactual conditional mediator densities (binary)**. The plot shows changes in the densities of conditional mediator probabilities in response to various values of δ . The conditional probabilities of hitting civilians, given airstrike locations and covariates, are shown.

With this setup, we estimate the indirect effects of increasing the probability of hitting civilians, while keeping the frequency and distribution of airstrikes constant. Figures S17 and S18 summarize

the main results. While we see some positive effects with $L = 3$, the results are not consistent across all time periods. We do not observe any consistent, statistically significant mediating effects of civilian casualties.

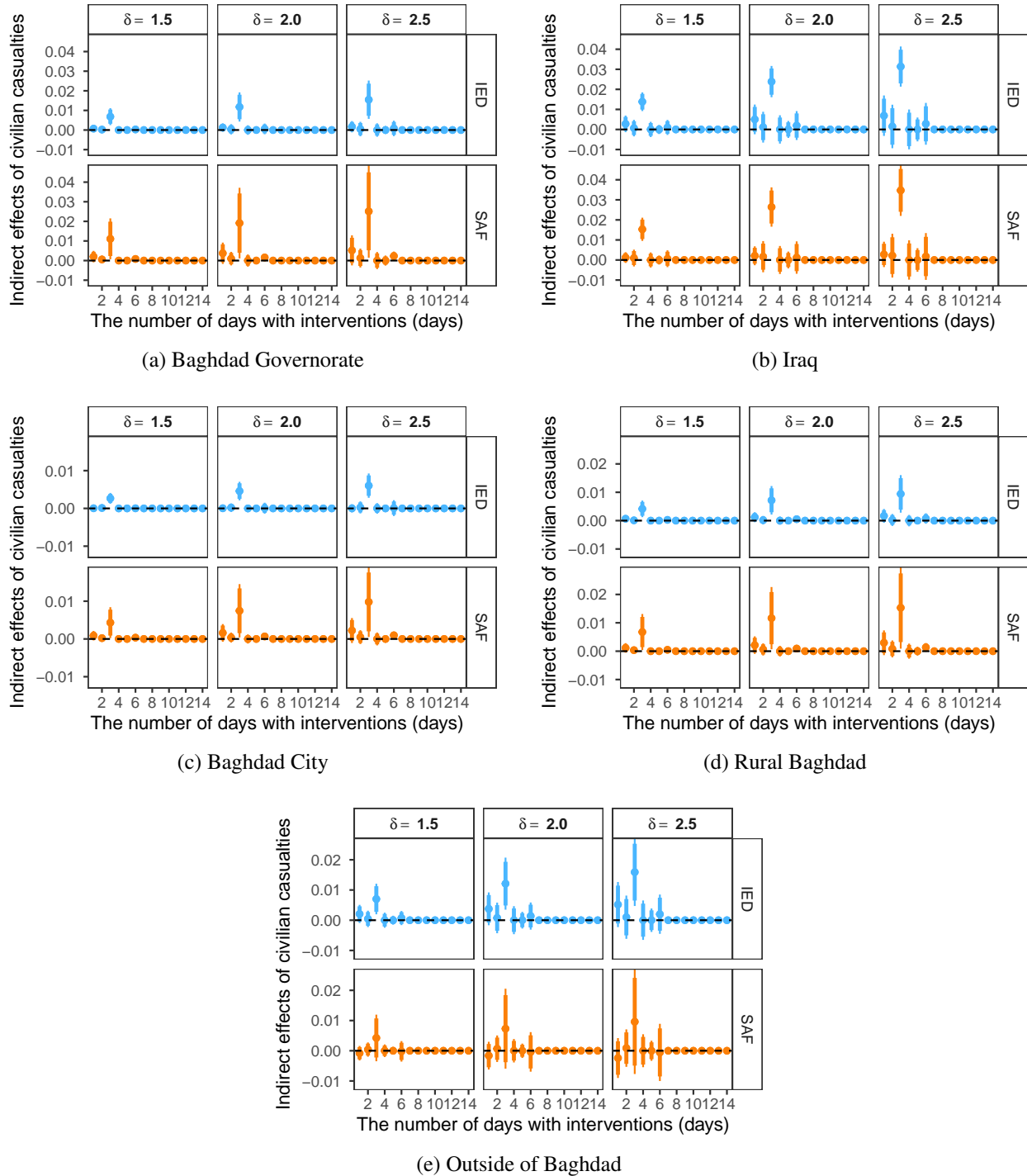


Figure S17: **Indirect effects of civilian casualties in other areas (binary), I.** Indirect effects in (a) Baghdad Governorate, (b) Iraq, (c) Baghdad City, (d) rural Baghdad, and (e) outside Baghdad are shown.

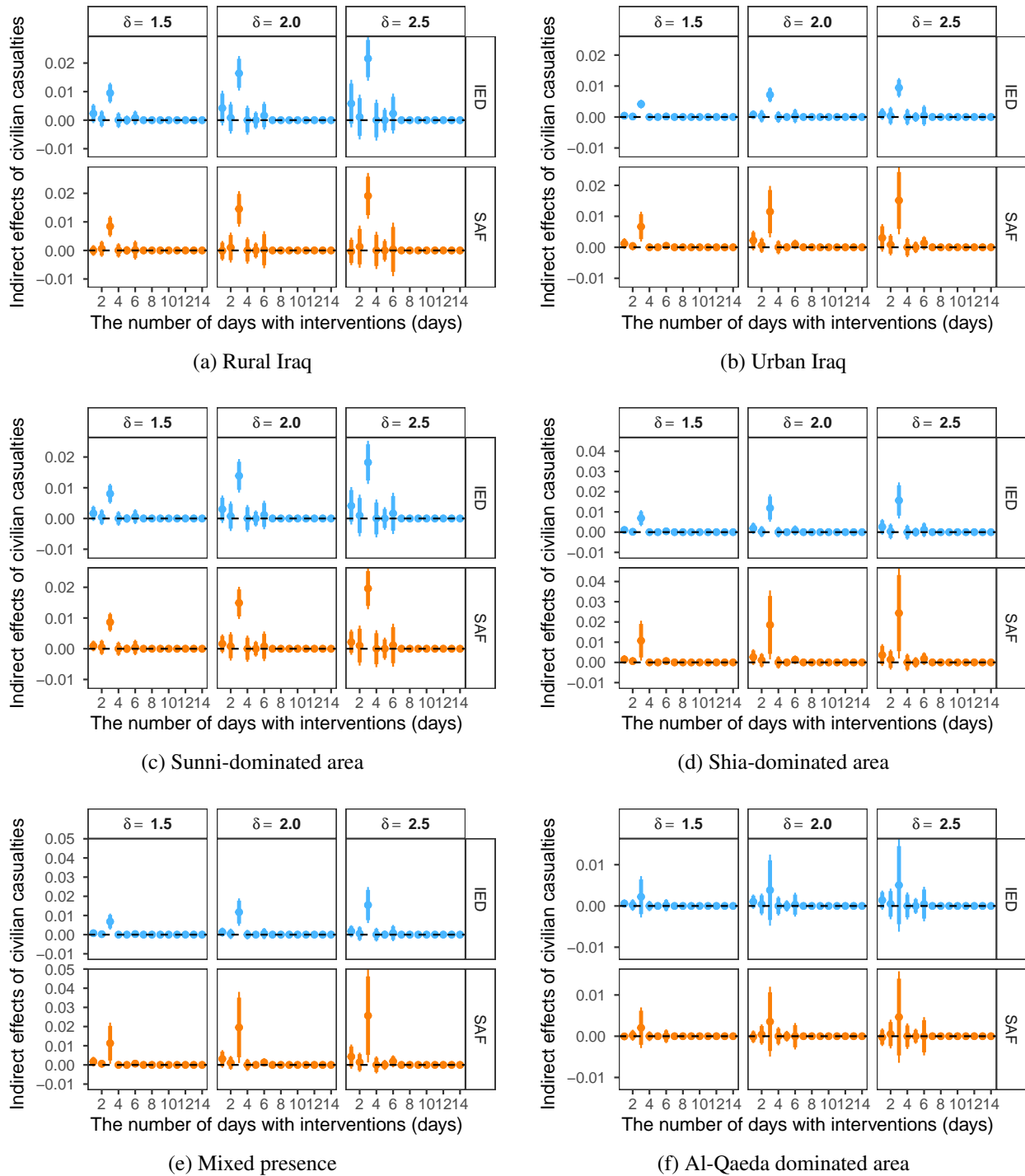


Figure S18: **Indirect effects of civilian casualties in other areas (binary), II.** Indirect effects in (a) rural Iraq, (b) urban Iraq, (c) areas with Sunni dominance, (d) areas with Shia dominance, (e) areas with Sunni/Shia mixed presence, and (e) Al-Qaeda dominated areas are shown.